Journal for ImmunoTherapy of Cancer

Quantifying the impact of immunotherapy on RNA dynamics in cancer

Ieva Usaite ,[1,2] Dhruva Biswas,[1,2,3] Krijn Dijkstra,[1,2,4,5] Thomas BK Watkins,[1] Oriol Pich,[2] Clare Puttick,[1,2] Mihaela Angelova,[2] Krupa Thakkar,[1,6] Crispin Hiley,[1,2,7] Nicolai Birkbak ,[8,9] Marleen Kok,[10] Simone Zaccaria ,[1,11] Yin Wu,[12,13] Kevin Litchfield,[1,6] Charles Swanton,[1,2] Nnennaya Kanu[1]

To cite: Usaite I, Biswas D, Dijkstra K, *et al*. Quantifying the impact of immunotherapy on RNA dynamics in cancer. *Journal for ImmunoTherapy of Cancer* 2023;**11**:e007870. doi:10.1136/jitc-2023-007870

► Additional supplemental material is published online only. To view, please visit the journal online (http://dx.doi.org/10.1136/jitc-2023-007870).

IU and DB contributed equally.

IU and DB are joint first authors.

Accepted 05 October 2023

For numbered affiliations see end of article.

Correspondence to
Dr Charles Swanton;
charles.swanton@crick.ac.uk

Dr Nnennaya Kanu;
n.kanu@ucl.ac.uk

Dr Kevin Litchfield;
k.litchfield@ucl.ac.uk

ABSTRACT

Background Checkpoint inhibitor (CPI) immunotherapies have provided durable clinical responses across a range of solid tumor types for some patients with cancer. Nonetheless, response rates to CPI vary greatly between cancer types. Resolving intratumor transcriptomic changes induced by CPI may improve our understanding of the mechanisms of sensitivity and resistance.

Methods We assembled a cohort of longitudinal pre-therapy and on-therapy samples from 174 patients treated with CPI across six cancer types by leveraging transcriptomic sequencing data from five studies.

Results Meta-analyses of published RNA markers revealed an on-therapy pattern of immune reinvigoration in patients with breast cancer, which was not discernible pre-therapy, providing biological insight into the impact of CPI on the breast cancer immune microenvironment. We identified 98 breast cancer-specific correlates of CPI response, including 13 genes which are known IO targets, such as toll-like receptors *TLR1*, *TLR4*, and *TLR8*, that could hold potential as combination targets for patients with breast cancer receiving CPI treatment. Furthermore, we demonstrate that a subset of response genes identified in breast cancer are already highly expressed pre-therapy in melanoma, and additionally we establish divergent RNA dynamics between breast cancer and melanoma following CPI treatment, which may suggest distinct immune microenvironments between the two cancer types.

Conclusions Overall, delineating longitudinal RNA dynamics following CPI therapy sheds light on the mechanisms underlying diverging response trajectories, and identifies putative targets for combination therapy.

WHAT IS ALREADY KNOWN ON THIS TOPIC

⇒ Explorations of molecular dynamics following checkpoint inhibitor (CPI) therapy within small cohorts have shed light on the biological activity of CPI-modulated immune responses such as early T-cell turnover and expansion. However, an understanding of the impact of CPI on transcriptomic changes and similarities and differences in mechanisms of response to CPI between solid tumor types remains limited.

WHAT THIS STUDY ADDS

⇒ This study integrates longitudinal pre-therapy and on-therapy transcriptomic data across solid tumor types to identify meaningful transcriptomic dynamics on-therapy, enabling a deeper insight into the mechanisms of CPI response and resistance and how these may differ across melanoma and breast cancer.

HOW THIS STUDY MIGHT AFFECT RESEARCH, PRACTICE OR POLICY

⇒ Findings from this study provide a rational for further investigation of promising putative targets for combination therapy with CPI to enhance response rates in breast cancer.

INTRODUCTION

A molecular understanding of immune checkpoints, and their aberrant activation in developing tumors, has led to the recent clinical development of immune checkpoint inhibitors (CPIs). Over the last decade, CPI agents have demonstrated durable responses across a range of cancer types and are FDA-approved for multiple indications, including as a first-line therapy option for metastatic disease.[1] However, only a minority of patients achieve clinical responses ranging from objective response rates of 45% in advanced melanoma cases,[2] to 5% to 10% in metastatic triple-negative breast cancers (TNBCs).[3 4]

Due to variability in CPI response rates between patients, numerous studies have attempted to identify molecular predictors of response. Using single timepoint data, collected prior to CPI treatment (pre-therapy), factors that have been linked to CPI sensitivity have been derived from tumor genomics and tumor microenvironmental (TME) studies.[5] Notably, baseline PD-L1 expression and tumor mutational burden are both FDA-approved as predictive biomarkers to stratify patients

for CPI therapy. Furthermore, numerous transcriptomic signatures have been developed, predominantly within melanoma, as putative RNA-based predictors of CPI sensitivity including signatures of interferon-gamma (IFNγ) signaling, cytolytic activity, and antigen presentation.[6–13]

Nevertheless, biomarkers of immune response, based on pre-therapy molecular profiles in discovery cohorts have displayed varying performance in large validation cohorts (n>1000 patients), particularly in a pan-cancer setting.[14 15] These markers implicitly assume that baseline molecular features are sufficient to encapsulate the dynamic impact of CPI on-therapy, including resculpting the cellular composition and functional states within the tumor microenvironment. Moreover, these factors do not account for the well-recognized interindividual variation in baseline immune status.

Paired longitudinal analyses of patients receiving CPI agents, with pre-therapy and on-therapy tumor biopsies, have the potential to address these limitations and decipher important factors driving an effective immune response. However, these analyses are complicated by the logistical challenges of tumor re-biopsy on treatment. To date, small exploratory cohorts (n≤20 patients) of this kind have reported a phenomenon termed T-cell "reinvigoration,"[16] whereby early T-cell turnover and expansion or persistence of high-frequency T-cell clonotypes are associated with CPI response,[17 18] and improved survival outcomes.[19 20] Other longitudinal CPI studies have demonstrated clonal replacement of T-cell clones on-therapy, which were not present within responding tumors pre-treatment.[21] In addition, other studies have demonstrated mechanisms of CPI treatment failure, such as defective antigen presentation,[22 23] impaired IFNγ signaling,[22] or neoantigen loss.[24] In metastatic TNBC, on-therapy increases in T-cell receptor (TCR) clonality and T-cell infiltration have been shown to be associated with response to CPI.[25] Furthermore, similar shifts in eosinophils were enriched in patients responding to CPI, possibly due to their role in enhancing CD8+ T-cell activation.[26]

Despite the small numbers of patients in these longitudinal studies, profiling molecular dynamics following CPI therapy has enabled the biological activity of CPI-modulated immune responses to be defined. In turn, this has improved our understanding of the mechanisms underpinning sensitivity or resistance. To build on this body of work, we established the CPI-Dynamics ("CPIΔ") multi-cancer cohort of 174 patients across six datasets, leveraging the power of paired longitudinal (pre-treatment and early on-treatment samples) to investigate transcriptomic changes during CPI therapy. The objectives of our approach were to better understand why some cancer types respond more favorably to CPI treatment than others, specifically melanoma compared with TNBC, by identifying correlates which underlie the biological mechanisms of response.

METHODS

Human clinical data

The CPIΔ cohort uses transcriptomic sequencing data from the following studies:

1. Voorwerk *et al*,[25] the metastatic TNBC anti-PD-1 (nivolumab) treated "breast" cohort.
2. Riaz *et al*,[27] the advanced melanoma anti-PD-1 (nivolumab) treated "melanoma (a)" and "melanoma (b)" cohorts.
3. Yang *et al*,[28] the pan-cancer anti-PD-1 (pembrolizumab) treated "pan-cancer" cohort.
4. Powles *et al*,[29] the advanced urothelial anti-PD-L1 (atezolizumab) treated "urothelial (a)" cohort.
5. Dijk *et al*,[30] the advanced urothelial anti-PD-1 (nivolumab) and anti-CTLA-4 (ipilimumab) treated "urothelial (b)" cohort.

Across all selected studies, patients provided written consent before enrollment into respective trials, furthermore, trial approval was obtained from each institutions medical-ethical committee/board, as described previously.[25 27–30] Inclusion criteria for the CPIΔ cohort were (1) treatment with CPI (anti-PD-1/PD-L1 or anti-CTLA4); (2) availability of longitudinal transcriptomic data at both pre-therapy and on-therapy timepoints; and (3) availability of clinical outcome data (overall survival (OS), radiological response and/or pathological response). These criteria yielded a total of 174 CPI-treated patients with paired samples across six cancer types. The individual cohorts comprising the CPIΔ study are henceforth referred to as the "breast" cohort (n=25 patients with TNBC), "melanoma (a)" cohort (n=23 patients with melanoma, CPI-naïve), "melanoma (b)" cohort (n=19 patients with melanoma, prior lines of CPI therapy), "pan-cancer" cohort (head and neck carcinoma n=3, TNBC n=3, high-grade serous ovarian cancer n=6, melanoma n=6, rare solid tumors n=12), "urothelial (a)" cohort (n=64), and "urothelial (b)" cohort (n=13). A breakdown of sample numbers for each study/cancer type and treatment course is contained in table 1 and online supplemental figure 1. The majority of our cohorts included patients with either metastatic or advanced disease, many of whom had other lines of systemic therapy prior to CPI. The details of those previous lines of therapy are included where available. For the "breast" cohort, patients had received one to three lines of prior systemic non-CPI treatment (chemotherapy) with disease progression on the last treatment regiment; however, all patients were CPI naïve prior to entering the trial (online supplemental figure 1A). For the "melanoma (a)" and "melanoma (b)" cohorts, patients with unresectable stage III or IV melanoma who were refractory, intolerant, or refused standard therapy for treatment of metastatic disease were enrolled. For the "melanoma (a)" cohort all patients had not received previous lines of CPI (online supplemental figure 1B), whereas patients within the "melanoma (b)" cohort had progressed following anti-CTLA-4 treatment prior to entering the trial (online supplemental figure 1C). For the "pan-cancer" cohort, patients had either

Table 1 CPIΔ cohort overview

Cohort	Cancer type	Pre-therapy (n)	Pre-therapy data type	On-therapy (n)	On-therapy data type	Paired longitudinal samples (n)	Longitudinal data type
Breast	Metastatic TNBC	44	RNA-seq	25	NanoString	25	NanoString
Melanoma (a)	Metastatic melanoma	29	RNA-seq	23	RNA-seq	23	RNA-seq
Melanoma (b)	Metastatic melanoma	19	RNA-seq	19	RNA-seq	19	RNA-seq
Pan-cancer	Metastatic solid tumors	30	RNA-seq	30	RNA-seq	30	RNA-seq
Urothelial (a)	Muscle-invasive urothelial cancer	64	RNA-seq	64	RNA-seq	64	RNA-seq
Urothelial (b)	Locoregionally advanced urothelial cancer	13	RNA-seq	13	RNA-seq	13	RNA-seq

CPI, immune checkpoint inhibitor ; RNA-seq, RNA sequencing; TNBC, triple-negative breast cancer.

failed prior systemic non-CPI treatment, had no standard non-CPI therapy options, or were not appropriate for standard non-CPI options. All patients in this cohort were CPI naïve prior to entering the trial (online supplemental figure 1D). For both the "urothelial (a)" and "urothelial (b)" cohorts, patients who refused neoadjuvant cisplatin-based chemotherapy or where neoadjuvant cisplatin-based therapy was not deemed appropriate, were enrolled onto the respective trials. Patients within both cohorts were CPI naïve prior to entering the trials (online supplemental figure 1E,F). Detailed treatment history and demographic data regarding, age, sex, and race were either limited or unavailable for selected cohorts and hence not used within our analyses.

Clinical endpoints and stratification

Across the CPIΔ cohorts, four had both OS and RECIST (Response Evaluation Criteria in Solid Tumors) radiological response available; the remaining two cohorts had pathological complete response (pCR) data available. Radiological clinical responses were harmonized across the studies to ensure consistency in this outcome measurement, with "responder" defined as complete response or partial response and "non-responder" as stable disease or progressive disease, as conducted previously.[14] Furthermore, for pathological response, "responder" was defined as pCR or major pathological response (MPR), and "non-responder" as no pCR or MPR. These definitions of response criteria were used for the stratification of samples within the CPIΔ cohorts into CPI-responding and CPI-non-responding tumors, per cohort, throughout the analyses. Additional stratification was applied using OS, splitting tumors into groups of either favorable or poorer clinical outcomes by a median split of OS per cohort. No other filters were used here to stratify patients, as the last follow-up time was not available for the majority of cohorts.

Longitudinal bulk transcriptomic data

Preprocessed transcriptomic data were accessed for every patient-tumor within the CPIΔ study. All cohorts included transcriptomic data from tumor biopsies collected from two specific timepoints; pre-therapy (baseline sample prior to CPI treatment) and on-therapy (after at least one cycle of CPI, ranging from 2 to 9 weeks). Across the CPIΔ cohorts, longitudinal transcriptomic information was available in the form of either RNA sequencing (n=6) or NanoString (n=1) data. For the "breast" cohort, transcriptomic data in the form of RNA sequencing was available pre-therapy only (n=44), whereas paired pre-therapy and on-therapy transcriptomic data were only available in the form of NanoString data, and hence these data were used for the majority of analyses. For the "breast" cohorts, a total of n=25 patients had NanoString data from both pre-therapy and on-therapy timepoints available. The melanoma cohorts ("melanoma (a)" and "melanoma (b)") had transcriptomic data available in the form of RNA sequencing. In total, all n=19 "melanoma (b)" patients had sequencing data available across both timepoints. Only 23/29 'Melanoma a' patients had sequencing data available from both timepoints. For both the urothelial cohorts, RNA sequencing was available across both timepoints for n=64 ('urothelial a') and n=13 ('urothelial b') patients. For analysis, all transcriptomic data, in the form of transcript per million (TPM), was transformed using log2(TPM+1). The exception to this was the RNA sequencing data from the pan-cancer cohort, where data was already log2 transformed and batch normalized for n=30 patients across both pre- and on-therapy timepoints.

CPI1000+ study samples

Transcriptomic data in the form of TPM were leveraged from the CPI1000+ study[14] consisting of pre-therapy RNA-sequencing data across four "melanoma" CPI-naïve cohorts: Liu *et al* (n=66), an advanced melanoma anti-PD-1

treated cohort[31] ; Snyder *et al* (n=20), an advanced melanoma anti-CTLA-4 treated cohort[32]; Hugo *et al* (n=26), an advanced melanoma anti-PD-1 treated cohort[6] ; Van Allen *et al* (n=39), an advanced melanoma anti-CTLA-4 treated cohort.[33] One melanoma CPI-pretreated cohort referred to as "melanoma (c)," Liu *et al* (n=55), an advanced melanoma anti-PD-1 treated cohort.[31] Two bladder cohorts: Snyder *et al* (n=21), an advanced urothelial cancer anti-PD-L1 treated cohort[34]; Mariathasan *et al* (n=331), an advanced urothelial cancer anti-PD-L1 treated cohort.[11] One renal cohort, McDermott *et al* (n=39), a metastatic renal cell carcinoma anti-PD-L1 treated cohort.[12] One lung cohort, Shim *et al* (n=195), an advanced non-small-cell lung cancer (NSCLC) anti-PD-L1 treated cohort.[35] One gastric cohort, Kim *et al* (n=55), an advanced gastric cancer anti-PD-1 treated cohort.[36] Unless otherwise stated, all data were log2(TPM+1) transformed.

Pre-therapy bulk transcriptomic data

For the purpose of comparing pre-therapy expression across both "melanoma (a)" and "breast" CPIΔ cohorts, pre-therapy RNA sequencing data for these cohorts were obtained from the CPI1000+ study.[14] Here, data were processed from raw sequencing reads, and standardized processing/quality control procedures were executed as described previously.[14]

Derivation of published signatures

The following published transcriptomic signatures/marker genes were tested for associations with response to CPI therapy, including 15 pre-therapy-derived signatures/markers: *CD8A*,[37] *CD274*(PD-L1),[38] *CXCL9*,[39] both MHC I and MHC II,[31] CD8 T-cell effector referred to as T-Effector,[12] and the CD8 T-cell effector signature from the POPLAR trial referred to as POPLAR,[40] stroma-EMT,[41]12-chemokine referred to as Chemokine,[42] T-cell inflamed signature referred to as IFNγ,[7] TGFβ pan fibroblast referred to as Pan-F-TBRS,[11] IMPRES,[8] cell proliferation,[43] 15 β-catenin target genes referred to as BCTGs,[44] and cytolytic score referred to as CYT.[45] An addition 17 signatures/markers derived at the on-therapy timepoint were evaluated including, CD8 exhaustion,[46] *CD27*, *CD69*, *CD8B*, *GZMA*, *GZMK*, *HAVCR2*, *ICOS*, *ENTPD1*, *EOMES*, *LAG3*, *PDCD1*, *CTLA4*, *TBX21*, *TIGIT*, *ZAP70*,[16] and *CXCR6*.[47]

TCGA analysis

The Cancer Genome Atlas (TCGA) data across two cancer types (breast cancer and melanoma) were acquired using R software (V.4.0.2). Gene expression data, Workflow Type: HTSeq-Counts and clinical data were downloaded from Genomic Data Commons Data Portal using the R/Bioconductor package TCGAbiolinks V.2.16.4.[48] Clinical data were used to select for CPI-naïve tumor samples and for patients with OS of at least 1 day, yielding 712 breast cancer and 67 melanoma cases. Gene expression counts were normalized using DESeq2 V.1.28.1[49] variance stabilizing transformation function and data were filtered for genes of interest. For survival analyses, OS was estimated from clinical data using "days_to_last_followup" and "days_to_death" and an OS event was defined from "vital_status" (Dead/Alive).

Sampling bias

Sampling bias analyses evaluating genes identified to change in expression on-therapy were conducted using two CPI-naïve-multi-region cohorts, including the TRACERx lung cohort (lung, TRACERx, n=797 regions from 278 patients)[50] and the ADAPTeR cohort (renal, ADAPTeR, n=26 regions from 5 patients).[18] Spatial RNA variation in these treatment-naïve cohorts were calculated as RNA intratumor heterogeneity (ITH) scores as previously performed.[51] Briefly, per tumor, the SDs of expression values for a particular gene across tumor regions were calculated, generating a gene-specific, patient-specific measure of variance. This variance was then summarized across all tumors (median). Generated scores, per given gene, were used to compare the spatial variance to longitudinal variance. Longitudinal variance was captured between longitudinal tumor samples (SD) and summarized across all tumors (median), generated using selected CPIΔ longitudinal cohorts per analysis. Both RNA-ITH and longitudinal variance scores were then compared. This analysis was conducted separately using CPIΔ CPI-responding tumors and CPIΔ CPI-non-responding tumors where appropriate.

Statistic selection

The statistic for capturing RNA expression change between the pre-therapy and on-therapy timepoints:

"Hedge's g"

$$delta = \left(mB - mA \right) / SD * d$$

Where m*A* is the mean expression of a given gene at the pre-therapy timepoint across selected tumor samples and m*B* is the mean expression on-therapy. *SD*d* is the pooled and weighted *SD* across tumor samples, accounting for biased estimates of effect size in small sample sizes.[52]

Statistics and reproducibility

The statistical tests used are indicated in the accompanying figure legends and are two sided, where applicable, unless otherwise stated. All findings were considered significant at a p value threshold of 0.05. Significant p values are indicated within the figures. Plots and graphs were generated with R Studio software (V.4.0.2). Ilustrations were created using BioRender (https://biorender.com).

RESULTS

Assembling the CPI-Dynamics ("CPIΔ") cohort

To assemble the CPIΔ cohort, we leveraged molecular data from six longitudinal CPI studies (table 1; online supplemental figure 1; Methods section). The individual cohorts comprising the CPIΔ study are henceforth referred to as the "breast" cohort (patients with TNBC),

"melanoma (a)" cohort (patients with melanoma, CPI-naïve), "melanoma (b)" cohort (patients with melanoma, prior lines of CPI therapy), "pan-cancer" cohort (head and neck carcinoma, TNBC, high-grade serous ovarian cancer, melanoma, rare solid tumors), "urothelial (a)" cohort, and a "urothelial (b)" cohort.

To explore known biological factors associated with CPI sensitivity, established published transcriptomic signatures and marker genes of CPI response were evaluated. Although the majority of selected signatures encompassed genes associated with immune response and were derived across a variety of cancer types, their pan-cancer applicability was unknown. First, 15 signatures previously derived as informative from pre-therapy samples were evaluated, consisting of both single- and multi-gene markers/signatures with several overlapping genes between signatures. To explore the pan-cancer utility of these signatures, we employed pre-therapy RNA sequencing data from the CPIΔ cohort in addition to 10 pre-therapy cohorts from the CPI1000+ dataset[14] (Methods section). Across the "CPIΔ plus CPI1000+" cohort (16 cohorts, n=1046 patients), each signature was evaluated individually and the generated effect sizes, OR based on RECIST response or pCR (Methods section), and generated SEs were combined in a meta-analysis across cohorts (figure 1A; Methods section).

Sixty percent (9/15) of pre-therapy derived signatures were significantly associated with CPI response in the pre-therapy meta-analysis (figure 1A; online supplemental table 1). However, at the individual cohort-level, for the "breast" pre-therapy CPIΔ cohort, no significant associations were observed (figure 1A; online supplemental table 2). Furthermore, most signatures did not validate in the cancer types in which they had been derived, specifically noted across melanoma (1/7), NSCLC (0/3), urothelial (1/2), and renal (0/1) derived signatures (figure 1A; online supplemental table 2). These data indicate that the majority of established signatures were not informative of CPI response in this breast cancer cohort, and that overall, a minority of RNA signatures are associated with response in more than one cohort.

Next, 17 signatures previously derived as informative of CPI response from on-therapy samples were evaluated using the on-therapy sequencing data from the CPIΔ cohorts. Eighty-eight percent (15/17) of on-therapy derived transcriptomic signatures were significantly associated with response within the on-therapy meta-analysis (figure 1B; online supplemental table 3). In the "breast" CPIΔ cohort, contrary to pre-treatment where no signatures were significantly associated with response, 50% (8/16) of assessable on-therapy derived signatures were significantly associated with response (figure 1B; online supplemental table 4), including markers of immune activation (*ZAP70*, p=0.046) and exhausted T-cell phenotypes (*GZMA*, p=0.020) among other immune checkpoint genes (*LAG3*, p=0.01; *CTLA*-4, p=0.02; TIGIT, p=0.02). These signals of immune reinvigoration could be detected on-therapy in CPI-treated breast tumors, which was not discernible in pre-therapy signature and samples, suggesting that on-therapy gene expression may provide additional biological insight into the impact of CPI on the breast cancer immune microenvironment.

Dynamics of published RNA markers following CPI therapy

Since in the "breast" CPIΔ cohort, the on-therapy derived RNA signatures demonstrated more informative signals on-therapy, we next used expression data for all evaluated gene signatures (both pre- and on-therapy derived) to explore the impact of CPI on transcriptomic expression changes between pre- and on-therapy timepoints at both the cohort- and patient-level, within the "breast" CPIΔ cohort (n=25).

Using this approach, the *CD8A* marker demonstrated a normal distribution of expression pre-therapy, which became flatter on-therapy, suggesting that tumors in this cohort exhibited either no change, an increase, or a decrease in *CD8A* expression after CPI (figure 2A, top). At the patient-level, a wide diversity in RNA trajectories were revealed following CPI therapy for the *CD8A* gene, whereby some tumors with the lowest pre-therapy *CD8A* expression shifted to the highest on-therapy expression levels, and vice versa (figure 2A, bottom). When assessing the dynamic changes in *CD8A* expression on-therapy compared with pre-therapy, we observed a striking association of dynamically increasing *CD8A* with improved favorable survival which would not be possible to determine using pre-treatment *CD8A* expression levels only (figure 2A, bottom). Lastly, correlating on-therapy expression shifts with clinical outcomes demonstrated a significant enrichment (p=0.0048) for favorable survival outcomes (OS>median, Methods section) within tumors with on-therapy increases in *CD8A* expression (77% (10/13)), while 75% (9/12) of tumors with decreased *CD8A* expression had poorer survival outcomes within the "breast" CPIΔ cohort (figure 2A, bottom). Across the remaining transcriptomic signatures, similar dynamics were observations (figure 2B–E). Furthermore, 76% (19/25) of other signatures were significantly enriched for favorable survival outcomes within breast tumors with dynamic on-therapy expression increases (figure 2E).

For the other CPIΔ cohorts, significant enrichments for favorable survival outcomes within tumors with expression increases were observed within the "melanoma (a)" for 13% of signatures (4/32) and the "urothelial (b)" cohort for (6%) of signatures (2/32) (online supplemental figure 2A,B). No other significant differences were observed (online supplemental figure 2C–E). Taken together these results highlight the importance of delineating changes which occur on-CPI as they may hold key biological information about the impact of CPI on the tumor microenvironment. Furthermore, these data emphasize the need to move beyond established gene signatures and examine RNA dynamics across all genes, which may aid in deciphering patterns of response or resistance to CPI in breast cancer.

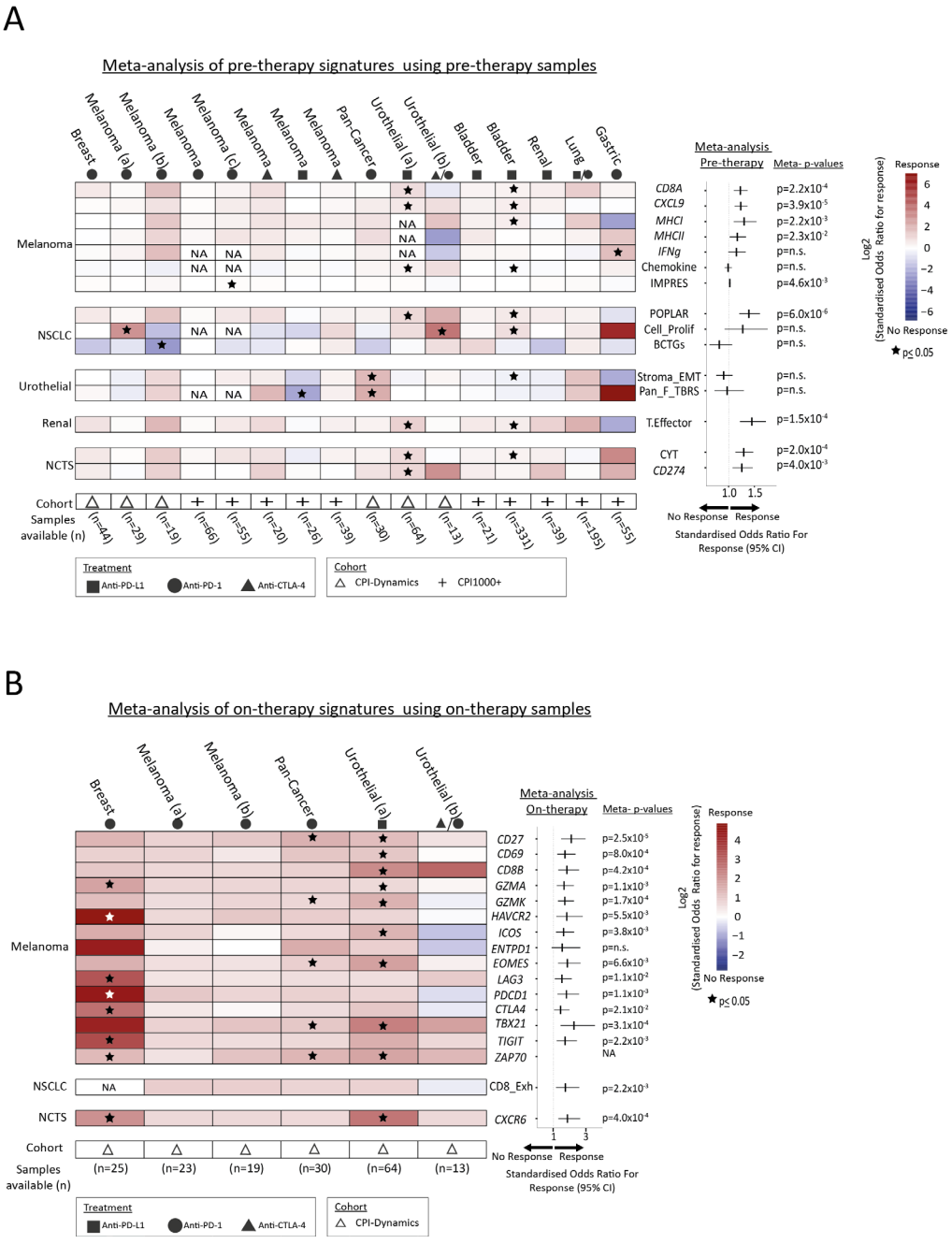

Figure 1 Meta-analysis of RNA signatures associated with CPI response. (A) Pre-therapy meta-analysis. Pre-therapy-derived signatures are shown as rows and individual cohorts within the "CPIΔ plus CPI1000+" cohorts as columns; studies in which each cohort was included are indicated (Δ=CPIΔ; +=CPI1000+; bottom of the heatmap). (B) On-therapy meta-analysis. Here on-therapy-derived signatures are shown as rows and individual cohorts within the CPIΔ cohort as columns. The heatmaps indicates the effect size of each signature in each cohort, measured using the log2 odds ratio (OR) for response versus non-response (RECIST criteria), derived from logistic regression. Red represents an association with response, blue an association with non-response, and significance indicated with an asterisk. Both cohort size (bottom of the heatmap) and drug received (top of the heatmap) are indicated. Signatures are split into the cancer type in which they were derived (left of heatmaps; melanoma, non-small-cell lung cancer (NSCLC), urothelial; renal; NCTS (non-cancer-type-specific)). The forest plots on the right display the overall effect size and significance (p values) of each signature in the meta-analysis across all studies, based on the effect sizes and SEs from each individual cohort. A random-effects model was used for the meta-analysis to account for different cancer types .

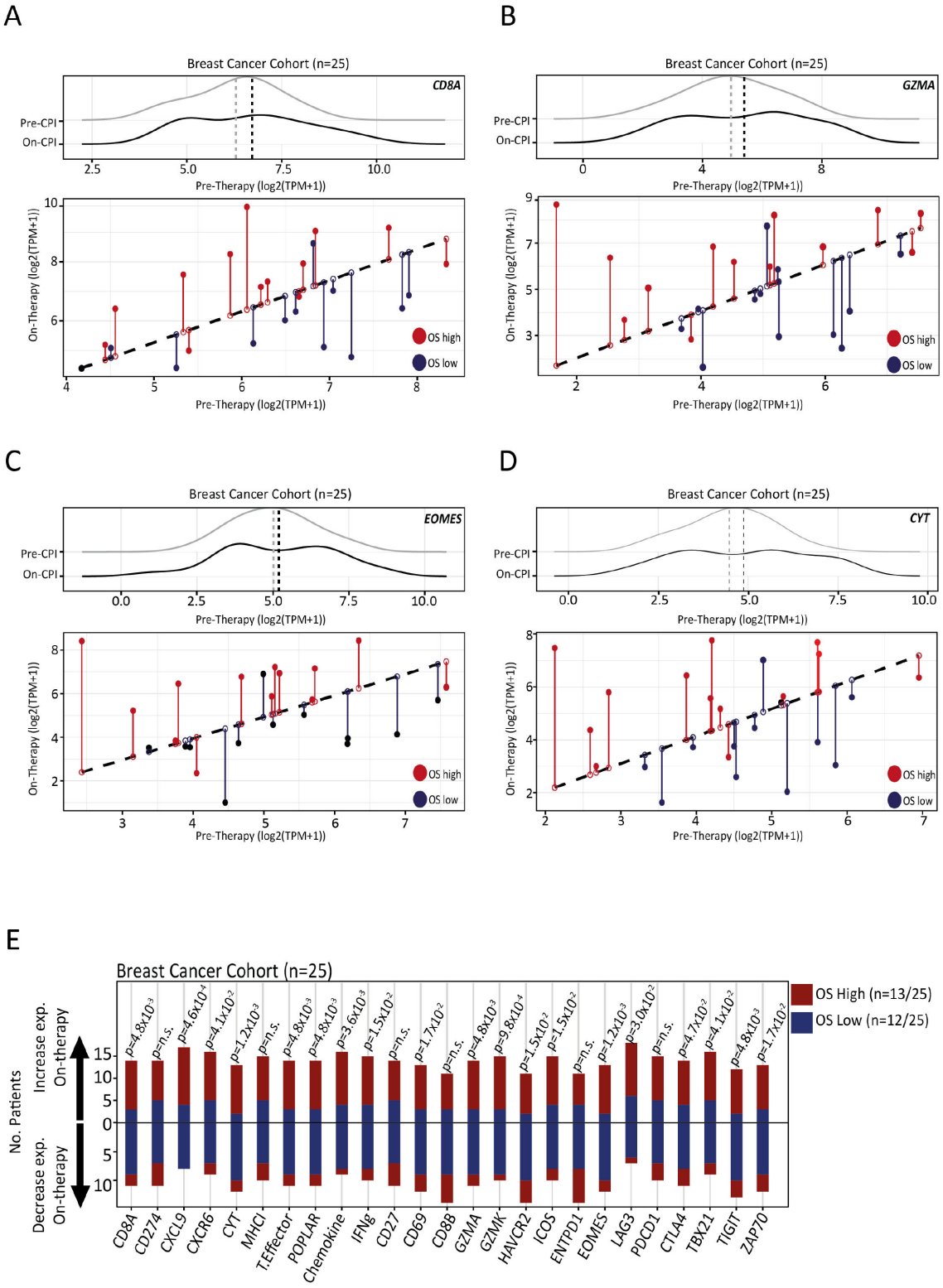

Figure 2 Dynamics of RNA signatures pre-therapy and on-therapy. (A–D) Longitudinal expression of (a) *CD8A*, (b) *GZMA*, (c) *EOMES*, (d) CYT marker genes within the "breast" CPIΔ cohort. Top density plots display pre-therapy (gray curve) and on-therapy (black curve) expression across the breast cancer cohort with longitudinal data available (n=25). Bottom residual plot demonstrates pre-therapy expression (log2(TPM+1)) plotted along the diagonal line (x-axis) and on-therapy (y-axis) expression which is joined to paired patient-level pre-therapy expression with a vertical line. Red indicates cohort stratification into patient-tumors with high overall survival (OS; >median (OS)) and dark blue indicates patient-tumors with low OS (OS<median (OS)). (E) Summary plot of all available signatures (n=25) within the breast cancer cohort. Signatures are depicted on the x-axis and number of patient tumors which either increase (top arrow) or decrease (bottom arrow) in expression for each signature on the y-axis. Bars in red (OS high) and dark blue (OS low) depict patient-tumor stratification based on OS. Significance was tested using a Fisher's exact test and displayed. CPI, checkpoint inhibitor.

RNA dynamics induced by CPI in breast cancer

Previous work has focused on delineating response signals by comparing responding and non-responding breast tumors using static pre-therapy or on-therapy timepoints separately. In light of the dynamic expression changes observed on-therapy, we next explored transcriptional changes associated with CPI treatment across the 778 immune-related genes from the immune NanoString panel, to achieve further insight into the biological mechanisms underpinning response in breast cancer. Here, we sought to quantify RNA dynamics from bulk pre-therapy and on-therapy transcriptomic data by applying the hedges' g statistic (Methods section) and identifying genes that either increase ("positive delta"), decrease ("negative delta") or do not change ("neutral delta") in expression on-therapy within individual CPI response groups (CPI-responding tumors and CPI-non-responding tumors; Methods).

To delineate expression modules with shared or diverging longitudinal patterns following CPI treatment, genes displaying dynamic expression shifts on-therapy were compared between the CPI response groups (figure 3A, diagram left; Methods section), yielding four classifications of genes (figure 3A, diagram right; online supplemental table 5). Two groups of genes were characterized by either positive or negative dynamic shifts in expression in CPI-responding tumors: "Response Pos" with n=135 genes and "Response Neg" with n=7 genes from the "breast" CPIΔ cohort (figure 3A, diagram right; online supplemental table 5). In addition to two groups of genes with either positive or negative dynamic shifts in expression in CPI-non-responding tumors only; "Resistance Pos" with n=7 genes and "Resistance Neg" with n=6 genes from the "breast" CPIΔ cohort (figure 3A, diagram right; online supplemental table 5). Classification of genes was conducted across all CPIΔ cohorts, subsetted to 778 immune genes within the immune NanoString panel. Within the breast cancer cohort 79% of genes (107/135) identified within the "Response Pos" group (figure 3B), 86% of genes (6/7) within the "Response Neg" and "Resistance Pos" (figure 3C; online supplemental figure 3A and tables 6 and 7), and 83% of genes (5/6) within the "Resistance Neg" group demonstrated dynamic expression shifts on-therapy in the "breast" CPIΔ cohort only (online supplemental figure 3B and tables 6 and 7).

Next, to address the limitation of single-region biopsies, which may lead to some identified genes within the "breast" CPIΔ cohort being confounded by tumor sampling bias, longitudinal RNA variation following CPI therapy was compared with spatial RNA variation in treatment-naïve tumors (multi-region samples; table 2) for each gene across CPI-responding and CPI-non-responding tumors (RECIST radiological response) within the CPIΔ "breast" cohort (Methods section). Ninety-eight percent (105/107) of the "Response Pos" genes, 83% (5/6) of the "Response Neg" genes, 50% (3/6) of the "Resistance Pos" genes, and 20% (1/5) of the "Resistance Neg" genes were not confounded by sampling bias, whereby spatial RNA variation underlying tumor sampling bias was surpassed by the changes in RNA expression during CPI therapy within the "breast" CPIΔ cohort (figure 3D).

CPI dynamics and clinical outcomes in breast cancer

After filtering out genes which were confounded by sampling bias (figure 3D), we explored whether the expression changes on-CPI of the remaining 114 genes were associated with clinical outcomes. Patient-level deltas (on-therapy – pre-therapy) expression change values were calculated for each individual gene, and both RECIST radiological response and OS clinical endpoints were evaluated within the "breast" CPIΔ cohort. Data were also leveraged from CPI-naïve-tumors from the TCGA breast cancer datasets, and OS was evaluated to distinguish CPI response signals from the prognostic signals.

Using these last filtering steps, 90/114 genes were significantly associated with favorable clinical outcomes (clinical outcome being OS) in patients with breast cancer treated with CPI (figure 3E, left; online supplemental table 8). Genes comprising this group included those expressed on macrophages (*C1QA* and *C1QB*), T-cells (*CD3G*), myeloid cell expressed genes (*FCGR1A*), chemokine receptors and ligands (*CCR5*, *CXCL10*, *CXCL11*, *XCL2*), IFNγ -induced genes associated with immune infiltration (*GBP1* and *GBP4*), crucial regulators of T-cell and NK-cell proliferation and differentiation (*IL21R*), genes involved in antigen processing (*PSMB9* and *B2M*), and genes expressed by NK cells and other cytotoxic immune cells such as *KLRK1* (*NKG2D*). Furthermore, 13/90 identified genes were also known IO targets (*CD38*, *CD7*, *CD80*, *CD27*, *SLAMF7*, *TIGIT*, *CD274*, *ICOS*, *TNFRSF9*, *JAK2*, *TLR1*, *TLR1*, and *TLR8*).

Crucially, 8/114 genes were identified as significantly associated with CPI response (RECIST radiological response; figure 3E, right; online supplemental table 8). These eight genes included, *FCGR3A*, the low-affinity Fc gamma receptor associated with cytotoxic lymphocytes and critical for antibody-dependent cytotoxicity, *REN*, an aspartic protease that is part of the renin–angiotensin–aldosterone system, *NRAS*, an oncogene associated with poor clinical outcomes in breast cancer, *PIK3R2*, a lipid kinase associated with tumor progression, *CCL3* a chemokine ligand which mediates macrophage chemotaxis and enhancing differentiation of T cells into effector T cells, *COL4A5*, a collagen type 4 alpha 5 chain associated with response to chemotherapy in breast cancer, *AQP9*, an aquaporin family member, and *H2AX*, a variant histone (figure 3E, right; online supplemental table 8). The remaining 16/114 genes were either not associated with clinical outcomes in patients with breast cancer treated with CPI or associated with clinical outcomes in CPI-naïve patients with breast cancer. Together these results suggest that genes identified to be associated with clinical outcomes (RECIST radiological response and OS) may play roles in response to CPI in breast cancer.

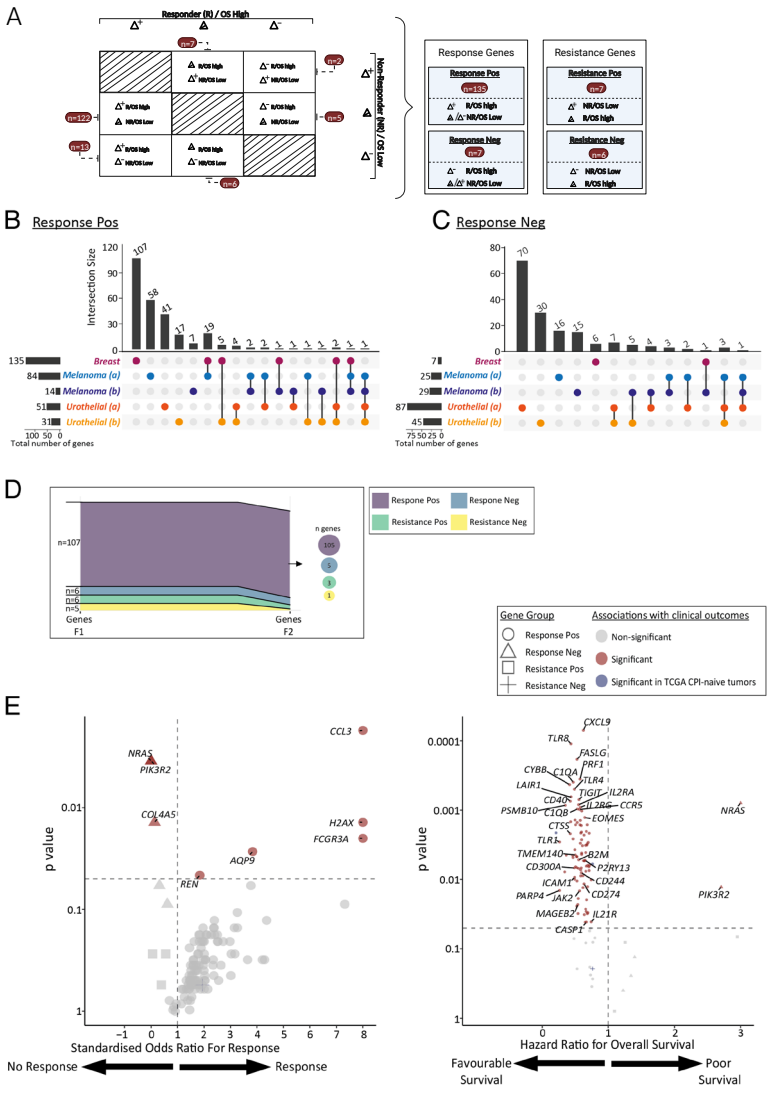

Figure 3 CPI induced gene expression dynamics in breast cancer. (A) Left diagram depicting RNA dynamics (Δ+ "increase," Δ– "decrease," Δ neutral expression change on-therapy) observed across tumors stratified into CPI-responding-tumors (RECIST Responder(R)/OS high (>median OS)) and CPI-non-responding-tumors (RECIST non-responder (NR)/OS low (<median OS)) within the "breast" CPIΔ cohort, with number of genes highlighted in red. Diagram on the right demonstrates the classification of genes into four categories, "Response Pos" (Δ+ in CPI-responding-tumors), "Response Neg" (Δ– in CPI-responding-tumors), "Resistance Pos" (Δ+ in CPI-non-responding-tumors), and "Resistance Neg" (Δ– in CPI-non-responding-tumors) genes, with total genes displayed. The illustrations were created using BioRender (https://biorender.com). (B, C) Upset plots of genes comprising the (B) "Response Pos" and (C) "Response Neg" categories across six of the CPIΔ cohorts, subsetted for 778 genes within the "breast" CPIΔ immune NanoString panel. For each upset plot, the left bar plots indicate the number of genes identified in each gene category per CPIΔ cohort, including "breast" (pink), "melanoma (a)" (light blue), "melanoma (b)" (dark blue), "urothelial (a)" (orange), "urothelial (b)" (yellow). The top bar plot indicates the total number of genes which are unique to each cohort and the number of shared genes between cohorts, with interactions highlighted in the bottom dot plot. (D) Proportion plots depicting gene identified to "increase" or "decrease" in expression on-therapy across gene categories ("Response Pos," purple; "Response Neg," blue; "Resistance Pos," green; "Resistance Neg," yellow) in the "breast" CPIΔ cohort only. Y axis indicates the number of genes identified per gene category at F1 (filter one), followed by the number of genes identified per gene category to not be confounded by sampling bias F2 (filter 2; Methods section) within the "breast" CPIΔ cohort. Analysis was conducted on 778 genes comprising the immune NanoString panel. (E) Scatter plot left, depicting the overall effect size (OR; x-axis) and significance (p value; y-axis) of identified genes (each point) identified within one of the four gene categories ("Response Pos," circle; "Response Neg," triangle; "Resistance Pos," square; "Resistance Neg," cross) and not confounded by sampling bias (results from figure 3D). Associations with clinical outcomes were assessed using RECIST radiological response across the "breast" CPIΔ cohort. Gray indicates genes with no association with CPI response, in red a significant association with CPI response, and in blue associated with clinical outcomes in CPI-naïve tumors within the TCGA dataset. Scatter plot right, depicting the hazard ratio (HR; x-axis) and significance (p value; y-axis) of identified genes. Associations with clinical outcomes were assessed using OS across the "breast" CPIΔ cohort. CPI, checkpoint inhibitor; OS, overall survival; RECIST, Response Evaluation Criteria in Solid Tumors.

Table 2 Treatment-naïve multi-region datasets

Cohort	Cancer type	Patients (n)	Regions (n)	Data type
TRACERx Lung	NSCLC	278	797	RNA-seq
ADAPTeR	Renal	7	26	RNA-seq

Gene-level explorations of differing mechanisms of CPI dynamics between breast cancer versus melanoma

To evaluate differences in biological mechanisms of CPI response between breast cancer and melanoma, we compared pre-therapy expression of the crucial genes identified to be associated with CPI-response (RECIST/OS) in breast cancer (n=98 genes) across both breast and CPI-naïve melanoma tumors ("melanoma (a)" CPIΔ cohort). To objectively compare gene expression data between these two cohorts and limit any variability which may arise due to varied data processing, here pre-therapy RNA sequencing data from these two cohorts were leveraged from the CPI1000+ study, whereby data were processed through the same pipeline (Methods section). In melanoma, 16 genes identified to increase in expression in CPI-responding breast tumors after treatment were expressed significantly higher within the melanoma tumors compared with breast tumors pre-therapy (figure 4A). Furthermore, 4/16 genes are known IO targets (*TLR8*, *TLR4*, *TLR1*, *JAK*). Likewise, two genes, *COL4A5* and *PRK3R2*, which were identified to decrease in expression in CPI-responding breast tumors after treatment, presented significantly lower expression in melanoma compared with breast tumors pre-therapy (figure 4B). These results suggest that patients with melanoma potentially respond better to CPI due to crucial genes already either being highly or lowly expressed pre-therapy and suggest that RNA dynamics following CPI treatment may differ between breast and melanoma tumors, which may partially inform the difference in response rates to CPI.

Next, exploring differences in RNA dynamics between pre-therapy and on-therapy timepoints between breast tumors and melanoma, the same approach used in the "breast" CPIΔ cohort was applied to the melanoma CPI-naïve ("melanoma (a)") CPIΔ cohort, evaluating the 778 genes from the immune NanoString panel. Of the genes identified to only change in expression within the melanoma cohort (genes from the "Response Pos," "Response Neg," "Resistance Pos," and "Resistance Neg" categories) a total of 64/95 genes were not confounded by sampling bias (figure 4C). Twenty-two percent of these genes (14/64) were associated with either response or non-response to CPI therapy, including seven genes which decreased in expression on-therapy in CPI-responding tumors and were significantly associated with non-response (figure 4D). These seven genes included *PMS2*, an essential gene in DNA mismatch repair, and *SOX10*, a melanocyte-inducing transcription factor, *BAMBI*, a TGFβ pseudo-receptor, two genes involved in cancer metabolism, *SLC16A*, a solute carrier family member that plays a role in the transport of lactate and pyruvate, and *LDHA*, a lactate dehydrogenase which converts pyruvate to lactate, and *SNCA*, which codes for alpha-synuclein, that has been associated with enhancing cell survival in melanoma (figure 4D).

Furthermore, three genes increased in expression in CPI-non-responding melanoma tumors and were associated with non-response, including *RAD51*, involved in homologous recombination and DNA repair, and has been linked to immune dysregulation, *MAGEA1*, the melanoma-associated antigen 1, and *BLM*, a helicase family member which plays a role in cellular metabolic processes (figure 4D). Lastly, three genes increased in expression on-CPI in CPI-responding melanoma tumors and were significantly associated with response to CPI in melanoma, including *RORC*, coding for a DNA-binding transcription factor (figure 4D). These genes were not observed to significantly change in expression on-therapy in breast tumors. Taken together, these results demonstrate varied response patterns between CPI-treated melanoma and breast tumors, which warrant further investigation as potential targets for combination therapy for patients with breast cancer.

DISCUSSION

CPIs have been shown to be effective in treating several types of cancer, including melanoma. Nonetheless, response rates in many other cancer types, most notably breast cancer which remains one of the most prevalent cancer worldwide, are far inferior. This differential efficacy could reflect different mechanisms of response to treatment within breast cancer and the complexities of the immune system's response to the disease. Here, we explored the transcriptomic response of cancers to CPI treatment through the analysis of our CPIΔ cohort. Our analysis of both pre- and on-therapy-derived published signatures demonstrated that most cancer-type-derived signatures did not inform clinical outcomes in the cancer type they were derived from. This lack of reliability highlights the potential differences in signals of response across tumor types. In the breast cancer cohort, unlike pre-therapy signatures, 50% of on-therapy signatures were associated with response. On-therapy signals within the breast cancer cohort were consistent with signals of immune reinvigoration of T-cell exhausted phenotypes on-therapy, as suggested by genes such as *CTLA-4*, *HAVCR2* (*TIM-3*), and *GZMA*, which have been shown to increase in expression following anti-PD-1 in melanoma.[16]

By exploring transcriptomic changes on CPI in the "breast" CPIΔ cohorts, we identified key breast cancer-specific correlates of CPI response. We identified eight genes which change in expression on-therapy and may define CPI response within breast cancer, including *FCGR3A*, an Fc gamma receptor, for which high expression on NK cells has been functionally shown to cause higher

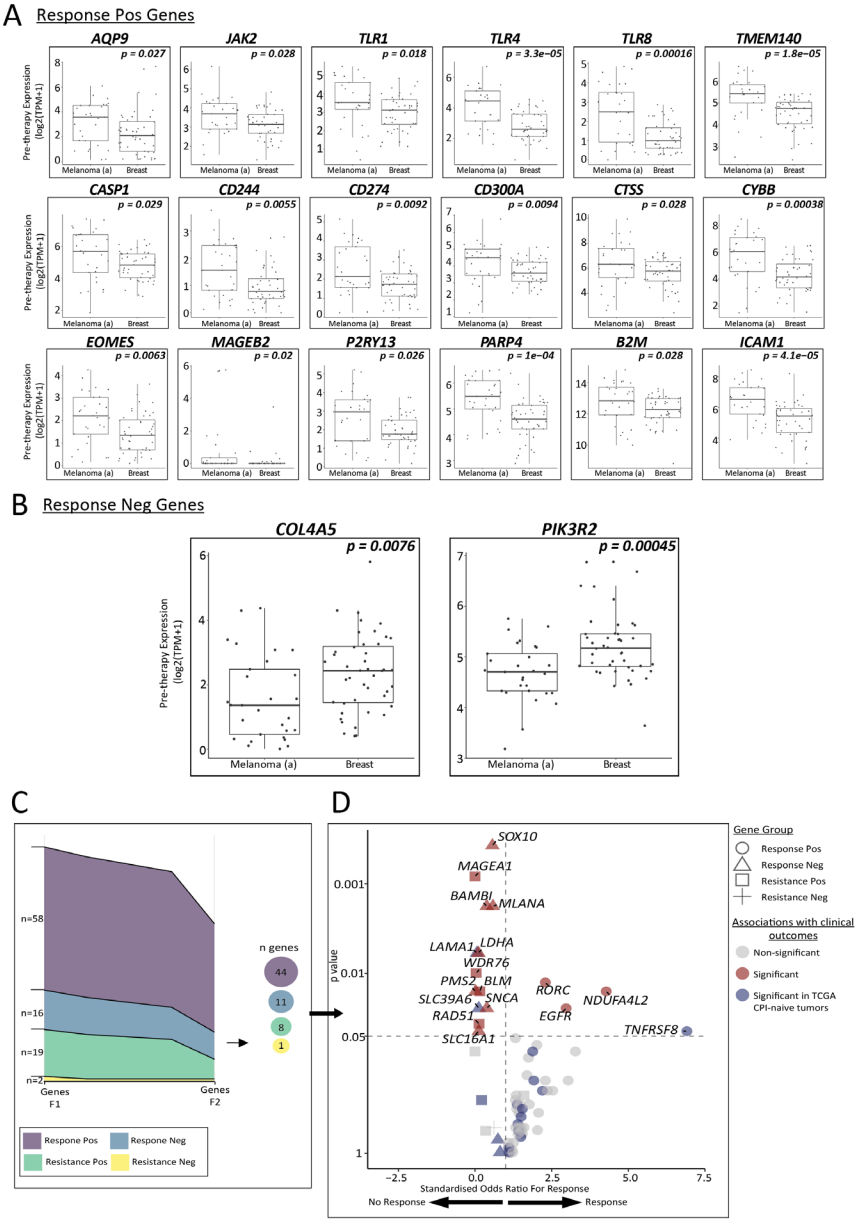

Figure 4 Differential mechanisms of CPI dynamics breast cancer versus melanoma. (A) Box plots comparing pre-therapy expression (y-axis) of genes identified to increase in expression on-therapy (Response Pos genes) and be associated with clinically favorable response to CPI in breast cancer (figure 2E, right), within the "melanoma (a)" and "breast" CPIΔ cohort (x-axis). This analysis used RNA sequencing data processed from FASTq to TPM matrix through a standardized pipeline allowing for comparison across both cohorts. Significance was tested using a Wilcoxon test and displayed. (B) Box plots comparing pre-therapy expression (y-axis) of genes identified to decrease in expression on-therapy (Response Neg genes) and observed to be associated with no response to CPI breast cancer (figure 2D, right), within the "melanoma (a)" and "breast" CPIΔ cohort (x-axis). Data used here were RNA sequencing across both cohorts processed from FASTq to TPM matrix through a standardized pipeline allowing for comparison. Significance was tested using a Wilcoxon test and displayed. (C) Proportion plots depicting gene identified to "increase" or "decrease" in expression across gene categories ("Response Pos," purple; "Response Neg," blue; "Resistance Pos," green; "Resistance Neg," yellow) on-therapy across the "melanoma (a)" CPIΔ cohort only. Y axis indicates the number of genes identified per gene category at F1 (filter one), followed by the number of genes identified per gene category to not be confounded by sampling bias F2 (filter 2; Methods section) within the "melanoma (a)" CPIΔ cohort. This analysis was conducted on 778 genes comprising the immune NanoString panel. (D) Scatter plot depicting the overall effect size (OR; x-axis) and significance (p value; y-axis) of identified genes (each point) identified within one of the four gene categories ("Response Pos," circle; "Response Neg," triangle; "Resistance Pos," square; "Resistance Neg," cross) and not confounded by sampling bias (results from figure 3D). Associations with clinical outcomes were assessed using RECIST radiological response across the "Melanoma (a)" cohort. Gray symbols indicates genes with no association with CPI response, in red a significant associations with CPI response, and in blue associated with clinical outcomes in CPI-naïve tumors within the TCGA dataset. CPI, checkpoint inhibitor; RECIST, Response Evaluation Criteria in Solid Tumors.

anti-PD-L1 antibody-dependent cellular cytotoxicity lysis of tumor cells.[53] Also, *CCL3*, a chemokine ligand, overexpression of which in colorectal cancer mouse models led to the rapid regression of tumors, increased proliferation, and functionality of tumor-infiltrating T cells and accelerated tumor-regression on CPI (anti-PD-1).[54] These genes may play roles in response to CPI in breast cancer and are putative targets for combination therapy, which in turn could aid in the delivery of immuno-oncology and enhancing CPI efficacy within breast cancer.

In parallel, we also identified 90 genes in breast cancer associated with favorable clinical outcomes in patients with breast cancer treated with CPI including *CCL5*, XCL1, *XCL2*, *KLRK1*, and *GZMB*, associated with the presence of functional cytotoxic NK cells.[55–58] Of these genes, *KLRK1* (*NKG2D*) has been reported not only to enhance the cytotoxicity of NK cells, aiding in the elimination of tumor cells, but also facilitate the activation of breast-resident vδ1 cells[57 59–62] and has been associated with good prognosis in breast cancers.[58] Together these results suggest the presence of functional cytotoxic NK cell phenotypes and other cytotoxic immune cells within the breast cancer TME may play a critical role in response to CPI in breast cancer.

We identified 18 genes which significantly increase in expression on-CPI in breast cancer responders but were already highly expressed in melanoma pre-therapy. These 18 genes included *B2M*, a component in MHC-I antigen processing and presentation,[63] and 3 Toll-like receptor genes (*TLR1*, *TLR4*, and *TLR8*), which have been suggested as potential IO targets.[64] Importantly, multiple TLR agonists have been investigated in combination with CPI to enhance efficacy across various cancer types.[65–68] Furthermore, of the genes identified to decrease in expression on-CPI in breast cancer, *PIK3R2* was already lowly expressed in melanoma tumors pre-therapy and has been associated with repressed cell proliferation, invasion, epithelial–mesenchymal transition, and cell apoptosis in melanoma cells,[69] which could hold potential applicability in breast cancer. These genes warrant further investigation and may be potential targets for combination therapy in IO refectory cancers like TNBC, particularly genes such as *TLR8*, *TLR4*, and *TLR1*, which are known IO targets.

We also identified 14 genes associated with either CPI response or non-response within the melanoma CPIΔ cohort, which did demonstrate significant expression changes on-CPI within the breast cancer cohort, including *SOX10*, *SLC16A*, *SNCA*, *BAMBI*, and *RAD51*. Of the genes identified to decrease in expression in melanoma responding tumors, *SOX10* has been shown to hinder immunogenicity in melanoma cell lines through the *IRF4–IRF1* axis and regulate PD-L1 expression.[70] Furthermore, suppression of *SOX10* has demonstrated increased efficacy to combination therapy including anti-PD-1 in melanoma.[70] *SLC16A*, has been associated with lower OS across cancer types,[71 72] and in breast cancer *SLC16A* has been associated with more aggressive phenotypes.[73] Knockout of *SNCA* in melanoma cells has been associated with higher rates of apoptosis in xenografts,[74] suggesting that lower expression observed in melanoma tumors treated with CPI may aid in cancer cell elimination, whereas knockout of *BAMBI*, has been associated with growth inhibition in TNBC cell lines.[75] Of the genes identified to increase in expression in CPI-non-responding tumors, *RAD51*, has been associated with poor survival in breast cancer and other cancer types, as well as with increased genomic instability and immune dysregulation.[76] These results highlight key genes associated with response to CPI in melanoma, which warrant further study to investigate their biological effect on immune response in the context of CPI, in addition to providing additional targets for combination therapy, which may prove to also be beneficial in the treatment of breast cancer.

Our study is not without limitations. The biggest challenge faced in longitudinal CPI response analyses is the difficulty in obtaining paired data from CPI-treated patients, resulting in small cohorts for such analyses, in addition to varied timing of biopsies on-treatment across cohorts, which may influence the biological composition of the TME following CPI therapy. Despite this, our study is the largest meta-analysis of its kind and provides valuable insights into the biology of CPI-mediated immune response. A further complication in leveraging data from multiple studies is the lack of standardized reporting of covariates such as patient demographics and detailed treatment histories. However, our study aimed to mitigate this limitation where possible by selecting cohorts with metastatic and advanced disease only, in addition to restricting more detailed comparisons exclusively between cohorts of patients reported as CPI-naïve prior to entering the trials. We explored data from various cohorts with RNA sequencing and NanoString data which were not unified in a single pipeline, which could potentially affect the comparability of the data. Nevertheless, the aforementioned limitation was addressed where possible by leveraging RNA sequencing data processed through a unified pipeline when conducting head-to-head comparisons of gene expression of identified genes. Furthermore, our meta-analyses still provide important insights into the biology of CPI-mediated immune response and contributes to an advancement of the field. However, the use of transcriptomic data generated from different platforms may lead to limitations in conclusions that could be drawn, as analyses were limited to 778 genes from the NanoString panel for comparison between cohorts as opposed to genome-wide, which may restrict our analysis. Although much of our data were obtained from a single sampled biopsy, which could introduce sampling bias, this limitation was mitigated by validating our findings in orthogonal multi-regional datasets to ensure that the intra-sample longitudinal variability was larger than the spatial treatment-naïve variability. However, we acknowledge the limitations introduced by the lack of concordant cancer type and stage-matched multi-region datasets

used. Nonetheless, our study creates a wealth of opportunities for further research to validate and expand on these findings, aiming to improve personalized treatment options for patients with cancer .

Author affiliations
[1]Cancer Research UK Lung Cancer Centre of Excellence, University College London Cancer Institute, London, UK
[2]Cancer Evolution and Genome Instability Laboratory, The Francis Crick Institute, London, UK
[3]Bill Lyons Informatics Centre, University College London Cancer Institute, London, UK
[4]Department of Molecular Oncology and Immunology, The Netherlands Cancer Institute, Amsterdam, The Netherlands
[5]Oncode Institute, Utrecht, The Netherlands
[6]Tumour Immunogenomics and Immunosurveillance Laboratory, University College London Cancer Institute, London, UK
[7]University College London Hospitals NHS Foundation Trust, London, UK
[8]Department of Molecular Medicine, Aarhus Universitet, Aarhus, Denmark
[9]Department of Clinical Medicine, Aarhus Universitet, Aarhus, Denmark
[10]Division of Tumor Biology & Immunology, Netherlands Cancer Institute, Amsterdam, The Netherlands
[11]Computational Cancer Genomics Research Group, University College London Cancer Institute, London, UK
[12]Department of Medical Oncology, Guy's and St. Thomas' NHS Foundation Trust, London, UK
[13]Peter Gorer Department of Immunobiology and Centre for Inflammation Biology and Cancer Immunology, King's College London, London, UK

Twitter Mihaela Angelova @__mihaela__

Acknowledgements We thank Lewis Au and Samra Turajilic for permission to use their published data for the sampling bias analysis. Most importantly, we thank the patients and their families.

Contributors IU and DB contributed equally to this paper. IU and DB designed, carried out, and/or interpreted bioinformatics analyses. IU, DB, YW, and NK wrote the manuscript. KD, TBKW, OP, CP, MA, KT, CH, NB, MK, and SZ provided experimental data and/or interpreted bioinformatics analyses. NK, KL, and CS supervised the project. NK, KL, and CS are responsible for the overall content as guarantors.

Funding This work was supported by Breast Cancer Research Foundation (BCRF-22-157). CS is a Royal Society Napier Research Professor (RSRP\R\210001). This work was supported by the Francis Crick Institute that receives its core funding from Cancer Research UK (CC2041), the UK Medical Research Council (CC2041), and the Wellcome Trust (CC2041). For the purpose of Open Access, the author has applied a CC BY public copyright license to any Author Accepted Manuscript version arising from this submission. CS is funded by Cancer Research UK (TRACERx (C11496/A17786), PEACE (C416/A21999), and CRUK Cancer Immunotherapy Catalyst Network); Cancer Research UK Lung Cancer Centre of Excellence (C11496/A30025); the Rosetrees Trust, Butterfield and Stoneygate Trusts; NovoNordisk Foundation (ID16584); Royal Society Professorship Enhancement Award (RP/EA/180007); National Institute for Health Research (NIHR) University College London Hospitals Biomedical Research Centre; the Cancer Research UK-University College London Centre; Experimental Cancer Medicine Centre; the Breast Cancer Research Foundation (US); and The Mark Foundation for Cancer Research Aspire Award (Grant 21-029-ASP). This work was supported by a Stand Up To Cancer-LUNGevity-American Lung Association Lung Cancer Interception Dream Team Translational Research Grant (Grant Number: SU2C-AACR-DT23-17 to S.M. Dubinett and A.E. Spira). Stand Up To Cancer is a division of the Entertainment Industry Foundation. Research grants are administered by the American Association for Cancer Research, the Scientific Partner of SU2C. CS is in receipt of an ERC Advanced Grant (PROTEUS) from the European Research Council under the European Union's Horizon 2020 research and innovation programme (grant agreement no. 835297). DB was supported by funding from a Cancer Research UK (CRUK) Early Detection and Diagnosis Project award, the Idea to Innovation (i2i) Crick translation scheme supported by the Medical Research Council, the National Institute for Health Research Biomedical Research Centre, and the Breast Cancer Research Foundation (BCRF-22-157). KD was supported by funding from the European Union's Horizon 2020 research and innovation programme under the Marie Skłodowska-Curie grant agreement No. 101024529. YW is supported by a Wellcome Trust Clinical Research Career Development Fellowship (no. 220589/Z/20/Z). NK is supported by CRUK and the Breast Cancer Research Foundation (BCRF-22-157) and receives research support from AstraZeneca.

Competing interests DB reports personal fees from NanoString and AstraZeneca, and has a patent PCT/GB2020/050221 issued on methods for cancer prognostication. KD provides consultancy services to Achilles Therapeutics. YW consults for PersonGen Biotherapeutics and E15 VC. MK received research funding paid to the institute from BMS, Roche, AstraZeneca, has advisory roles compensated to the institute for: Daiichi Sankyo, BMS, MSD, Novartis, Roche outside the submitted work, and speakers' fee paid to the institute from: Roche, BMS and Gilead. CS acknowledges grant support from AstraZeneca, Boehringer-Ingelheim, Bristol Myers Squibb, Pfizer, Roche-Ventana, Invitae (previously Archer Dx Inc—collaboration in minimal residual disease sequencing technologies) and Ono Pharmaceutical. CS is an AstraZeneca Advisory Board member and chief investigator for the AZ MeRmaiD 1 and 2 clinical trials, and is also co-chief investigator of the NHS Galleri trial, funded by GRAIL, and a paid member of GRAIL's Scientific Advisory Board. He receives consultant fees from Achilles Therapeutics (where he is also a Scientific Advisory Board member), Bicycle Therapeutics (where he is also a Scientific Advisory Board member), Genentech, Medicxi, Roche Innovation Centre—Shanghai, Metabomed (until July 2022) and the Sarah Cannon Research Institute, had stock options in Apogen Biotechnologies and GRAIL until June 2021, currently has stock options in Epic Bioscience and Bicycle Therapeutics, and has stock options in and is co-founder of Achilles Therapeutics. CS is an inventor on a European patent application relating to assay technology to detect tumor recurrence (PCT/GB2017/053289); the patent has been licensed to commercial entities and under his terms of employment CS is due a revenue share of any revenue generated from such license(s). CS holds patents relating to targeting neoantigens (PCT/EP2016/059401), identifying clinical response to immune checkpoint blockade (PCT/EP2016/071471), determining HLA loss of heterozygosity (PCT/GB2018/052004), predicting survival rates of patients with cancer (PCT/GB2020/050221), identifying patients whose cancer responds to treatment (PCT/GB2018/051912), detecting tumor mutations (PCT/US2017/28013), methods for lung cancer detection (US20190106751A1), and identifying insertion/deletion mutation targets (European and US, PCT/GB2018/051892), and is co-inventor to a patent application to determine methods and systems for tumor monitoring (PCT/EP2022/077987). CS is a named inventor on a provisional patent protection related to a ctDNA detection algorithm.

Patient consent for publication Not applicable.

Ethics approval Not applicable.

Provenance and peer review Not commissioned; externally peer reviewed.

Data availability statement Data are available in a public, open access repository. Data are available upon reasonable request. The tumor region RNA sequencing data (in each case from the TRACERx study) used during this study has been deposited at the European Genome–phenome Archive (EGA), which is hosted by The European Bioinformatics Institute and the Centre for Genomic Regulation under the accession code under the accession code EGAS00001006517 (RNA sequencing); access is controlled by the TRACERx data access committee. Details on how to apply for access are available on the linked page. Details of all published datasets obtained from third parties used in this study are as follows. Data are available on reasonable request. Multi-region RNA sequencing data from the ADAPTeR trial (NCT02446860) are available at EGA (EGAD00001008163). For the "breast" cohort, from the TONIC trial (NTC02499367), RNA sequencing data have been deposited in the European Genome phenome Archive (EGA) under accession number EGAS0001003535 and will be made available from the corresponding author on reasonable request. Data requests for RNA sequencing and NanoString data will be reviewed by the institutional review board of the Netherlands Cancer Institute (NKI) and applying researchers will need to sign a data access agreement with the NKI after approval. RNA sequencing from the "urothelial (a)" cohort from the ABACUS trial (NCT02662309) is available at EGA (EGAC00001001602) and from the "urothelial (b)" cohort from the NABUCCO trial (NCT03387761) is available at EGA (EGAS00001001648). Data are available in a public, open access repository. RNA sequencing data from the "melanoma (a)" and "melanoma (b)" cohorts are available at the Gene Expression Omnibus under GSE91061. "Pan-cancer" cohort transcriptomic and clinical data from the INSPIRE trial (NCT02644369) were downloaded as SourceData_Fig4.zip from Yang et al (https://doi.org/10.1038/s41467-021-25432-7). The dataset for the 2 TCGA cancer cohorts can be downloaded from the genomic data commons data portal (https://portal.gdc.cancer.gov/).

ORCID iDs
Ieva Usaite http://orcid.org/0000-0001-6154-0447
Nicolai Birkbak http://orcid.org/0000-0003-1613-9587
Simone Zaccaria http://orcid.org/0000-0002-5265-7392

REFERENCES

1 Johnson DB, Nebhan CA, Moslehi JJ, *et al*. Immune-Checkpoint inhibitors: long-term implications of toxicity. *Nat Rev Clin Oncol* 2022;19:254–67.
2 Larkin J, Chiarion-Sileni V, Gonzalez R, *et al*. Five-year survival with combined Nivolumab and Ipilimumab in advanced Melanoma. *N Engl J Med* 2019;381:1535–46.
3 Adams S, Loi S, Toppmeyer D, *et al*. Pembrolizumab monotherapy for previously untreated, PD-L1-positive, metastatic triple-negative breast cancer: cohort B of the phase II KEYNOTE-086 study. *Ann Oncol* 2019;30:405–11.
4 Emens LA, Cruz C, Eder JP, *et al*. Long-term clinical outcomes and biomarker analyses of Atezolizumab therapy for patients with metastatic triple-negative breast cancer: A phase 1 study. *JAMA Oncol* 2019;5:74–82.
5 Havel JJ, Chowell D, Chan TA. The evolving landscape of biomarkers for Checkpoint inhibitor Immunotherapy. *Nat Rev Cancer* 2019;19:133–50.
6 Hugo W, Zaretsky JM, Sun L, *et al*. Genomic and Transcriptomic features of response to anti-PD-1 therapy in metastatic Melanoma. *Cell* 2016;165:35–44.
7 Ayers M, Lunceford J, Nebozhyn M, *et al*. IFN-Γ-related mRNA profile predicts clinical response to PD-1 blockade. *J Clin Invest* 2017;127:2930–40.
8 Auslander N, Zhang G, Lee JS, *et al*. Robust prediction of response to immune Checkpoint blockade therapy in metastatic Melanoma. *Nat Med* 2018;24:1545–9.
9 Cristescu R, Mogg R, Ayers M, *et al*. Pan-tumor Genomic biomarkers for PD-1 Checkpoint blockade-based Immunotherapy. *Science* 2018;362:eaar3593.
10 Jiang P, Gu S, Pan D, *et al*. Signatures of T cell dysfunction and exclusion predict cancer Immunotherapy response. *Nat Med* 2018;24:1550–8.
11 Mariathasan S, Turley SJ, Nickles D, *et al*. TGFβ attenuates tumour response to PD-L1 blockade by contributing to exclusion of T cells. *Nature* 2018;554:544–8.
12 McDermott DF, Huseni MA, Atkins MB, *et al*. Clinical activity and molecular correlates of response to Atezolizumab alone or in combination with Bevacizumab versus Sunitinib in renal cell carcinoma. *Nat Med* 2018;24:749–57.
13 Thompson JC, Davis C, Deshpande C, *et al*. Gene signature of antigen processing and presentation machinery predicts response to Checkpoint blockade in non-small cell lung cancer (NSCLC) and Melanoma. *J Immunother Cancer* 2020;8:e000974.
14 Litchfield K, Reading JL, Puttick C, *et al*. Meta-analysis of Tumor- and T cell-intrinsic mechanisms of sensitization to Checkpoint inhibition. *Cell* 2021;184:596–614.
15 Chowell D, Yoo S-K, Valero C, *et al*. Improved prediction of immune Checkpoint blockade efficacy across multiple cancer types. *Nat Biotechnol* 2022;40:499–506.
16 Huang AC, Postow MA, Orlowski RJ, *et al*. T-cell invigoration to tumour burden ratio associated with anti-PD-1 response. *Nature* 2017;545:60–5.
17 Valpione S, Galvani E, Tweedy J, *et al*. Immune-awakening revealed by peripheral T cell Dynamics after one cycle of Immunotherapy. *Nat Cancer* 2020;1:210–21.
18 Au L, Hatipoglu E, Robert de Massy M, *et al*. Determinants of anti-PD-1 response and resistance in clear cell renal cell carcinoma. *Cancer Cell* 2021;39:1497–1518.
19 Cha E, Klinger M, Hou Y, *et al*. Improved survival with T cell Clonotype stability after anti–CTLA-4 treatment in cancer patients. *Sci Transl Med* 2014;6:238ra70.
20 Fairfax BP, Taylor CA, Watson RA, *et al*. Peripheral Cd8+ T cell characteristics associated with durable responses to immune Checkpoint blockade in patients with metastatic Melanoma. *Nat Med* 2020;26:193–9.
21 Yost KE, Satpathy AT, Wells DK, *et al*. Clonal replacement of tumor-specific T cells following PD-1 blockade. *Nat Med* 2019;25:1251–9.
22 Zaretsky JM, Garcia-Diaz A, Shin DS, *et al*. Mutations associated with acquired resistance to PD-1 blockade in Melanoma. *N Engl J Med* 2016;375:819–29.
23 Sade-Feldman M, Jiao YJ, Chen JH, *et al*. Resistance to Checkpoint blockade therapy through inactivation of antigen presentation. *Nat Commun* 2017;8.
24 Anagnostou V, Smith KN, Forde PM, *et al*. Evolution of Neoantigen landscape during immune Checkpoint blockade in non-small cell lung cancer. *Cancer Discov* 2017;7:264–76.
25 Voorwerk L, Slagter M, Horlings HM, *et al*. Immune induction strategies in metastatic triple-negative breast cancer to enhance the sensitivity to PD-1 blockade: the TONIC trial. *Nat Med* 2019;25:1175.
26 Blomberg OS, Spagnuolo L, Garner H, *et al*. IL-5-producing $Cd4^+$ T cells and Eosinophils cooperate to enhance response to immune Checkpoint blockade in breast cancer. *Cancer Cell* 2023;41:106–23.
27 Riaz N, Havel JJ, Makarov V, *et al*. Tumor and Microenvironment evolution during Immunotherapy with Nivolumab. *Cell* 2017;171:934–49.
28 Cindy Yang SY, Lien SC, Wang BX, *et al*. Pan-cancer analysis of longitudinal metastatic tumors reveals Genomic alterations and immune landscape Dynamics associated with Pembrolizumab sensitivity. *Nat Commun* 2021;12:5137.
29 Powles T, Kockx M, Rodriguez-Vida A, *et al*. Clinical efficacy and biomarker analysis of Neoadjuvant Atezolizumab in operable urothelial carcinoma in the ABACUS trial. *Nat Med* 2019;25:1706–14.
30 van Dijk N, Gil-Jimenez A, Silina K, *et al*. Preoperative Ipilimumab plus Nivolumab in Locoregionally advanced urothelial cancer: the NABUCCO trial. *Nat Med* 2020;26:1839–44.
31 Liu D, Schilling B, Liu D, *et al*. Integrative molecular and clinical modeling of clinical outcomes to Pd1 blockade in patients with metastatic Melanoma. *Nat Med* 2019;25:1916–27.
32 Snyder A, Makarov V, Merghoub T, *et al*. Genetic basis for clinical response to CTLA-4 blockade in Melanoma. *N Engl J Med* 2014;371:2189–99.
33 Van Allen EM, Miao D, Schilling B, *et al*. Genomic correlates of response to CTLA-4 blockade in metastatic Melanoma. *Science* 2015;350:207–11.
34 Snyder A, Nathanson T, Funt SA, *et al*. Contribution of systemic and somatic factors to clinical response and resistance to PD-L1 blockade in urothelial cancer: an exploratory multi-Omic analysis. *PLoS Med* 2017;14:e1002309.
35 Shim JH, Kim HS, Cha H, *et al*. HLA-corrected tumor Mutation burden and Homologous Recombination deficiency for the prediction of response to PD-(L)1 blockade in advanced non-small-cell lung cancer patients. *Annals of Oncology* 2020;31:902–11.
36 Kim ST, Cristescu R, Bass AJ, *et al*. Comprehensive molecular characterization of clinical responses to PD-1 inhibition in metastatic gastric cancer. *Nat Med* 2018;24:1449–58.
37 Tumeh PC, Harview CL, Yearley JH, *et al*. PD-1 blockade induces responses by inhibiting adaptive immune resistance. *Nature* 2014;515:568–71.
38 Gibney GT, Weiner LM, Atkins MB. Predictive biomarkers for Checkpoint inhibitor-based Immunotherapy. *Lancet Oncol* 2016;17:e542–51.
39 Chow MT, Ozga AJ, Servis RL, *et al*. Intratumoral activity of the Cxcr3 Chemokine system is required for the efficacy of anti-PD-1 therapy. *Immunity* 2019;50:1498–512.
40 Fehrenbacher L, Spira A, Ballinger M, *et al*. Atezolizumab versus Docetaxel for patients with previously treated non-small-cell lung cancer (POPLAR): a Multicentre, open-label, phase 2 randomised controlled trial. *The Lancet* 2016;387:1837–46.
41 Wang L, Saci A, Szabo PM, *et al*. EMT- and Stroma-related gene expression and resistance to PD-1 blockade in urothelial cancer. *Nat Commun* 2018;9.
42 Messina JL, Fenstermacher DA, Eschrich S, *et al*. 12-Chemokine gene signature identifies lymph node-like structures in Melanoma: potential for patient selection for Immunotherapy? *Sci Rep* 2012;2:765.

43 Pabla S, Conroy JM, Nesline MK, *et al*. Proliferative potential and resistance to immune Checkpoint blockade in lung cancer patients. *J Immunotherapy Cancer* 2019;7.
44 Takeuchi Y, Tanegashima T, Sato E, *et al*. Highly Immunogenic cancer cells require activation of the WNT pathway for immunological escape. *Sci Immunol* 2021;6:eabc6424.
45 Rooney MS, Shukla SA, Wu CJ, *et al*. Molecular and genetic properties of tumors associated with local immune Cytolytic activity. *Cell* 2015;160:48–61.
46 Caushi JX, Zhang J, Ji Z, *et al*. Transcriptional programs of Neoantigen-specific TIL in anti-PD-1-treated lung cancers. *Nature* 2021;596:126–32.
47 Jerby-Arnon L, Tooley K, Escobar G, *et al*. Pan-cancer mapping of single t cell profiles reveals a tcf1:cxcr6-cxcl16 regulatory axis essential for effective anti-tumor immunity. *Immunology* [Preprint] 2021.
48 Colaprico A, Silva TC, Olsen C, *et al*. Tcgabiolinks: an R/Bioconductor package for integrative analysis of TCGA data. *Nucleic Acids Res* 2016;44:e71.
49 Love MI, Huber W, Anders S. Moderated estimation of fold change and dispersion for RNA-Seq data with Deseq2. *Genome Biol* 2014;15:550.
50 Martínez-Ruiz C, Black JRM, Puttick C, *et al*. Genomic–Transcriptomic evolution in lung cancer and metastasis. *Nature* 2023;616:543–52.
51 Biswas D, Birkbak NJ, Rosenthal R, *et al*. A Clonal expression biomarker Associates with lung cancer mortality. *Nat Med* 2019;25:1540–8.
52 Cumming G. The new Statistics: why and how. *Psychol Sci* 2014;25:7–29.
53 Park J-E, Kim S-E, Keam B, *et al*. Anti-tumor effects of NK cells and anti-PD-L1 antibody with antibody-dependent cellular cytotoxicity in PD-L1-positive cancer cell lines. *J Immunother Cancer* 2020;8:e000873.
54 Kang TG, Park HJ, Moon J, *et al*. Enriching Ccl3 in the tumor Microenvironment facilitates T cell responses and improves the efficacy of anti-PD-1 therapy. *Immune Netw* 2021;21:e23.
55 de Andrade LF, Lu Y, Luoma A, *et al*. Discovery of specialized NK cell populations infiltrating human Melanoma metastases. *JCI Insight* 2019;4. 10.1172/jci.insight.133103 Available: https://insight.jci.org/articles/view/133103
56 Ji S, Chen H, Yang K, *et al*. Peripheral cytokine levels as predictive biomarkers of benefit from immune Checkpoint inhibitors in cancer therapy. *Biomedicine & Pharmacotherapy* 2020;129:110457.
57 van der Leun AM, Thommen DS, Schumacher TN. Cd8+ T cell States in human cancer: insights from single-cell analysis. *Nat Rev Cancer* 2020;20:218–32.
58 Tan W, Liu M, Wang L, *et al*. Novel immune-related genes in the tumor Microenvironment with Prognostic value in breast cancer. *BMC Cancer* 2021;21:126.
59 Wu Y, Kyle-Cezar F, Woolf RT, *et al*. An innate-like Vδ1+ Γδ T cell compartment in the human breast is associated with remission in triple-negative breast cancer. *Sci Transl Med* 2019;11.
60 Wu Y, Biswas D, Usaite I, *et al*. A local human Vδ1 T cell population is associated with survival in Nonsmall-cell lung cancer. *Nat Cancer* 2022;3:696–709.
61 von Linsingen R, Pinho de França P, de Carvalho NS, *et al*. MICA and Klrk1 genes and their impact in Cervical intraepithelial Neoplasia development in the Southern Brazilian population. *Human Immunology* 2020;81:249–53.
62 Zlatareva I, Wu Y. Local Γδ T cells: translating promise to practice in cancer Immunotherapy. *Br J Cancer* 2023;129:393–405.
63 Gettinger S, Choi J, Hastings K, *et al*. Impaired HLA class I antigen processing and presentation as a mechanism of acquired resistance to immune Checkpoint inhibitors in lung cancer. *Cancer Discovery* 2017;7:1420–35.
64 Szekely B, Bossuyt V, Li X, *et al*. Immunological differences between primary and metastatic breast cancer. *Ann Oncol* 2018;29:2232–9.
65 Farias A, Soto A, Puttur F, *et al*. A Tlr4 agonist improves immune Checkpoint blockade treatment by increasing the ratio of Effector to regulatory cells within the tumor Microenvironment. *Sci Rep* 2021;11.
66 Jeon D, McNeel DG. Toll-like receptor agonist combinations augment Mouse T-cell anti-tumor immunity via IL-12- and interferon Ss-mediated suppression of immune Checkpoint receptor expression. *Oncoimmunology* 2022;11:2054758.
67 Lee WS, Kim DS, Kim JH, *et al*. Intratumoral Immunotherapy using a Tlr2/3 agonist, L-Pampo, induces robust antitumor immune responses and enhances immune Checkpoint blockade. *J Immunother Cancer* 2022;10:e004799.
68 Gonzalez C, Williamson S, Gammon ST, *et al*. Tlr5 agonists enhance anti-tumor immunity and overcome resistance to immune Checkpoint therapy. *Commun Biol* 2023;6:31:31.:.
69 Wang J, Cai S, Xiong Q, *et al*. Pik3R2 predicts poor outcomes for patients with Melanoma and contributes to the malignant progression via Pi3K/AKT/NF-ΚB axis. *Clin Transl Oncol* 2023;25:1402–12.
70 Yokoyama S, Takahashi A, Kikuchi R, *et al*. Sox10 regulates Melanoma Immunogenicity through an Irf4-Irf1 axis. *Cancer Res* 2021;81:6131–41.
71 Xie J, Zhu Z, Cao Y, *et al*. Solute carrier transporter Superfamily member Slc16A1 is a potential Prognostic biomarker and associated with immune infiltration in skin cutaneous Melanoma. *Channels* 2021;15:483–95.
72 Zhang L, Song ZS, Wang ZS, *et al*. n.d. High expression of Slc16A1 as a biomarker to predict poor prognosis of Urological cancers. *Front Oncol*;11. 10.3389/fonc.2021.706883 Available: https://www.frontiersin.org/articles/10.3389/fonc.2021.706883
73 Johnson JM, Cotzia P, Fratamico R, *et al*. n.d. Mct1 in invasive Ductal carcinoma: Monocarboxylate metabolism and aggressive breast cancer. *Front Cell Dev Biol*;5. 10.3389/fcell.2017.00027 Available: https://www.frontiersin.org/articles/10.3389/fcell.2017.00027
74 Shekoohi S, Rajasekaran S, Patel D, *et al*. Knocking out alpha-Synuclein in Melanoma cells Dysregulates cellular iron metabolism and suppresses tumor growth. *Sci Rep* 2021;11:5267.
75 Raisner R, Bainer R, Haverty PM, *et al*. Super-enhancer acquisition drives Oncogene expression in triple negative breast cancer. *PLoS ONE* 2020;15:e0235343.
76 Liao C, Talluri S, Zhao J, *et al*. Rad51 is implicated in DNA damage, Chemoresistance and immune dysregulation in solid tumors. *Cancers (Basel)* 2022;14:5697.

Supplementary Figure 1. Overview of the CPIΔ cohorts. Summarising longitudinal sample collections, treatments course, sequencing, and clinical outcome data availability.

A) 'Breast' cohort. Metastatic TNBC cohort consisting of n=25 patients with longitudinal data available (diagram, left). Patients were randomised into 4 arms (timeline, bottom), receiving either low-dose induction therapy or no induction prior to immunotherapy, followed by CPI every 2 weeks (Nivolumab, PD-1) until progression or for a maximum of 12 months. Two biopsies were collected (timeline, top), the first (T1) prior to any treatment and second (T2) after 3-cycles of CPI. This cohort consists of NanoString RNA sequencing data and has clinical outcome data in the form of both overall survival (OS) and response defined by RECIST (table, right).

B) "Melanoma (a)" cohort. Advanced melanoma cohort. Cohort consists of n=23 patients who were CPI naïve prior to starting the course of treatment and have longitudinal data available. All patients received CPI every 2 weeks (Pembrolizumab, PD-1), until progression, or for a maximum of 2 years. Two biopsies were collected from each patient (timeline, top), the first (T1) prior to any treatment and second (T2) after 1-cycle of CPI (23-29 days). This cohort consists of RNA-sequencing data, with clinical outcome data in the form of both overall survival (OS) and response defined by RECIST available (table, right).

C) "Melanoma (b)" cohort. Advanced melanoma cohort. Cohort consists of n=19 patients who had previously received CPI (CTLA-4) with longitudinal data available. All patients received CPI every 2 weeks (Pembrolizumab, PD-1), until progression, or for a maximum of 2 years. Two biopsies were collected from each patient (timeline, top), the first (T1) prior to any treatment and second (T2) after 1-cycle of CPI (23-29 days). This cohort consists of RNA-sequencing data, with clinical outcome data in the form of both overall survival (OS) and response defined by RECIST (table, right).

D) "Pan-cancer" cohort. Metastatic solid tumor cohort consisting of n=30 patients with longitudinal data available (diagram, left) across > 5 different cancer types including, head & neck (n=3), TNBC (n=3), high-grade serous ovarian (n=6), melanoma (n=6), and a group of patients with rare solid tumors (n=12). All patients received CPI every 3 weeks (Pembrolizumab, PD-1), until progression, or for a maximum of 2 years. Two biopsies were collected from each patient (timeline, top), the first (T1) prior to any treatment and the second

Usaite I, *et al. J Immunother Cancer* 2023; 11:e007870. doi: 10.1136/jitc-2023-007870

(T2) after 2 or 3 cycles of CPI. This cohort consists of RNA-sequencing data, with clinical outcome data in the form of both overall survival (OS) and response defined by RECIST (table, right).

E) "Urothelial (a)" cohort. Urothelial cohort consisting of n=64 patients with longitudinal data available (diagram, left). All patients received CPI 3 times weekly (Atezolizumab, PD-L1). Two biopsies were collected from each patient (timeline, top), the first (T1) prior to any treatment and second (T2) after all cycles of CPI. This cohort consists of RNA-sequencing data, with clinical outcome data in the form of pathological response (pCR) available (table, right).

F) "Urothelial (b)" cohort. Urothelial cohort consisting of n=13 patients with longitudinal data available (diagram, left). All patients received CPI 3 times across 42 days (ipilimumab, CTLA-4, day 1; ipilimumab + nivolumab, CTLA-4 +PD-1, day 22; ipilimumab, CTLA-4, day 42). Two biopsies were collected from each patient (timeline, top), the first (T1) prior to any treatment and second (T2) after all cycles of CPI. This cohort consists of RNA-sequencing data, with clinical outcome data in the form of pathological response (pCR) available (table, right). The illustrations in **a-f** were created using BioRender (https://biorender.com).

Supplementary Figure 2. Transcriptomic signature shifts in expression on-therapy across cancer-types.

A) Summary plot of all available signatures (n=32) within the 'melanoma (a)' cohort. Signatures are depicted on the x-axis and the proportion of patient-tumors which increase (top arrow) or decrease (bottom arrow) in expression on-therapy for each signature is indicated on the y-axis. Bars in red (OS high) and blue (OS low) depict patient stratification based on OS. Significance was tested using a Fisher's Exact Test which is displayed.

B) Summary plot of all available signatures (n=32) within the 'Urothelial (b)' cohort. Bars in green (non-response) and yellow (response) depict patient stratification based of pCR.

C) Summary plot of all available signatures (n=32) within the 'melanoma (b)' cohort. Bars in red (OS high) and blue (OS low) depict patient stratification based on OS. Significance was tested using a Fisher's Exact Test which is displayed.
D) Summary plot of all available signatures (n=32) within the 'Pan-cancer' cohort. Bars in red (OS high) and blue (OS low) depict patient stratification based on OS. Significance was tested using a Fisher's Exact Test which is displayed.
E) Summary plot of all available signatures (n=28) within the 'Urothelial (a)' cohort. Bars in green (non-response) and yellow (response) depict patient stratification based of pCR. Significance was tested using a Fisher's Exact Test.

Supplementary Figure 3. Genes comprising the Resistance categories across CPIΔ cohorts

A-B) Upset plots of genes comprising the **a)** 'Resistance Pos' and **b)** 'Resistance Neg' categories across the CPIΔ cohorts sub-setting for 778 genes within the NanoString Immune panel. For each upset plot, the left bar plots indicate the number of genes identified in each gene category per CPIΔ cohort, including 'breast' (pink), 'melanoma (a)' (light blue), 'melanoma (b)' (dark blue), 'urothelial (a)' (orange), 'urothelial (b)' (yellow). The top bar plot indicates the total number of genes which are unique to each cohort and the number of shared genes between cohorts, with interactions highlighted in the bottom dot plot.

Usaite I, *et al. J Immunother Cancer* 2023; 11:e007870. doi: 10.1136/jitc-2023-007870

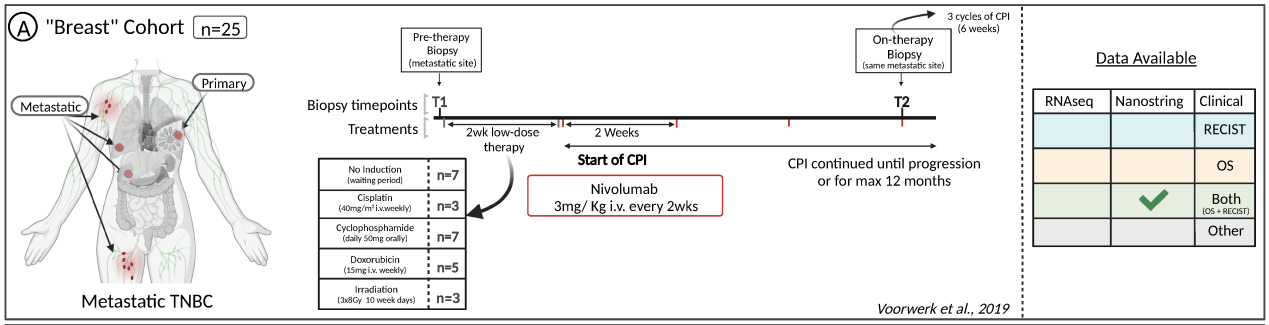
A "Breast" Cohort n=25
Metastatic
Primary
Metastatic TNBC
Pre-therapy Biopsy (metastatic site)
On-therapy Biopsy (same metastatic site)
3 cycles of CPI (6 weeks)
Biopsy timepoints
Treatments
T1
T2
2wk low-dose therapy
2 Weeks
Start of CPI
CPI continued until progression or for max 12 months
No Induction (waiting period) n=7
Cisplatin (40mg/m² i.v.weekly) n=3
Cyclophosphamide (daily 50mg orally) n=7
Doxorubicin (15mg i.v. weekly) n=5
Irradiation (3x8Gy 10 week days) n=3
Nivolumab 3mg/ Kg i.v. every 2wks
Voorwerk et al., 2019
Data Available
RNAseq
Nanostring
Clinical
RECIST
OS
Both (OS + RECIST)
Other

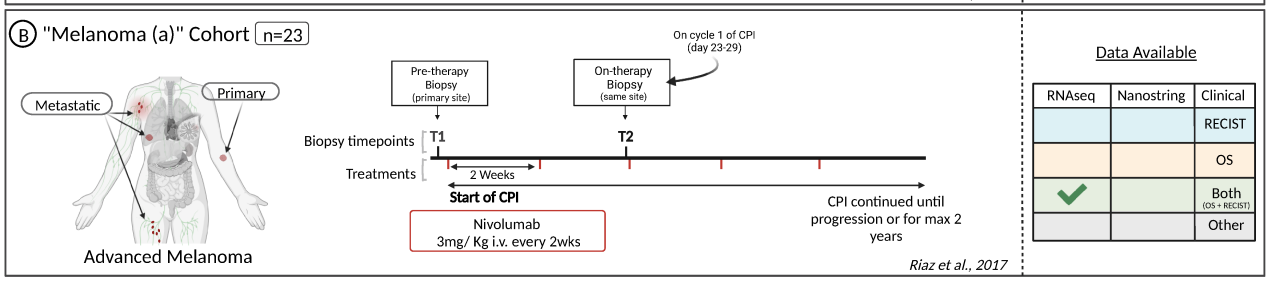
B "Melanoma (a)" Cohort n=23
Metastatic
Primary
Advanced Melanoma
Pre-therapy Biopsy (primary site)
On-therapy Biopsy (same site)
On cycle 1 of CPI (day 23-29)
Biopsy timepoints
Treatments
T1
T2
2 Weeks
Start of CPI
CPI continued until progression or for max 2 years
Nivolumab 3mg/ Kg i.v. every 2wks
Riaz et al., 2017
Data Available
RNAseq
Nanostring
Clinical
RECIST
OS
Both (OS + RECIST)
Other

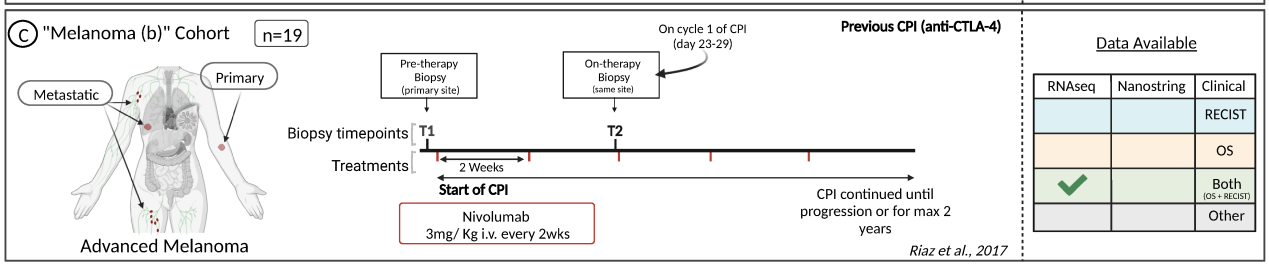
C "Melanoma (b)" Cohort n=19
Metastatic
Primary
Advanced Melanoma
Pre-therapy Biopsy (primary site)
On-therapy Biopsy (same site)
On cycle 1 of CPI (day 23-29)
Previous CPI (anti-CTLA-4)
Biopsy timepoints
Treatments
T1
T2
2 Weeks
Start of CPI
CPI continued until progression or for max 2 years
Nivolumab 3mg/ Kg i.v. every 2wks
Riaz et al., 2017
Data Available
RNAseq
Nanostring
Clinical
RECIST
OS
Both (OS + RECIST)
Other

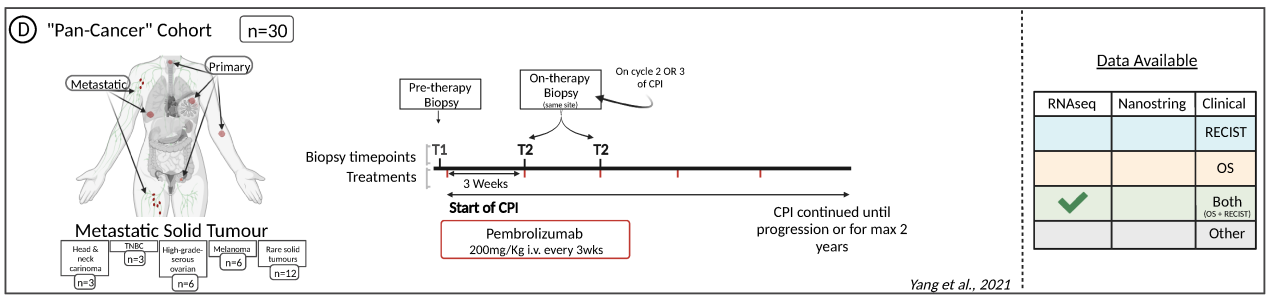
D "Pan-Cancer" Cohort n=30
Metastatic
Primary
Metastatic Solid Tumour
Head & neck carinoma n=3
TNBC n=3
High-grade-serous ovarian n=6
Melanoma n=6
Rare solid tumours n=12
Pre-therapy Biopsy
On-therapy Biopsy (same site)
On cycle 2 OR 3 of CPI
Biopsy timepoints
Treatments
T1
T2
T2
3 Weeks
Start of CPI
CPI continued until progression or for max 2 years
Pembrolizumab 200mg/Kg i.v. every 3wks
Yang et al., 2021
Data Available
RNAseq
Nanostring
Clinical
RECIST
OS
Both (OS + RECIST)
Other

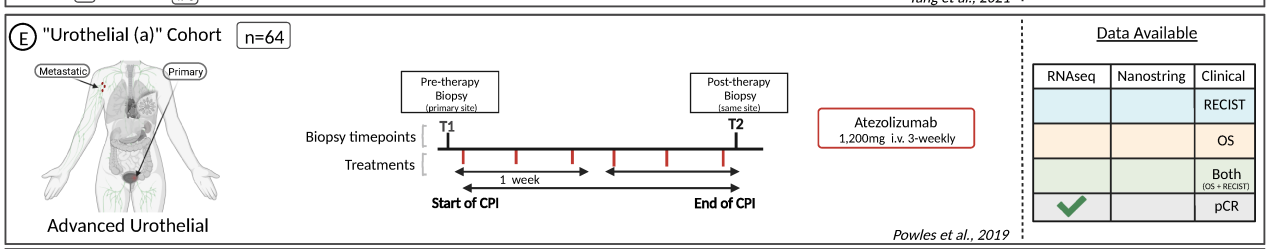
E "Urothelial (a)" Cohort n=64
Metastatic
Primary
Advanced Urothelial
Pre-therapy Biopsy (primary site)
Post-therapy Biopsy (same site)
Biopsy timepoints
Treatments
T1
T2
1 week
Start of CPI
End of CPI
Atezolizumab 1,200mg i.v. 3-weekly
Powles et al., 2019
Data Available
RNAseq
Nanostring
Clinical
RECIST
OS
Both (OS + RECIST)
pCR

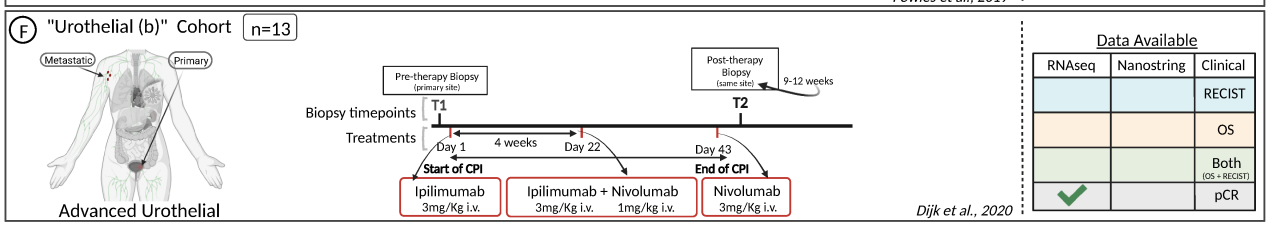
F "Urothelial (b)" Cohort n=13
Metastatic
Primary
Advanced Urothelial
Pre-therapy Biopsy (primary site)
Post-therapy Biopsy (same site)
9-12 weeks
Biopsy timepoints
Treatments
T1
T2
Day 1
4 weeks
Day 22
Day 43
Start of CPI
End of CPI
Ipilimumab 3mg/Kg i.v.
Ipilimumab + Nivolumab 3mg/Kg i.v. 1mg/kg i.v.
Nivolumab 3mg/Kg i.v.
Dijk et al., 2020
Data Available
RNAseq
Nanostring
Clinical
RECIST
OS
Both (OS + RECIST)
pCR

A

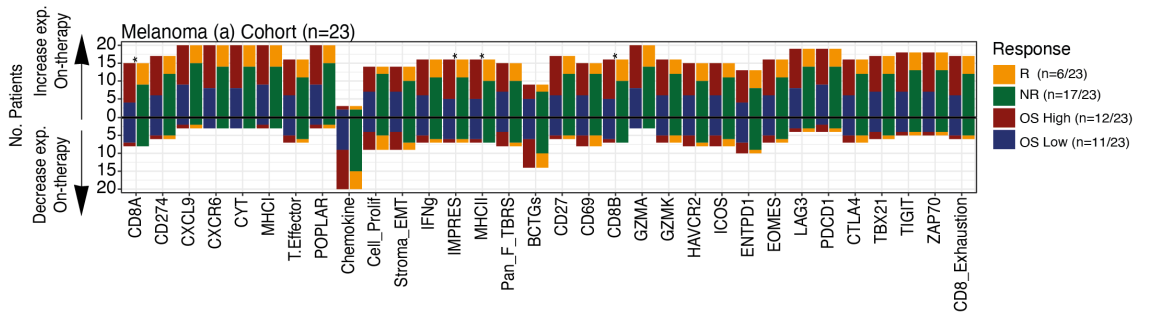
Melanoma (a) Cohort (n=23)
No. Patients
Increase exp. On-therapy
Decrease exp. On-therapy
Response
R (n=6/23)
NR (n=17/23)
OS High (n=12/23)
OS Low (n=11/23)
CD8A CD274 CXCL9 CXCR6 CYT MHCI T.Effector POPLAR Chemokine Cell_Prolif Stroma_EMT IFNg IMPRES MHCII Pan_F_TBRS BCTGs CD27 CD69 CD8B GZMA GZMK HAVCR2 ICOS ENTPD1 EOMES LAG3 PDCD1 CTLA4 TBX21 TIGIT ZAP70 CD8_Exhaustion

B

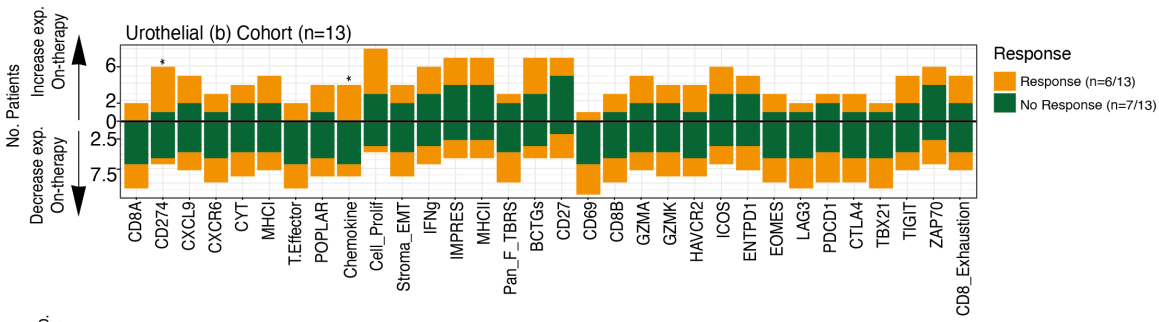
Urothelial (b) Cohort (n=13)
No. Patients
Increase exp. On-therapy
Decrease exp. On-therapy
Response
Response (n=6/13)
No Response (n=7/13)
CD8A CD274 CXCL9 CXCR6 CYT MHCI T.Effector POPLAR Chemokine Cell_Prolif Stroma_EMT IFNg IMPRES MHCII Pan_F_TBRS BCTGs CD27 CD69 CD8B GZMA GZMK HAVCR2 ICOS ENTPD1 EOMES LAG3 PDCD1 CTLA4 TBX21 TIGIT ZAP70 CD8_Exhaustion

C

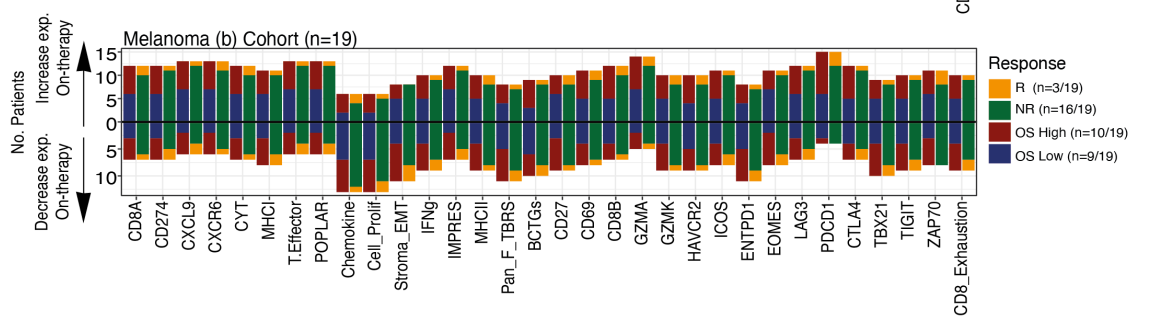
Melanoma (b) Cohort (n=19)
No. Patients
Increase exp. On-therapy
Decrease exp. On-therapy
Response
R (n=3/19)
NR (n=16/19)
OS High (n=10/19)
OS Low (n=9/19)
CD8A CD274 CXCL9 CXCR6 CYT MHCI T.Effector POPLAR Chemokine Cell_Prolif Stroma_EMT IFNg IMPRES MHCII Pan_F_TBRS BCTGs CD27 CD69 CD8B GZMA GZMK HAVCR2 ICOS ENTPD1 EOMES LAG3 PDCD1 CTLA4 TBX21 TIGIT ZAP70 CD8_Exhaustion

D

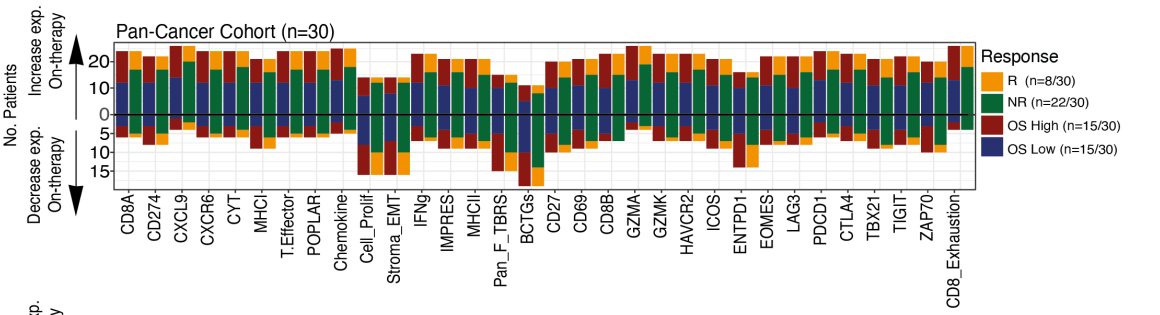
Pan-Cancer Cohort (n=30)
No. Patients
Increase exp. On-therapy
Decrease exp. On-therapy
Response
R (n=8/30)
NR (n=22/30)
OS High (n=15/30)
OS Low (n=15/30)
CD8A CD274 CXCL9 CXCR6 CYT MHCI T.Effector POPLAR Chemokine Cell_Prolif Stroma_EMT IFNg IMPRES MHCII Pan_F_TBRS BCTGs CD27 CD69 CD8B GZMA GZMK HAVCR2 ICOS ENTPD1 EOMES LAG3 PDCD1 CTLA4 TBX21 TIGIT ZAP70 CD8_Exhaustion

E

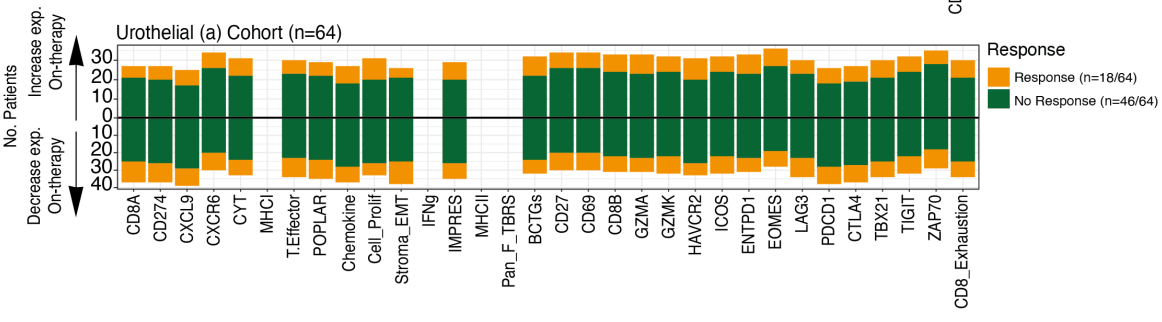
Urothelial (a) Cohort (n=64)
No. Patients
Increase exp. On-therapy
Decrease exp. On-therapy
Response
Response (n=18/64)
No Response (n=46/64)
CD8A CD274 CXCL9 CXCR6 CYT MHCI T.Effector POPLAR Chemokine Cell_Prolif Stroma_EMT IFNg IMPRES MHCII Pan_F_TBRS BCTGs CD27 CD69 CD8B GZMA GZMK HAVCR2 ICOS ENTPD1 EOMES LAG3 PDCD1 CTLA4 TBX21 TIGIT ZAP70 CD8_Exhaustion

A Resistance Pos

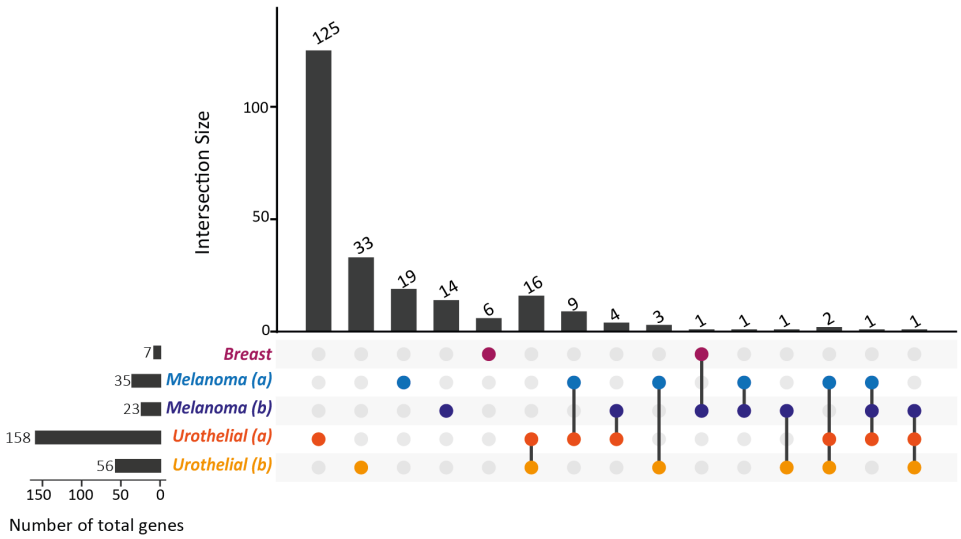

B Resistance Neg

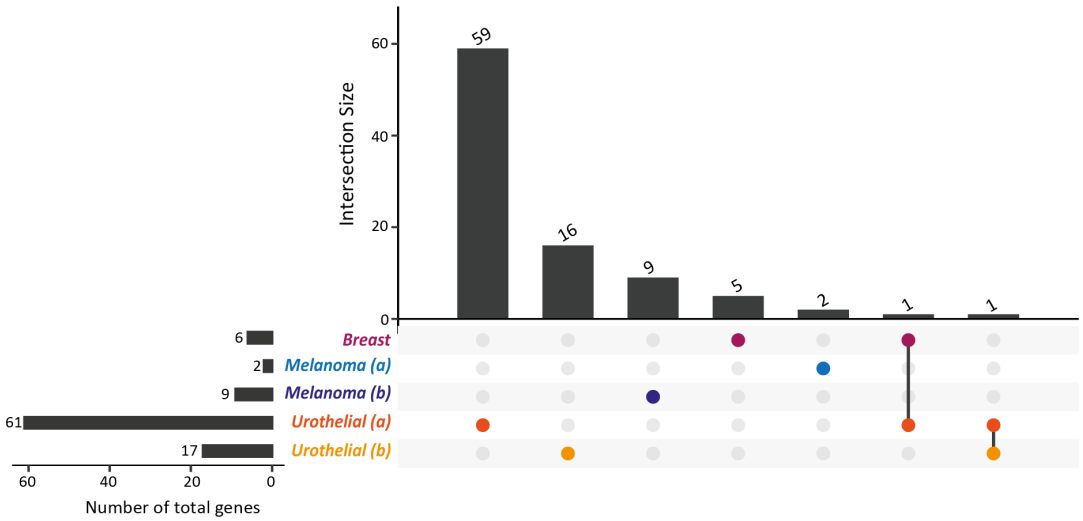

Supplementary Table 1: Pre-therapy Meta-analysis results across the CPI-Dynamics & CPI1000+ cohorts (n=16)

Signature	OR	Meta_Pval
CD8A	1.227054501	0.000223335
CD274	1.256900214	0.003997711
CXCL9	1.235147721	3.99E-05
CYT	1.29313745	0.000149581
MHCI	1.301381527	0.002178177
T.Effector	1.449905878	2.56E-05
POPLAR	1.392469393	5.95E-06
Chemokine	0.990350278	0.787128495
Cell_Prolif	1.273772588	0.14054066
Stroma_EMT	0.90375055	0.257522693
IFNg	1.150240919	0.060880528
IMPRES	1.02185141	0.004551108
MHCII	1.168625716	0.023471345
Pan_F_TBRS	0.970110769	0.837103795
BCTGs	0.819067	0.140472469

Supplementary Table 2: Pre-therapy Odds ratio results per dataset (CPI1000+ cohort & CPI-Dynamics cohorts)

Signatures	OR	P_Val	Cohort	Dataset
CD8A	0.66627771	0.835664336	Urothelial (b)	CPI-Dynamics
CD274	7.97144205	0.137529138	Urothelial (b)	CPI-Dynamics
CXCL9	1.79448657	0.533799534	Urothelial (b)	CPI-Dynamics
CYT	0.95351342	0.835664336	Urothelial (b)	CPI-Dynamics
MHCI	2.99882756	0.835664336	Urothelial (b)	CPI-Dynamics
T.Effector	1.0667453	0.835664336	Urothelial (b)	CPI-Dynamics
POPLAR	4.38125083	0.365967366	Urothelial (b)	CPI-Dynamics
Chemokine	1.78991092	0.137529138	Urothelial (b)	CPI-Dynamics
Cell_Prolif	13.7034486	0.034965035	Urothelial (b)	CPI-Dynamics
Stroma_EMT	1.17224537	0.945221445	Urothelial (b)	CPI-Dynamics
Pan_F_TBRS	0.97946567	0.835664336	Urothelial (b)	CPI-Dynamics
IFNg	0.37377887	0.365967366	Urothelial (b)	CPI-Dynamics
IMPRES	0.89443286	0.294871795	Urothelial (b)	CPI-Dynamics
MHCII	0.16420351	0.101398601	Urothelial (b)	CPI-Dynamics
BCTGs	1.79437988	0.628205128	Urothelial (b)	CPI-Dynamics
CD8A	0.95899809	1	Hugo_2016_Melanoma	CPI1000+
CD274	1.06744993	0.578767187	Hugo_2016_Melanoma	CPI1000+
CXCL9	0.9815608	0.840250947	Hugo_2016_Melanoma	CPI1000+
CYT	0.72135502	0.511438186	Hugo_2016_Melanoma	CPI1000+
MHCI	1.48704474	0.310733035	Hugo_2016_Melanoma	CPI1000+
T.Effector	0.90604213	0.840250947	Hugo_2016_Melanoma	CPI1000+
POPLAR	0.91143464	0.840250947	Hugo_2016_Melanoma	CPI1000+
Chemokine	1.0720175	0.578767187	Hugo_2016_Melanoma	CPI1000+
Cell_Prolif	0.4647657	0.203541719	Hugo_2016_Melanoma	CPI1000+
Stroma_EMT	0.43774027	0.101430879	Hugo_2016_Melanoma	CPI1000+
Pan_F_TBRS	0.19842144	0.016408669	Hugo_2016_Melanoma	CPI1000+
IFNg	0.90819337	0.801041863	Hugo_2016_Melanoma	CPI1000+
IMPRES	0.97400879	0.448300867	Hugo_2016_Melanoma	CPI1000+
MHCII	1.25182812	0.479322924	Hugo_2016_Melanoma	CPI1000+
BCTGs	1.04126358	1	Hugo_2016_Melanoma	CPI1000+
CD8A	1.19309505	0.869543309	Kim_2018_Gastric	CPI1000+
CD274	4.34891194	0.599121894	Kim_2018_Gastric	CPI1000+
CXCL9	0.96257636	0.984583805	Kim_2018_Gastric	CPI1000+
CYT	9.74040855	0.534267615	Kim_2018_Gastric	CPI1000+
MHCI	0.17419471	0.534267615	Kim_2018_Gastric	CPI1000+
T.Effector	0.2109699	0.612498873	Kim_2018_Gastric	CPI1000+
POPLAR	0.58381266	0.916356377	Kim_2018_Gastric	CPI1000+
Chemokine	1.305434	0.681217965	Kim_2018_Gastric	CPI1000+
Cell_Prolif	59.2203248	0.10301113	Kim_2018_Gastric	CPI1000+
Stroma_EMT	0.21500229	0.473078088	Kim_2018_Gastric	CPI1000+
Pan_F_TBRS	130.763284	0.215342884	Kim_2018_Gastric	CPI1000+
IFNg	3.40199961	0.030069232	Kim_2018_Gastric	CPI1000+

IMPRES	0.91545698	0.901218716	Kim_2018_Gastric	CPI1000+
MHCII	2.77640153	0.46130917	Kim_2018_Gastric	CPI1000+
BCTGs	0.58362975	0.612498873	Kim_2018_Gastric	CPI1000+
CD8A	1.03788719	0.902843949	Liu_2018_Melanoma	CPI1000+
CD274	1.02760319	0.836986353	Liu_2018_Melanoma	CPI1000+
CXCL9	1.04362356	0.767598005	Liu_2018_Melanoma	CPI1000+
CYT	1.15091292	0.704644771	Liu_2018_Melanoma	CPI1000+
MHCI	1.16402686	0.720816592	Liu_2018_Melanoma	CPI1000+
T.Effector	1.10554208	0.953894413	Liu_2018_Melanoma	CPI1000+
POPLAR	1.11118319	0.928829653	Liu_2018_Melanoma	CPI1000+
Stroma_EMT	0.9651659	0.989819746	Liu_2018_Melanoma	CPI1000+
IMPRES	1.00826091	0.711279179	Liu_2018_Melanoma	CPI1000+
MHCII	1.14143297	0.260121897	Liu_2018_Melanoma	CPI1000+
BCTGs	0.96268526	0.77889646	Liu_2018_Melanoma	CPI1000+
Chemokine	NA	NA	Liu_2018_Melanoma	CPI1000+
Cell_Prolif	NA	NA	Liu_2018_Melanoma	CPI1000+
Pan_F_TBRS	NA	NA	Liu_2018_Melanoma	CPI1000+
IFNg	NA	NA	Liu_2018_Melanoma	CPI1000+
CD8A	1.21866289	0.392677542	Liu_2018_Melanoma (c)	CPI1000+
CD274	1.02843651	0.526438837	Liu_2018_Melanoma (c)	CPI1000+
CXCL9	1.4251478	0.062096926	Liu_2018_Melanoma (c)	CPI1000+
CYT	1.65201456	0.105387412	Liu_2018_Melanoma (c)	CPI1000+
MHCI	1.26706807	0.588203298	Liu_2018_Melanoma (c)	CPI1000+
T.Effector	1.46192324	0.257335778	Liu_2018_Melanoma (c)	CPI1000+
POPLAR	1.60903805	0.169098131	Liu_2018_Melanoma (c)	CPI1000+
Stroma_EMT	1.37539607	0.434854899	Liu_2018_Melanoma (c)	CPI1000+
IMPRES	1.05497528	0.045578396	Liu_2018_Melanoma (c)	CPI1000+
MHCII	1.64096931	0.127225922	Liu_2018_Melanoma (c)	CPI1000+
BCTGs	0.58593155	0.07983895	Liu_2018_Melanoma (c)	CPI1000+
Chemokine	NA	NA	Liu_2018_Melanoma (c)	CPI1000+
Cell_Prolif	NA	NA	Liu_2018_Melanoma (c)	CPI1000+
Pan_F_TBRS	NA	NA	Liu_2018_Melanoma (c)	CPI1000+
IFNg	NA	NA	Liu_2018_Melanoma (c)	CPI1000+
CD8A	1.25328691	0.018399969	Mariathasan_2018_Bladder	CPI1000+
CD274	1.19374794	0.091121622	Mariathasan_2018_Bladder	CPI1000+
CXCL9	1.36342075	0.000182643	Mariathasan_2018_Bladder	CPI1000+
CYT	1.25487746	0.041847066	Mariathasan_2018_Bladder	CPI1000+
MHCI	1.37816134	0.039573675	Mariathasan_2018_Bladder	CPI1000+
T.Effector	1.45038057	0.030820607	Mariathasan_2018_Bladder	CPI1000+
POPLAR	1.5028487	0.002717792	Mariathasan_2018_Bladder	CPI1000+
Chemokine	0.92899553	0.032307512	Mariathasan_2018_Bladder	CPI1000+
Cell_Prolif	1.80889147	0.000547623	Mariathasan_2018_Bladder	CPI1000+

Stroma_EMT	0.7858278	0.034839223	Mariathasan_2018_Bladder	CPI1000+
Pan_F_TBRS	0.79721183	0.183219444	Mariathasan_2018_Bladder	CPI1000+
IFNg	1.15392642	0.282378504	Mariathasan_2018_Bladder	CPI1000+
IMPRES	1.00247843	0.696789951	Mariathasan_2018_Bladder	CPI1000+
MHCII	1.03631955	0.67552721	Mariathasan_2018_Bladder	CPI1000+
BCTGs	0.75057774	0.130625695	Mariathasan_2018_Bladder	CPI1000+
CD8A	1.38217575	0.34575036	McDermot_2018_Renal	CPI1000+
CD274	3.02426271	0.117517924	McDermot_2018_Renal	CPI1000+
CXCL9	1.24623087	0.401482107	McDermot_2018_Renal	CPI1000+
CYT	1.34722927	0.441345576	McDermot_2018_Renal	CPI1000+
MHCI	0.93017173	0.905028868	McDermot_2018_Renal	CPI1000+
T.Effector	2.28305809	0.141659965	McDermot_2018_Renal	CPI1000+
POPLAR	1.39767077	0.57303518	McDermot_2018_Renal	CPI1000+
Chemokine	0.91687058	0.483293053	McDermot_2018_Renal	CPI1000+
Cell_Prolif	1.03428491	0.771900698	McDermot_2018_Renal	CPI1000+
Stroma_EMT	0.7493167	0.720192079	McDermot_2018_Renal	CPI1000+
Pan_F_TBRS	0.74288763	0.720192079	McDermot_2018_Renal	CPI1000+
IFNg	1.03426041	0.905028868	McDermot_2018_Renal	CPI1000+
IMPRES	1.05107116	0.462065315	McDermot_2018_Renal	CPI1000+
MHCII	1.0988245	0.549907428	McDermot_2018_Renal	CPI1000+
BCTGs	0.34938528	0.596598439	McDermot_2018_Renal	CPI1000+
CD8A	1.90175057	0.01095456	Urothelial (a)	CPI-Dynamics
CD274	2.11603529	0.003610008	Urothelial (a)	CPI-Dynamics
CXCL9	1.57219484	0.006883502	Urothelial (a)	CPI-Dynamics
CYT	1.97353952	0.005672464	Urothelial (a)	CPI-Dynamics
T.Effector	2.35907689	0.002930938	Urothelial (a)	CPI-Dynamics
POPLAR	2.02688762	0.005672464	Urothelial (a)	CPI-Dynamics
Chemokine	1.21261039	0.010003949	Urothelial (a)	CPI-Dynamics
Cell_Prolif	1.86302521	0.220155576	Urothelial (a)	CPI-Dynamics
Stroma_EMT	0.84240207	0.772937352	Urothelial (a)	CPI-Dynamics
IMPRES	1.04093718	0.099247669	Urothelial (a)	CPI-Dynamics
BCTGs	0.8971702	0.619938747	Urothelial (a)	CPI-Dynamics
MHCI	NA	NA	Urothelial (a)	CPI-Dynamics
Pan_F_TBRS	NA	NA	Urothelial (a)	CPI-Dynamics
IFNg	NA	NA	Urothelial (a)	CPI-Dynamics
MHCII	NA	NA	Urothelial (a)	CPI-Dynamics
CD8A	1.09962135	0.635744948	Melanoma (a)	CPI-Dynamics
CD274	0.9331953	0.610254669	Melanoma (a)	CPI-Dynamics
CXCL9	1.15597835	0.468684888	Melanoma (a)	CPI-Dynamics
CYT	1.05900189	0.822715565	Melanoma (a)	CPI-Dynamics
MHCI	0.971503	0.78415664	Melanoma (a)	CPI-Dynamics
T.Effector	1.08817815	0.900967465	Melanoma (a)	CPI-Dynamics
POPLAR	1.15273514	0.635744948	Melanoma (a)	CPI-Dynamics
Chemokine	0.93789834	0.438307769	Melanoma (a)	CPI-Dynamics

Cell_Prolif	7.78618294	0.027868117	Melanoma (a)	CPI-Dynamics
Stroma_EMT	0.75910286	0.600480529	Melanoma (a)	CPI-Dynamics
Pan_F_TBRS	0.70873756	0.500128141	Melanoma (a)	CPI-Dynamics
IFNg	1.22183419	0.600480529	Melanoma (a)	CPI-Dynamics
IMPRES	1.0287712	0.532615743	Melanoma (a)	CPI-Dynamics
MHCII	1.14839034	0.822715565	Melanoma (a)	CPI-Dynamics
BCTGs	0.61627861	0.438307769	Melanoma (a)	CPI-Dynamics
CD8A	3.22023357	0.063983488	Melanoma (b)	CPI-Dynamics
CD274	2.34596799	0.210526316	Melanoma (b)	CPI-Dynamics
CXCL9	1.70934859	0.17131063	Melanoma (b)	CPI-Dynamics
CYT	2.57821707	0.109391125	Melanoma (b)	CPI-Dynamics
MHCI	2.72735996	0.210526316	Melanoma (b)	CPI-Dynamics
T.Effector	3.80558864	0.138286894	Melanoma (b)	CPI-Dynamics
POPLAR	2.90072548	0.138286894	Melanoma (b)	CPI-Dynamics
Chemokine	0.74304159	0.138286894	Melanoma (b)	CPI-Dynamics
Cell_Prolif	0.30893479	0.109391125	Melanoma (b)	CPI-Dynamics
Stroma_EMT	1.96206307	0.421052632	Melanoma (b)	CPI-Dynamics
Pan_F_TBRS	2.27628686	0.559339525	Melanoma (b)	CPI-Dynamics
IFNg	3.4203074	0.063983488	Melanoma (b)	CPI-Dynamics
IMPRES	1.12169641	0.109391125	Melanoma (b)	CPI-Dynamics
MHCII	2.19694914	0.210526316	Melanoma (b)	CPI-Dynamics
BCTGs	0.15344328	0.04747162	Melanoma (b)	CPI-Dynamics
CD8A	2.55991045	0.060601345	Shim_2020_Lung	CPI1000+
CD274	1.06671373	0.96600907	Shim_2020_Lung	CPI1000+
CXCL9	0.90990314	0.492740863	Shim_2020_Lung	CPI1000+
CYT	0.8874593	0.981355981	Shim_2020_Lung	CPI1000+
MHCI	2.57740472	0.058373285	Shim_2020_Lung	CPI1000+
T.Effector	4.44950418	0.069807953	Shim_2020_Lung	CPI1000+
POPLAR	1.27417683	0.891750365	Shim_2020_Lung	CPI1000+
Chemokine	1.02770701	0.503207583	Shim_2020_Lung	CPI1000+
Cell_Prolif	1.52038746	0.994516009	Shim_2020_Lung	CPI1000+
Stroma_EMT	3.13985768	0.17572877	Shim_2020_Lung	CPI1000+
Pan_F_TBRS	2.77035031	0.165437101	Shim_2020_Lung	CPI1000+
IFNg	0.84340227	0.769675743	Shim_2020_Lung	CPI1000+
IMPRES	1.09936487	0.103323065	Shim_2020_Lung	CPI1000+
MHCII	1.24940536	0.61005655	Shim_2020_Lung	CPI1000+
BCTGs	1.45607877	0.12199015	Shim_2020_Lung	CPI1000+
CD8A	1.77043179	0.257894737	Snyder_2014_Melanoma	CPI1000+
CD274	2.36508857	0.215789474	Snyder_2014_Melanoma	CPI1000+
CXCL9	1.59919049	0.215789474	Snyder_2014_Melanoma	CPI1000+
CYT	1.69141334	0.305263158	Snyder_2014_Melanoma	CPI1000+
MHCI	1.68517576	0.357894737	Snyder_2014_Melanoma	CPI1000+
T.Effector	1.94247824	0.257894737	Snyder_2014_Melanoma	CPI1000+
POPLAR	1.7679437	0.257894737	Snyder_2014_Melanoma	CPI1000+
Chemokine	0.85858061	0.415789474	Snyder_2014_Melanoma	CPI1000+
Cell_Prolif	0.59218368	0.689473684	Snyder_2014_Melanoma	CPI1000+

Stroma_EMT	1.43549834	0.545614035	Snyder_2014_Melanoma	CPI1000+
Pan_F_TBRS	3.86991125	0.215789474	Snyder_2014_Melanoma	CPI1000+
IFNg	1.54985968	0.415789474	Snyder_2014_Melanoma	CPI1000+
IMPRES	1.05394946	0.257894737	Snyder_2014_Melanoma	CPI1000+
MHCII	1.47971249	0.357894737	Snyder_2014_Melanoma	CPI1000+
BCTGs	0.64785276	0.545614035	Snyder_2014_Melanoma	CPI1000+
CD8A	1.20548728	0.387818572	Snyder_2017_Bladder	CPI1000+
CD274	1.42374421	0.369090966	Snyder_2017_Bladder	CPI1000+
CXCL9	1.27556663	0.294696818	Snyder_2017_Bladder	CPI1000+
CYT	1.21644909	0.45549259	Snyder_2017_Bladder	CPI1000+
MHCI	1.30628432	0.535259718	Snyder_2017_Bladder	CPI1000+
T.Effector	1.46358101	0.400257998	Snyder_2017_Bladder	CPI1000+
POPLAR	1.23999365	0.584571723	Snyder_2017_Bladder	CPI1000+
Chemokine	0.99118887	0.971018232	Snyder_2017_Bladder	CPI1000+
Cell_Prolif	1.13934418	0.913123495	Snyder_2017_Bladder	CPI1000+
Stroma_EMT	0.83232325	0.535259718	Snyder_2017_Bladder	CPI1000+
Pan_F_TBRS	0.92626725	0.855744754	Snyder_2017_Bladder	CPI1000+
IFNg	1.19632084	0.584571723	Snyder_2017_Bladder	CPI1000+
IMPRES	1.02741959	0.487960096	Snyder_2017_Bladder	CPI1000+
MHCII	1.50109728	0.400257998	Snyder_2017_Bladder	CPI1000+
BCTGs	2.1515785	0.487960096	Snyder_2017_Bladder	CPI1000+
CD8A	1.13803019	0.498343009	Vanallen_2015_Melanoma	CPI1000+
CD274	0.96038561	0.985399544	Vanallen_2015_Melanoma	CPI1000+
CXCL9	1.13117775	0.578400393	Vanallen_2015_Melanoma	CPI1000+
CYT	1.24635097	0.418650177	Vanallen_2015_Melanoma	CPI1000+
MHCI	1.42742502	0.378068904	Vanallen_2015_Melanoma	CPI1000+
T.Effector	1.33112042	0.240162352	Vanallen_2015_Melanoma	CPI1000+
POPLAR	1.28419373	0.358679578	Vanallen_2015_Melanoma	CPI1000+
Chemokine	0.91852129	0.43982457	Vanallen_2015_Melanoma	CPI1000+
Cell_Prolif	2.05033277	0.198560335	Vanallen_2015_Melanoma	CPI1000+
Stroma_EMT	1.25935532	0.843989024	Vanallen_2015_Melanoma	CPI1000+
Pan_F_TBRS	1.32496814	0.554011761	Vanallen_2015_Melanoma	CPI1000+
IFNg	1.10815212	0.603257656	Vanallen_2015_Melanoma	CPI1000+
IMPRES	1.01009787	0.733771031	Vanallen_2015_Melanoma	CPI1000+
MHCII	1.07027016	0.872094333	Vanallen_2015_Melanoma	CPI1000+
BCTGs	1.43101492	0.43982457	Vanallen_2015_Melanoma	CPI1000+
CD8A	1.4870418	0.282046498	Breast	CPI-Dynamics
CD274	1.42917216	0.521022175	Breast	CPI-Dynamics
CXCL9	1.05911386	0.753573747	Breast	CPI-Dynamics

CYT	1.56702404	0.133790658	Breast	CPI-Dynamics
MHCI	0.99623319	0.974974275	Breast	CPI-Dynamics
T.Effector	1.73100266	0.254192057	Breast	CPI-Dynamics
POPLAR	1.46234368	0.35999837	Breast	CPI-Dynamics
Chemokine	0.89004654	0.254192057	Breast	CPI-Dynamics
Cell_Prolif	0.98598199	0.925016873	Breast	CPI-Dynamics
Stroma_EMT	1.0014955	0.974974275	Breast	CPI-Dynamics
Pan_F_TBRS	1.12902949	0.925016873	Breast	CPI-Dynamics
IFNg	1.08360875	0.875340418	Breast	CPI-Dynamics
IMPRES	1.05083958	0.151740757	Breast	CPI-Dynamics
MHCII	0.95970483	0.94997214	Breast	CPI-Dynamics
BCTGs	0.36055135	0.171376061	Breast	CPI-Dynamics
CD8A	1.08073301	0.730335345	Pan-cancer	CPI-Dynamics
CD274	1.71806477	0.169911967	Pan-cancer	CPI-Dynamics
CXCL9	1.43975626	0.117617431	Pan-cancer	CPI-Dynamics
CYT	1.25828621	0.596740946	Pan-cancer	CPI-Dynamics
MHCI	1.7135558	0.419546808	Pan-cancer	CPI-Dynamics
T.Effector	1.25237887	0.50420465	Pan-cancer	CPI-Dynamics
POPLAR	1.26223598	0.565080878	Pan-cancer	CPI-Dynamics
Chemokine	1.1777488	0.106667008	Pan-cancer	CPI-Dynamics
Cell_Prolif	0.77157136	0.836238633	Pan-cancer	CPI-Dynamics
Stroma_EMT	3.65478281	0.023658256	Pan-cancer	CPI-Dynamics
Pan_F_TBRS	4.60938583	0.030770598	Pan-cancer	CPI-Dynamics
IFNg	1.30015298	0.185247205	Pan-cancer	CPI-Dynamics
IMPRES	1.04553551	0.218808203	Pan-cancer	CPI-Dynamics
MHCII	1.87662753	0.117617431	Pan-cancer	CPI-Dynamics
BCTGs	0.39836765	0.050221385	Pan-cancer	CPI-Dynamics

Supplementary Table 3: On-therapy Meta-analysis results across the CPI-Dynamics Cohort

Signature	OR	Meta_Pval
CXCR6	1.871012808	0.00039963
CD27	2.104834837	2.51E-05
CD69	1.722456266	0.000799152
CD8B	1.839082099	0.000415132
GZMA	1.663655143	0.001130337
GZMK	1.713323435	0.000171436
HAVCR2	1.831092963	0.005522387
ICOS	1.636093942	0.003766034
ENTPD1	1.552975769	0.10676932
EOMES	1.866750098	0.000664883
LAG3	1.535181409	0.01098131
PDCD1	1.807679224	0.001100671
CTLA4	1.452947707	0.021175073
TBX21	2.270518334	0.000307242
TIGIT	1.726905207	0.002152139
ZAP70	NA	NA
CD8_Exhaustion	1.745041983	0.006032447

Supplementary Table 4: On-therapy Odds ratio results per dataset (CPI-Dynamics cohort)

Signatures	OR	P_Val	Studies
CXCR6	1.653108342	0.730769231	Urothelial (b)
ICOS	0.636983757	0.533799534	Urothelial (b)
HAVCR2	0.952594626	0.234265734	Urothelial (b)
CTLA4	0.850835239	0.945221445	Urothelial (b)
LAG3	1.957953387	0.533799534	Urothelial (b)
TIGIT	1.651692857	0.835664336	Urothelial (b)
CD69	1.027376471	0.730769231	Urothelial (b)
ENTPD1	0.659152511	0.730769231	Urothelial (b)
CD27	1.451098381	0.365967366	Urothelial (b)
EOMES	1.227438754	0.628205128	Urothelial (b)
TBX21	3.501335027	0.445221445	Urothelial (b)
PDCD1	0.773173847	0.835664336	Urothelial (b)
CD8B	7.46761438	0.945221445	Urothelial (b)
GZMA	1.13178734	1	Urothelial (b)
GZMK	0.881387435	0.628205128	Urothelial (b)
ZAP70	2.56710286	0.445221445	Urothelial (b)
CD8_Exhaustion	0.8573509	0.730769231	Urothelial (b)
CXCR6	6.126799666	0.001620728	Urothelial (a)
ICOS	2.668504477	0.023693012	Urothelial (a)
HAVCR2	1.68806368	0.330175663	Urothelial (a)
CTLA4	2.027729191	0.097262288	Urothelial (a)
LAG3	1.507312548	0.539952836	Urothelial (a)
TIGIT	2.84833206	0.077399122	Urothelial (a)
CD69	2.087935281	0.02041894	Urothelial (a)
ENTPD1	1.861815068	0.217081189	Urothelial (a)
CD27	2.369693892	0.036227052	Urothelial (a)
EOMES	3.510157782	0.014993477	Urothelial (a)
TBX21	5.417513872	0.023693012	Urothelial (a)
PDCD1	1.709570535	0.287269597	Urothelial (a)
CD8B	4.705238231	0.048548617	Urothelial (a)
GZMA	1.624013461	0.023693012	Urothelial (a)
GZMK	2.729165024	0.003022976	Urothelial (a)
ZAP70	3.323718595	0.010835913	Urothelial (a)
CD8_Exhaustion	1.769967433	0.148444247	Urothelial (a)
CXCR6	1.665220759	0.201095624	Melanoma (a)
ICOS	1.75931078	0.073642605	Melanoma (a)
HAVCR2	1.644098787	0.657592598	Melanoma (a)
CTLA4	1.352729244	0.286308657	Melanoma (a)
LAG3	1.43797114	0.31925664	Melanoma (a)
TIGIT	1.597366526	0.155091286	Melanoma (a)
CD69	1.747200901	0.135100597	Melanoma (a)
ENTPD1	1.216465131	0.864849872	Melanoma (a)

CD27	1.778976304	0.086500837	Melanoma (a)
EOMES	1.489371147	0.354324547	Melanoma (a)
TBX21	1.783674437	0.233837277	Melanoma (a)
PDCD1	2.01583	0.06234955	Melanoma (a)
CD8B	1.652358049	0.177003774	Melanoma (a)
GZMA	1.681479884	0.135100597	Melanoma (a)
GZMK	1.550844054	0.100924247	Melanoma (a)
ZAP70	1.447700057	0.155091286	Melanoma (a)
CD8_Exhaustion	1.91050777	0.155091286	Melanoma (a)
CXCR6	1.663496883	0.210526316	Melanoma (b)
ICOS	1.121624386	0.957688338	Melanoma (b)
HAVCR2	2.059221698	0.253869969	Melanoma (b)
CTLA4	1.08756994	0.792569659	Melanoma (b)
LAG3	1.438442014	0.421052632	Melanoma (b)
TIGIT	1.528717382	0.487100103	Melanoma (b)
CD69	1.373865709	0.467200815	Melanoma (b)
ENTPD1	1.003836292	0.957688338	Melanoma (b)
CD27	2.001086544	0.210526316	Melanoma (b)
EOMES	1.459637136	0.559339525	Melanoma (b)
TBX21	2.161115088	0.253869969	Melanoma (b)
PDCD1	1.737047759	0.210526316	Melanoma (b)
CD8B	1.638519143	0.198337204	Melanoma (b)
GZMA	1.680490263	0.253869969	Melanoma (b)
GZMK	1.724497081	0.138286894	Melanoma (b)
ZAP70	2.198393654	0.131041303	Melanoma (b)
CD8_Exhaustion	1.862774937	0.17131063	Melanoma (b)
CXCR6	4.221242768	0.035652174	Breast
ICOS	2.981894158	0.072173913	Breast
HAVCR2	24.5384959	0.013913043	Breast
CTLA4	6.660360867	0.02	Breast
LAG3	9.641925946	0.009565217	Breast
TIGIT	10.79956478	0.02	Breast
CD69	1.845399225	0.23826087	Breast
ENTPD1	20.10549907	0.151304348	Breast
CD27	2.57451459	0.072173913	Breast
EOMES	2.77646845	0.05826087	Breast
TBX21	18.72494423	0.088695652	Breast
PDCD1	21.89559609	0.021442108	Breast
CD8B	2.008474295	0.088695652	Breast
GZMA	3.394087471	0.02	Breast
GZMK	2.350608975	0.088695652	Breast
ZAP70	2.521560348	0.046086957	Breast
CXCR6	1.61969001	0.117617431	Pan-Cancer
ICOS	1.570129343	0.117617431	Pan-Cancer
HAVCR2	1.902266827	0.08710619	Pan-Cancer
CTLA4	1.546488658	0.155501053	Pan-Cancer

LAG3	1.51034443	0.218808203	Pan-Cancer
TIGIT	1.642566639	0.129381805	Pan-Cancer
CD69	2.115823483	0.050221385	Pan-Cancer
ENTPD1	2.990501065	0.106667008	Pan-Cancer
CD27	2.782124922	0.00301832	Pan-Cancer
EOMES	1.878637336	0.030770598	Pan-Cancer
TBX21	2.046482943	0.034929544	Pan-Cancer
PDCD1	1.849042372	0.05636293	Pan-Cancer
CD8B	1.857646302	0.070431109	Pan-Cancer
GZMA	1.728959776	0.070431109	Pan-Cancer
GZMK	1.694060052	0.04462145	Pan-Cancer
ZAP70	2.602432641	0.006115575	Pan-Cancer
CD8_Exhaustion	1.766053565	0.096512086	Pan-Cancer

Supplementary Table 5: Breast cancer genes comprising the various gene categories

Gene_symbol	ENTREZID	Category
ADGRE1	2015	Response_pos
APOL6	80830	Response_pos
AQP9	366	Response_pos
B2M	567	Response_pos
C1QA	712	Response_pos
C1QB	713	Response_pos
C2	717	Response_pos
CASP1	834	Response_pos
CCL3	6348	Response_pos
CCL5	6352	Response_pos
CCL8	6355	Response_pos
CCR5	1234	Response_pos
CD2	914	Response_pos
CD244	51744	Response_pos
CD247	919	Response_pos
CD27	939	Response_pos
CD274	29126	Response_pos
CD300A	11314	Response_pos
CD38	952	Response_pos
CD3D	915	Response_pos
CD3E	916	Response_pos
CD3G	917	Response_pos
CD4	920	Response_pos
CD40	958	Response_pos
CD48	962	Response_pos
CD5	921	Response_pos
CD69	969	Response_pos
CD7	924	Response_pos
CD80	941	Response_pos
CD8A	925	Response_pos
CD96	10225	Response_pos
CLEC7A	64581	Response_pos
CTSS	1520	Response_pos
CTSW	1521	Response_pos
CXCL10	3627	Response_pos
CXCL11	6373	Response_pos
CXCL13	10563	Response_pos
CXCL9	4283	Response_pos
CXCR6	10663	Response_pos
CYBB	1536	Response_pos
EOMES	8320	Response_pos

FASLG	356	Response_pos
FCGR1A	2209	Response_pos
FCGR3A	2214	Response_pos
GBP1	2633	Response_pos
GBP4	115361	Response_pos
GIMAP4	55303	Response_pos
GZMA	3001	Response_pos
GZMB	3002	Response_pos
GZMH	2999	Response_pos
GZMK	3003	Response_pos
GZMM	3004	Response_pos
H2AX	3014	Response_pos
HCK	3055	Response_pos
HDC	3067	Response_pos
HLA-A	3105	Response_pos
HLA-B	3106	Response_pos
HLA-C	3107	Response_pos
HLA-DMA	3108	Response_pos
HLA-DOB	3112	Response_pos
HLA-E	3133	Response_pos
HSD11B1	3290	Response_pos
ICAM1	3383	Response_pos
ICAM3	3385	Response_pos
ICOS	29851	Response_pos
IL10RA	3587	Response_pos
IL12RB2	3595	Response_pos
IL18	3606	Response_pos
IL1B	3553	Response_pos
IL21R	50615	Response_pos
IL2RA	3559	Response_pos
IL2RB	3560	Response_pos
IL2RG	3561	Response_pos
IL32	9235	Response_pos
IRF1	3659	Response_pos
IRF2	3660	Response_pos
IRF3	3661	Response_pos
IRF5	3663	Response_pos
ITGAL	3683	Response_pos
ITGAX	3687	Response_pos
ITGB2	3689	Response_pos
JAK2	3717	Response_pos
JAK3	3718	Response_pos
KLRD1	3824	Response_pos
KLRK1	22914	Response_pos
LAIR1	3903	Response_pos
LCK	3932	Response_pos

LILRA1	11024	Response_pos
LILRB2	10288	Response_pos
LILRB4	11006	Response_pos
LYZ	4069	Response_pos
MAGEB2	4113	Response_pos
MAP3K12	7786	Response_pos
NFAM1	150372	Response_pos
NFKBIE	4794	Response_pos
NKG7	4818	Response_pos
NLRC5	84166	Response_pos
NOD2	64127	Response_pos
P2RY13	53829	Response_pos
PARP4	143	Response_pos
PDCD1	5133	Response_pos
PDCD1LG2	80380	Response_pos
PIK3CD	5293	Response_pos
PPARG	5468	Response_pos
PRF1	5551	Response_pos
PSMB10	5699	Response_pos
PSMB8	5696	Response_pos
PSMB9	5698	Response_pos
PTGER4	5734	Response_pos
REN	5972	Response_pos
RIPK3	11035	Response_pos
SERPINA1	5265	Response_pos
SH2D1A	4068	Response_pos
SIRPB2	284759	Response_pos
SLAMF7	57823	Response_pos
STAT1	6772	Response_pos
STAT4	6775	Response_pos
TAPBP	6892	Response_pos
TAPBPL	55080	Response_pos
TIGIT	201633	Response_pos
TLR1	7096	Response_pos
TLR4	7099	Response_pos
TLR7	51284	Response_pos
TLR8	51311	Response_pos
TMEM140	55281	Response_pos
TNF	7124	Response_pos
TNFAIP3	7128	Response_pos
TNFRSF14	8764	Response_pos
TNFRSF1B	7133	Response_pos
TNFRSF9	3604	Response_pos
TP53	7157	Response_pos
TRAT1	50852	Response_pos
XCL1	6375	Response_pos

XCL2	6846	Response_pos
ZAP70	7535	Response_pos
ANGPT2	285	Response_Neg
COL4A5	1287	Response_Neg
ERBB2	2064	Response_Neg
ICAM5	7087	Response_Neg
NRAS	4893	Response_Neg
PIK3R2	5296	Response_Neg
THBS1	7057	Response_Neg
BNIP3L	665	Resistance_Pos
BRCA2	675	Resistance_Pos
CD58	965	Resistance_Pos
IER3	8870	Resistance_Pos
MRE11	4361	Resistance_Pos
S100A8	6279	Resistance_Pos
S100A9	6280	Resistance_Pos
CDH5	1003	Resistance_Neg
GPC4	2239	Resistance_Neg
ITPK1	3705	Resistance_Neg
LRRC32	2615	Resistance_Neg
MMRN2	79812	Resistance_Neg
MYCT1	80177	Resistance_Neg

Supplmentary Table 6. Response Pos/Neg genes across all CPI-Dyanamics cohorts (subsetting on nanostring 778 gene panel)

Gene	Breast Pos	Breast Neg	Mel (a) Pos	Mel (a) Neg	Mel (b) Pos	Mel (b) Neg	Uro (a) Pos	Uro (a) Neg	Uro (b) Pos	Uro (b) Neg
A2M	0	0	0	0	0	0	1	0	0	0
ACVR1C	0	0	0	0	0	0	0	1	0	0
ADGRE1	1	0	1	0	0	0	0	0	0	0
ADM	0	0	0	0	0	0	1	0	0	0
ANGPT2	0	1	0	0	0	1	0	0	0	0
APLNR	0	0	1	0	0	0	0	0	0	0
APOE	0	0	0	0	1	0	0	0	1	0
APOL6	1	0	0	0	0	0	0	1	0	0
AQP9	1	0	0	0	0	0	0	0	0	0
ARID1A	0	0	0	0	0	0	0	1	0	0
AXIN1	0	0	0	0	1	0	0	0	0	0
AXL	0	0	0	0	0	0	1	0	0	0
B2M	1	0	0	0	0	0	0	0	0	0
BAD	0	0	0	0	0	0	0	0	0	1
BAMBI	0	0	0	1	0	0	0	0	0	0
BBC3	0	0	0	0	0	0	0	1	0	0
BCAT1	0	0	0	0	0	0	1	0	0	0
BCL2	0	0	0	0	0	0	0	0	1	0
BCL6B	0	0	0	0	0	0	1	0	0	0
BID	0	0	1	0	0	0	0	0	0	1
BIRC5	0	0	0	0	0	0	0	0	0	1
BNIP3L	0	0	0	0	0	0	1	0	0	0
BRCA1	0	0	0	0	0	1	0	0	0	1
BRD4	0	0	0	0	0	1	0	0	0	0
BRIP1	0	0	0	0	0	0	0	0	0	1
C1QA	1	0	0	0	0	0	0	0	0	0
C1QB	1	0	0	0	0	0	0	0	0	0
C2	1	0	0	0	0	0	0	0	0	0
CASP1	1	0	0	0	0	1	0	0	0	0
CASP3	0	0	0	0	0	0	0	0	0	1
CASP8	0	0	0	0	0	0	0	1	0	0
CCL14	0	0	1	0	0	0	0	0	0	0
CCL20	0	0	0	0	1	0	0	0	0	1
CCL22	0	0	1	0	0	0	0	0	0	0
CCL3	1	0	0	0	0	0	0	0	0	0
CCL5	1	0	0	0	0	0	0	0	0	0
CCL8	1	0	0	0	0	0	0	1	0	0
CCNB1	0	0	0	0	0	0	0	0	0	1
CCND2	0	0	0	0	0	0	1	0	0	0
CCNO	0	0	0	0	0	0	0	0	0	1
CCR2	0	0	1	0	0	0	0	0	0	0

CCR4	0	0	1	0	0	0	0	0	0	0
CCR5	1	0	0	0	0	0	0	0	0	0
CD19	0	0	1	0	0	0	0	0	0	0
CD1C	0	0	0	0	0	0	1	0	0	0
CD2	1	0	0	0	0	0	0	0	0	0
CD244	1	0	0	0	0	0	0	0	0	0
CD247	1	0	0	0	0	0	0	0	1	0
CD27	1	0	0	0	0	0	0	0	0	0
CD274	1	0	0	0	0	0	0	1	0	0
CD300A	1	0	0	0	0	0	0	0	0	0
CD38	1	0	0	0	0	0	0	0	0	0
CD3D	1	0	0	0	0	0	0	0	0	0
CD3E	1	0	0	0	0	0	0	0	0	0
CD3G	1	0	0	0	0	0	0	0	0	0
CD4	1	0	0	0	0	0	0	0	0	0
CD40	1	0	0	0	0	0	0	0	0	0
CD40LG	0	0	1	0	0	0	0	0	0	0
CD47	0	0	0	0	0	0	0	1	0	0
CD48	1	0	0	0	0	0	0	0	0	0
CD5	1	0	1	0	0	0	0	0	0	0
CD69	1	0	0	0	0	0	0	0	0	0
CD7	1	0	0	0	0	0	0	0	0	0
CD80	1	0	0	0	0	0	0	0	0	0
CD8A	1	0	0	0	0	0	0	0	0	0
CD96	1	0	0	0	0	0	0	0	0	0
CDC20	0	0	0	0	0	0	0	0	0	1
CDC6	0	0	0	0	0	1	0	0	0	1
CDH1	0	0	0	0	0	1	0	0	0	1
CDH2	0	0	0	0	0	0	1	0	0	0
CDH3	0	0	0	0	0	1	0	1	0	0
CDH5	0	0	0	0	0	0	1	0	0	0
CDK2	0	0	0	1	0	1	0	0	0	0
CDKN1C	0	0	0	0	0	0	1	0	0	0
CDKN2A	0	0	0	0	0	0	0	1	0	0
CENPF	0	0	0	0	0	0	0	1	0	1
CEP55	0	0	0	0	0	0	0	1	0	0
CES3	0	0	0	0	1	0	0	0	0	0
CGAS	0	0	0	0	0	0	0	1	0	0
CHUK	0	0	0	1	0	1	0	1	0	0
CLEC14A	0	0	0	0	0	0	1	0	0	0
CLEC7A	1	0	0	0	0	0	0	0	0	0
CNTFR	0	0	0	0	0	0	1	0	0	0
COL11A2	0	0	0	0	0	0	0	1	0	0
COL4A5	0	1	0	0	0	0	0	0	0	0
COL5A1	0	0	0	0	0	0	0	0	1	0
CPA3	0	0	0	0	0	0	1	0	0	0

CSF1	0	0	1	0	0	0	0	0	0	0
CSF2	0	0	0	0	0	0	0	1	0	0
CST2	0	0	0	0	0	1	0	0	0	1
CTNNB1	0	0	0	0	0	1	0	0	0	0
CTSS	1	0	0	0	0	0	0	0	0	0
CTSW	1	0	0	0	0	0	0	0	0	0
CX3CL1	0	0	1	0	0	0	0	0	0	0
CX3CR1	0	0	1	0	0	0	0	0	0	0
CXCL1	0	0	0	0	0	0	0	0	0	1
CXCL10	1	0	0	0	0	0	0	1	0	0
CXCL11	1	0	0	0	0	0	0	1	0	0
CXCL13	1	0	1	0	0	0	0	0	0	0
CXCL6	0	0	0	0	0	0	0	1	0	0
CXCL9	1	0	0	0	0	0	0	1	0	0
CXCR2	0	0	0	1	0	0	0	0	0	0
CXCR3	0	0	1	0	0	0	0	0	0	0
CXCR6	1	0	0	0	0	0	0	0	0	0
CYBB	1	0	0	0	0	0	0	0	0	0
DAB2	0	0	0	0	0	0	1	0	0	0
DIPK2B	0	0	0	0	0	0	1	0	0	0
DLL1	0	0	0	0	0	0	1	0	0	0
DLL4	0	0	0	0	0	0	1	0	0	0
DPP4	0	0	1	0	0	0	0	0	0	0
DTX3L	0	0	0	0	0	0	0	1	0	0
DTX4	0	0	0	0	0	0	0	0	0	1
DUSP2	0	0	1	0	0	0	1	0	0	0
EGFR	0	0	1	0	0	0	0	0	0	0
EIF2AK2	0	0	0	0	0	0	0	0	0	1
EIF4EBP1	0	0	0	1	0	0	0	0	0	0
EIF5AL1	0	0	0	0	0	1	0	1	0	0
ENTPD1	0	0	1	0	0	0	0	0	0	0
EOMES	1	0	0	0	0	0	0	0	0	0
EPCAM	0	0	0	0	0	0	0	0	0	1
ERBB2	0	1	0	0	0	0	0	0	0	0
ESR1	0	0	1	0	0	0	0	0	0	0
EXO1	0	0	0	0	0	1	0	0	0	1
F2RL1	0	0	0	0	0	0	0	1	0	0
FAM30A	0	0	1	0	0	0	0	0	0	0
FASLG	1	0	0	0	0	0	0	0	0	0
FCGR1A	1	0	0	0	0	0	0	0	0	0
FCGR3A	1	0	0	0	0	0	0	1	0	0
FCGR3B	0	0	0	0	0	0	0	1	0	0
FCGRT	0	0	1	0	1	0	1	0	1	0
FCN1	0	0	1	0	0	0	0	0	0	0
FGF13	0	0	0	1	0	0	1	0	0	0
FGF9	0	0	0	0	0	0	1	0	0	0

FGFR1	0	0	0	0	0	0	0	0	1	0
FOXP3	0	0	1	0	0	0	0	0	0	0
FSTL3	0	0	0	1	0	0	1	0	0	0
FZD9	0	0	0	0	0	1	0	0	0	0
GBP1	1	0	0	0	0	0	0	0	0	0
GBP2	0	0	0	0	0	0	0	1	0	0
GBP4	1	0	0	0	0	0	0	1	0	0
GIMAP4	1	0	1	0	0	0	0	0	0	0
GIMAP6	0	0	0	0	0	0	0	0	1	0
GLI1	0	0	0	0	0	0	1	0	0	0
GLUD1	0	0	0	0	0	1	0	0	0	0
GPC4	0	0	0	0	0	0	1	0	0	0
GPR160	0	0	0	0	0	0	0	0	0	1
GPSM3	0	0	0	0	0	0	0	0	1	0
GZMA	1	0	0	0	0	0	0	0	0	0
GZMB	1	0	0	0	0	0	0	0	0	0
GZMH	1	0	0	0	0	0	0	0	0	0
GZMK	1	0	0	0	0	0	0	0	0	0
GZMM	1	0	0	0	0	0	0	0	1	0
H2AX	1	0	0	0	0	0	0	0	0	0
HCK	1	0	0	0	0	0	0	0	0	0
HDAC11	0	0	0	0	1	0	0	0	0	0
HDAC4	0	0	0	0	0	0	1	0	1	0
HDAC5	0	0	0	0	0	0	0	0	1	0
HDC	1	0	0	0	0	0	1	0	1	0
HERC6	0	0	0	0	0	0	0	1	0	1
HLA-A	1	0	0	0	0	0	0	0	0	0
HLA-B	1	0	0	0	0	0	0	0	0	0
HLA-C	1	0	0	0	0	0	0	0	0	0
HLA-DMA	1	0	0	0	0	0	0	0	0	0
HLA-DOB	1	0	1	0	0	0	0	0	0	0
HLA-E	1	0	0	0	0	0	0	0	1	0
HSD11B1	1	0	0	0	0	0	0	0	0	0
ICAM1	1	0	0	0	0	0	0	0	0	0
ICAM2	0	0	0	0	0	0	1	0	0	0
ICAM3	1	0	1	0	0	0	0	0	0	0
ICAM5	0	1	0	0	0	0	0	0	0	0
ICOS	1	0	0	0	0	0	0	0	0	0
ID4	0	0	0	0	0	0	1	0	0	0
IFI27	0	0	1	0	0	0	0	0	0	0
IFI35	0	0	1	0	0	0	0	1	0	0
IFI6	0	0	0	0	0	0	0	1	0	0
IFIH1	0	0	1	0	0	0	0	1	0	0
IFIT1	0	0	0	0	0	0	0	1	0	1
IFIT2	0	0	0	0	0	0	0	1	0	0
IFIT3	0	0	0	0	0	0	0	1	0	0

IFITM1	0	0	1	0	0	0	0	0	0	0
IFITM2	0	0	1	0	0	0	0	0	0	0
IFNG	0	0	0	0	0	0	0	1	0	0
IFNGR2	0	0	0	0	0	0	0	0	0	1
IKBKG	0	0	0	0	1	0	0	0	0	0
IL10	0	0	1	0	0	0	0	0	0	0
IL10RA	1	0	1	0	0	0	0	0	0	0
IL11RA	0	0	0	0	0	0	1	0	1	0
IL12RB2	1	0	0	0	0	0	0	1	0	0
IL18	1	0	0	0	0	0	0	0	0	0
IL18R1	0	0	1	0	1	0	0	0	0	0
IL1A	0	0	0	0	0	0	0	1	0	0
IL1B	1	0	0	0	0	0	0	0	0	0
IL21R	1	0	0	0	0	0	0	1	0	0
IL2RA	1	0	0	0	0	0	0	0	0	0
IL2RB	1	0	0	0	0	0	0	0	0	0
IL2RG	1	0	0	0	0	0	0	0	0	0
IL32	1	0	0	0	0	0	0	0	0	0
IL34	0	0	0	0	0	0	0	0	1	0
IRF1	1	0	0	0	0	0	0	1	0	0
IRF2	1	0	0	0	0	0	0	1	0	0
IRF3	1	0	1	0	1	0	0	0	0	0
IRF5	1	0	1	0	0	0	0	0	0	0
IRF7	0	0	1	0	0	0	0	1	0	0
IRF8	0	0	1	0	0	0	0	0	0	0
IRF9	0	0	0	0	0	0	0	1	0	0
ITGA2	0	0	0	0	0	0	0	1	0	0
ITGAE	0	0	0	0	0	0	0	1	0	0
ITGAL	1	0	0	0	0	0	0	0	0	0
ITGAX	1	0	1	0	0	0	0	0	0	0
ITGB2	1	0	0	0	0	0	0	0	0	0
ITGB3	0	0	0	0	0	0	1	0	0	0
JAK2	1	0	0	0	0	0	0	0	0	0
JAK3	1	0	1	0	0	0	0	0	0	0
KAT2B	0	0	0	0	0	1	0	0	0	0
KDR	0	0	1	0	0	0	0	0	0	0
KIR3DL2	0	0	1	0	0	0	0	0	0	0
KIT	0	0	0	0	0	0	1	0	0	0
KLRB1	0	0	1	0	0	0	0	0	0	0
KLRD1	1	0	0	0	0	0	0	0	0	0
KLRK1	1	0	1	0	0	0	0	0	0	0
KRAS	0	0	0	0	0	0	0	1	0	1
KRT5	0	0	0	0	0	0	0	1	0	1
LAIR1	1	0	0	0	0	0	0	0	0	0
LAMA1	0	0	0	1	0	0	0	0	0	0
LAMC2	0	0	0	0	0	0	0	1	0	0

LCK	1	0	0	0	0	0	0	0	0	0
LDHA	0	0	0	1	0	0	0	0	0	0
LILRA1	1	0	1	0	0	0	0	0	0	0
LILRB2	1	0	0	0	0	0	0	0	0	0
LILRB4	1	0	0	0	0	0	0	0	0	0
LOXL2	0	0	0	0	0	0	1	0	0	0
LRRC32	0	0	0	0	0	0	0	0	1	0
LTB	0	0	1	0	0	0	0	0	0	0
LTBP1	0	0	0	0	0	0	1	0	0	0
LY9	0	0	1	0	0	0	0	0	0	0
LYZ	1	0	1	0	0	0	0	0	0	0
MAGEA1	0	0	0	0	0	0	0	1	0	0
MAGEA12	0	0	0	0	0	0	0	1	0	0
MAGEA3	0	0	0	1	0	0	0	1	0	1
MAGEA6	0	0	0	0	0	0	0	1	0	0
MAGEB2	1	0	0	0	0	0	0	0	0	0
MAML2	0	0	0	0	0	0	1	0	0	0
MAP3K12	1	0	0	0	0	0	1	0	1	0
MARCO	0	0	1	0	1	0	0	0	0	0
MFNG	0	0	1	0	0	0	0	0	1	0
MGMT	0	0	0	0	0	0	0	0	1	0
MICB	0	0	0	0	0	0	0	1	0	0
MLANA	0	0	0	1	0	0	0	0	0	0
MLH1	0	0	0	0	0	1	0	0	0	0
MMP11	0	0	1	0	0	0	0	1	0	0
MMP7	0	0	0	0	0	0	0	0	0	1
MMRN2	0	0	1	0	0	0	0	0	0	0
MS4A2	0	0	0	0	0	0	1	0	0	0
MSH2	0	0	0	0	0	1	0	0	0	0
MTOR	0	0	0	0	0	1	0	0	0	0
MX1	0	0	1	0	0	0	0	1	0	1
MYC	0	0	0	1	0	1	1	0	0	0
MYD88	0	0	1	0	0	0	0	1	0	0
NDC80	0	0	0	0	0	0	0	1	0	0
NDUFA4L2	0	0	1	0	0	0	0	0	0	0
NECTIN1	0	0	0	0	0	0	0	0	0	1
NECTIN2	0	0	1	0	0	0	0	0	0	0
NFAM1	1	0	0	0	0	0	0	0	0	0
NFATC2	0	0	1	0	0	0	0	0	0	0
NFKBIE	1	0	0	0	0	1	0	0	0	0
NKG7	1	0	0	0	0	0	0	0	1	0
NLRC5	1	0	0	0	0	0	0	0	0	0
NOD2	1	0	0	0	0	0	0	0	0	0
NRAS	0	1	0	0	0	0	0	0	0	0
NUF2	0	0	0	0	0	0	0	0	0	1
OAS1	0	0	0	0	0	0	0	0	0	1

OAS2	0	0	0	0	0	0	0	1	0	0
OASL	0	0	1	0	0	0	0	1	0	0
ORC6	0	0	0	0	0	0	0	0	0	1
OTOA	0	0	1	0	0	0	1	0	0	0
P2RY13	1	0	0	0	0	0	0	0	0	0
P4HA2	0	0	0	0	1	0	1	0	0	0
PARP12	0	0	0	0	0	0	0	1	0	0
PARP4	1	0	0	0	0	0	0	0	0	0
PARP9	0	0	1	0	0	0	0	1	0	0
PDCD1	1	0	0	0	1	0	0	0	0	0
PDCD1LG	1	0	0	0	0	0	0	0	0	0
PFKFB3	0	0	0	0	0	0	1	0	0	0
PIAS4	0	0	0	0	1	0	0	0	0	0
PIK3CA	0	0	0	0	0	0	0	1	0	0
PIK3CD	1	0	0	0	0	0	0	0	0	0
PIK3CG	0	0	1	0	0	0	0	0	0	0
PIK3R1	0	0	0	0	0	0	1	0	0	0
PIK3R2	0	1	0	0	0	0	0	0	0	0
PIK3R5	0	0	0	0	0	0	0	0	1	0
PLA1A	0	0	0	0	0	1	0	0	0	0
PMS2	0	0	0	1	0	0	0	0	0	0
PPARG	1	0	1	0	0	0	0	0	0	0
PRF1	1	0	0	0	0	0	0	0	0	0
PSMB10	1	0	0	0	0	0	0	1	0	0
PSMB5	0	0	0	1	0	1	0	0	0	0
PSMB8	1	0	0	0	0	0	0	1	0	0
PSMB9	1	0	0	0	0	0	0	1	0	0
PTGER4	1	0	1	0	0	0	0	0	0	0
PTPN11	0	0	0	0	0	1	0	1	0	0
PTTG1	0	0	0	1	0	0	0	1	0	1
PVRIG	0	0	1	0	0	0	0	0	0	0
RAD51C	0	0	0	1	0	0	0	1	0	0
RELA	0	0	0	0	0	0	0	1	0	0
REN	1	0	0	0	0	0	0	0	0	0
RICTOR	0	0	0	0	0	0	0	1	0	0
RIPK1	0	0	0	0	0	1	0	0	0	0
RIPK2	0	0	0	0	0	0	0	1	0	0
RIPK3	1	0	1	0	0	0	0	0	0	0
ROBO4	0	0	0	0	0	0	1	0	1	0
RORC	0	0	1	0	0	0	0	0	0	0
RPL23	0	0	0	1	0	0	0	0	0	0
RPL7A	0	0	0	1	0	0	0	0	0	0
RRM2	0	0	0	0	0	0	0	0	0	1
RSAD2	0	0	0	0	0	0	0	1	0	0
S100A8	0	0	0	0	0	0	0	1	0	0
SAMD9	0	0	0	0	0	0	0	1	0	0

SBNO2	0	0	0	0	0	0	0	1	0	0
SELL	0	0	1	0	0	0	0	0	0	0
SELP	0	0	0	0	0	0	1	0	0	0
SERPINA1	1	0	0	0	0	0	0	0	0	0
SFRP1	0	0	0	0	0	0	0	0	1	0
SFXN1	0	0	0	0	0	0	0	0	0	1
SH2D1A	1	0	0	0	0	0	0	0	0	0
SHC2	0	0	0	0	0	0	1	0	1	0
SIGLEC1	0	0	0	0	0	0	0	0	1	0
SIGLEC5	0	0	0	0	1	0	0	0	0	0
SIGLEC8	0	0	1	0	0	0	0	0	0	0
SIRPB2	1	0	0	0	0	0	0	0	0	0
SLAMF7	1	0	0	0	0	0	0	0	0	0
SLC16A1	0	0	0	1	0	0	0	0	0	0
SLC39A6	0	0	0	1	0	0	0	0	0	0
SLC7A5	0	0	0	1	0	0	0	1	0	0
SMAD5	0	0	0	1	0	0	0	0	0	0
SNCA	0	0	0	1	0	0	1	0	0	0
SOX10	0	0	0	1	0	0	1	0	0	0
SOX11	0	0	0	0	0	0	0	0	0	1
SOX2	0	0	0	0	0	0	0	0	0	1
SPRY4	0	0	0	0	0	1	0	0	0	0
SRP54	0	0	0	0	0	1	0	1	0	0
STAT1	1	0	0	0	0	0	0	1	0	0
STAT3	0	0	0	0	0	1	0	0	0	0
STAT4	1	0	1	0	0	0	0	0	0	0
TAP1	0	0	0	0	0	0	0	1	0	0
TAP2	0	0	0	0	0	0	0	1	0	0
TAPBP	1	0	0	0	0	0	0	0	0	0
TAPBPL	1	0	0	0	0	0	0	0	0	0
TGFB1	0	0	1	0	0	0	0	0	0	0
TGFB2	0	0	0	0	0	0	1	0	0	0
TGFBR2	0	0	0	0	0	0	1	0	0	0
THBS1	0	1	1	0	0	0	0	0	0	0
TICAM1	0	0	1	0	0	0	0	0	0	0
TIE1	0	0	0	0	0	0	0	0	1	0
TIGIT	1	0	0	0	0	0	0	0	0	0
TLR1	1	0	0	0	0	0	0	0	0	0
TLR3	0	0	0	0	0	0	0	1	0	0
TLR4	1	0	0	0	0	0	0	0	0	0
TLR7	1	0	0	0	0	0	0	0	0	0
TLR8	1	0	0	0	0	0	0	0	0	0
TMEM140	1	0	0	0	0	0	0	0	0	0
TMEM45B	0	0	0	0	0	0	0	0	0	1
TNF	1	0	0	0	0	0	0	0	0	0
TNFAIP3	1	0	0	0	0	0	0	0	0	0

TNFRSF1(	0	0	1	0	0	0	0	0	0	0
TNFRSF14	1	0	0	0	0	0	0	0	1	0
TNFRSF18	0	0	1	0	0	0	0	0	0	0
TNFRSF1E	1	0	0	0	0	0	0	0	0	0
TNFRSF25	0	0	0	0	0	0	0	1	0	0
TNFRSF8	0	0	1	0	0	0	0	0	0	0
TNFRSF9	1	0	0	0	0	0	0	0	0	0
TNFSF10	0	0	1	0	0	0	0	1	0	0
TNFSF12	0	0	0	0	0	0	0	0	1	0
TNFSF13	0	0	1	0	0	0	0	0	0	0
TP53	1	0	0	0	0	0	0	0	0	1
TPM1	0	0	0	0	0	0	0	0	1	0
TRAF1	0	0	1	0	0	0	0	0	0	0
TRAT1	1	0	0	0	0	0	0	0	0	0
TREM2	0	0	1	0	0	0	0	0	0	0
TRIM21	0	0	1	0	0	0	0	1	0	0
TSLP	0	0	0	0	0	0	1	0	0	0
TTC30A	0	0	0	0	0	0	0	0	0	1
TWF1	0	0	0	0	0	0	0	0	0	1
TYMP	0	0	0	0	0	0	0	1	0	0
TYMS	0	0	0	0	0	0	0	1	0	0
UBA7	0	0	0	0	0	0	0	0	1	0
UBE2C	0	0	0	0	0	0	0	0	0	1
UBE2T	0	0	0	0	0	0	0	1	0	1
ULBP2	0	0	0	1	0	0	0	1	0	1
VSIR	0	0	0	0	0	0	0	0	1	0
WDR76	0	0	0	0	0	0	0	0	0	1
WNT2B	0	0	0	0	0	0	1	0	0	0
XCL1	1	0	0	0	0	1	0	0	0	0
XCL2	1	0	1	0	0	0	0	0	0	0
ZAP70	1	0	1	0	0	0	0	0	0	0
ZC3H12A	0	0	1	0	0	0	0	0	0	0

Supplmentary Table 7. Resistance Pos/Neg genes across all CPI-Dyanamics cohorts (subsetting on nanostring 778 gene panel)

Gene	Breast Pos	Breast Neg	Mel (a) Pos	Mel (a) Neg	Mel (b) Pos	Mel (b) Neg	Uro (a) Pos	Uro (a) Neg	Uro (b) Pos	Uro (b) Neg
ADAM12	0	0	0	0	0	1	0	0	0	0
ADGRE1	0	0	0	0	0	0	0	0	0	1
ALDOC	0	0	0	0	0	0	0	1	0	0
ANGPT2	0	0	0	0	0	0	0	1	0	0
AQP9	0	0	0	0	0	0	1	0	0	0
AREG	0	0	0	0	1	0	0	0	1	0
ARG2	0	0	0	0	0	0	0	1	0	0
ARNT2	0	0	0	0	0	0	0	1	0	0
ATF3	0	0	0	0	1	0	0	0	0	0
B2M	0	0	0	0	0	0	1	0	0	0
BAMBI	0	0	0	0	0	0	0	1	0	0
BBC3	0	0	0	0	1	0	0	0	0	0
BBS1	0	0	0	0	0	0	0	1	0	0
BIRC3	0	0	0	0	1	0	1	0	0	0
BLM	0	0	1	0	0	0	0	0	0	0
BLVRA	0	0	1	0	0	0	0	0	0	0
BMP2	0	0	0	0	0	0	0	1	0	0
BNIP3	0	0	0	0	0	0	0	1	0	0
BNIP3L	1	0	0	0	0	0	0	0	0	0
BRCA2	1	0	0	0	0	0	0	0	0	0
BRD4	0	0	0	0	0	0	0	1	0	0
BTLA	0	0	0	0	0	0	1	0	0	0
CASP1	0	0	0	0	0	0	1	0	0	0
CASP9	0	0	0	0	0	0	0	1	0	0
CCL19	0	0	0	0	0	0	1	0	0	0
CCL2	0	0	0	0	0	0	1	0	0	0
CCL22	0	0	0	0	0	0	0	0	0	1
CCL3	0	0	0	0	0	0	1	0	0	0
CCL4	0	0	0	0	0	0	1	0	1	0
CCL5	0	0	0	0	0	0	1	0	1	0
CCNA1	0	0	0	0	0	0	0	0	1	0
CCND1	0	0	0	0	0	0	0	1	0	0
CCR2	0	0	0	0	0	0	1	0	0	0
CD14	0	0	0	0	0	0	1	0	0	1
CD163	0	0	1	0	0	0	1	0	0	0
CD19	0	0	0	0	0	0	0	0	0	1
CD2	0	0	0	0	0	0	1	0	0	0
CD247	0	0	0	0	0	0	1	0	0	0
CD27	0	0	0	0	0	0	1	0	0	0
CD28	0	0	0	0	0	0	1	0	0	0
CD300A	0	0	0	0	0	0	1	0	0	0
CD38	0	0	0	0	0	0	1	0	0	0

CD3D	0	0	0	0	0	0	1	0	0	0
CD3E	0	0	0	0	0	0	1	0	0	0
CD3G	0	0	0	0	0	0	1	0	0	0
CD4	0	0	0	0	0	0	1	0	0	0
CD44	0	0	0	0	0	0	1	0	0	0
CD47	0	0	0	0	1	0	0	0	0	0
CD48	0	0	0	0	0	0	1	0	0	0
CD5	0	0	0	0	0	0	1	0	0	0
CD58	1	0	0	0	0	0	0	0	0	0
CD6	0	0	0	0	0	0	1	0	0	0
CD69	0	0	1	0	0	0	0	0	1	0
CD7	0	0	0	0	0	0	1	0	0	0
CD74	0	0	0	0	0	0	1	0	0	0
CD79A	0	0	0	0	0	0	0	0	0	1
CD79B	0	0	0	0	0	0	0	0	0	1
CD84	0	0	0	0	0	0	1	0	0	0
CD86	0	0	0	0	0	0	1	0	0	0
CD8A	0	0	0	0	0	0	1	0	1	0
CD8B	0	0	0	0	0	0	1	0	1	0
CDH11	0	0	0	0	0	0	0	0	1	0
CDH5	0	1	0	0	0	0	0	0	0	0
CDKN1A	0	0	0	0	1	0	0	0	0	0
CDKN2A	0	0	0	1	0	0	0	0	0	0
CDKN2B	0	0	0	0	0	0	0	1	0	0
CEBPB	0	0	1	0	0	0	0	0	0	0
CES3	0	0	0	0	0	0	0	1	0	0
CLEC7A	0	0	1	0	0	0	1	0	0	0
CMKLR1	0	0	1	0	0	0	1	0	0	0
COL11A1	0	0	0	0	0	0	0	0	1	0
COL17A1	0	0	0	0	0	0	0	1	0	1
CSF1	0	0	0	0	0	0	1	0	0	0
CSF2RB	0	0	0	0	0	0	1	0	0	0
CSF3R	0	0	0	0	0	0	1	0	0	0
CTLA4	0	0	0	0	1	0	1	0	1	0
CTNNB1	0	0	0	0	0	0	0	1	0	0
CTSS	0	0	0	0	0	0	1	0	0	0
CX3CL1	0	0	0	0	0	0	1	0	0	0
CX3CR1	0	0	0	0	0	0	0	1	0	0
CXCL1	0	0	1	0	0	0	1	0	0	0
CXCL11	0	0	1	0	0	0	0	0	1	0
CXCL13	0	0	0	0	0	0	1	0	0	0
CXCL14	0	0	0	0	0	0	0	1	0	0
CXCL2	0	0	1	0	0	0	0	0	0	0
CXCL3	0	0	1	0	0	0	1	0	0	0
CXCL5	0	0	0	0	0	0	1	0	0	0
CXCL6	0	0	1	0	0	1	0	0	0	0

CXCL8	0	0	0	0	0	0	1	0	0	0
CXCL9	0	0	0	0	1	0	0	0	0	0
CXCR4	0	0	0	0	0	0	0	0	1	0
CXCR6	0	0	0	0	0	0	1	0	1	0
CXXC5	0	0	0	0	0	0	0	1	0	0
CYBB	0	0	0	0	0	0	1	0	0	0
DAB2	0	0	0	0	0	1	0	0	1	0
DKK 1.00	0	0	0	0	0	0	0	1	0	0
DUSP5	0	0	0	0	0	0	0	0	1	0
E2F3	0	0	0	0	0	0	0	0	1	0
EDN1	0	0	0	0	0	0	0	0	1	0
EGR1	0	0	0	0	0	0	0	0	1	0
ENTPD1	0	0	0	0	0	0	1	0	0	0
EOMES	0	0	0	0	0	0	1	0	1	0
FAM30A	0	0	0	0	0	0	0	0	0	1
FAP	0	0	0	0	0	0	0	0	1	0
FAS	0	0	0	0	0	0	1	0	1	0
FASLG	0	0	0	0	0	0	1	0	0	0
FBP1	0	0	0	0	0	0	0	1	0	0
FCN1	0	0	0	0	0	0	1	0	0	0
FCRL2	0	0	0	0	0	0	0	0	0	1
FGFR4	0	0	0	0	0	0	0	0	0	1
FLT1	0	0	0	0	0	0	0	1	0	0
FOSL1	0	0	0	0	1	0	1	0	0	0
FOXC1	0	0	0	0	0	0	0	1	0	0
FOXP3	0	0	0	0	0	0	1	0	0	0
FPR1	0	0	0	0	0	0	1	0	0	0
FPR3	0	0	0	0	0	0	1	0	0	0
FYN	0	0	1	0	0	0	0	0	1	0
GBP1	0	0	0	0	0	0	1	0	1	0
GIMAP4	0	0	0	0	0	0	1	0	0	0
GLS	0	0	0	0	0	0	1	0	1	0
GLUD1	0	0	1	0	0	0	0	1	0	0
GLUL	0	0	1	0	0	0	0	0	0	0
GMIP	0	0	0	0	0	0	0	1	0	0
GNG4	0	0	0	0	0	0	1	0	0	0
GNLY	0	0	0	0	0	0	1	0	0	0
GPC4	0	1	0	0	0	0	0	0	0	0
GPSM3	0	0	0	0	0	0	1	0	0	0
GZMA	0	0	0	0	0	0	1	0	0	0
GZMB	0	0	0	0	0	0	1	0	0	0
GZMH	0	0	0	0	0	0	1	0	0	0
GZMK	0	0	0	0	0	0	1	0	0	0
H2AX	0	0	0	0	0	0	0	0	0	1
HAVCR2	0	0	0	0	0	0	1	0	1	0
HCK	0	0	0	0	0	0	0	0	0	1

HDAC3	0	0	0	0	0	0	0	1	0	0
HDAC5	0	0	0	0	0	0	0	1	0	0
HEY1	0	0	0	0	0	0	0	1	0	0
HIF1A	0	0	0	0	0	0	0	0	1	0
HLA-A	0	0	0	0	0	0	1	0	0	0
HLA-DMA	0	0	0	0	0	0	1	0	0	0
HLA-DOB	0	0	0	0	0	0	1	0	0	0
HLA-DQB1	0	0	0	0	0	0	1	0	0	0
HLA-DRB1	0	0	0	0	0	0	1	0	0	0
HLA-DRB5	0	0	0	0	0	0	1	0	0	0
HLA-F	0	0	0	0	0	0	1	0	0	0
HSD11B1	0	0	0	0	1	0	1	0	0	0
ICAM1	0	0	1	0	0	0	1	0	0	0
ICAM3	0	0	0	0	0	0	0	0	0	1
ICOS	0	0	0	0	1	0	1	0	0	0
IDO1	0	0	0	0	0	0	1	0	0	0
IER3	1	0	0	0	0	0	0	0	0	0
IFI16	0	0	0	0	0	0	1	0	0	0
IFI6	0	0	0	0	0	0	0	0	0	1
IFITM1	0	0	0	0	0	0	1	0	0	0
IKBKG	0	0	0	0	0	0	0	1	0	0
IL10	0	0	0	0	0	0	1	0	0	0
IL10RA	0	0	0	0	0	0	1	0	0	0
IL12RB2	0	0	0	0	0	0	0	0	1	0
IL15	0	0	0	0	0	0	1	0	0	0
IL18R1	0	0	0	0	0	0	1	0	1	0
IL1R2	0	0	1	0	0	0	1	0	0	0
IL24	0	0	0	0	0	0	1	0	0	0
IL2RA	0	0	1	0	1	0	1	0	0	0
IL2RB	0	0	0	0	0	0	1	0	0	0
IL2RG	0	0	0	0	0	0	1	0	0	0
IL32	0	0	0	0	0	0	1	0	0	0
IL7R	0	0	0	0	0	0	0	0	1	0
INHBA	0	0	0	0	1	0	0	0	0	0
IRF4	0	0	0	0	0	0	0	0	0	1
ITGA4	0	0	0	0	0	0	1	0	0	0
ITGAL	0	0	0	0	0	0	1	0	0	0
ITGAM	0	0	0	0	0	0	1	0	0	0
ITGB2	0	0	0	0	0	0	1	0	0	0
ITPK1	0	1	0	0	0	0	0	0	0	0
JAK2	0	0	0	0	0	0	1	0	0	0
JAK3	0	0	0	0	0	0	1	0	0	0
KAT2B	0	0	0	0	0	0	0	1	0	0
KDR	0	0	0	0	0	0	0	1	0	0
KIR3DL2	0	0	0	0	0	0	1	0	0	0
KLRD1	0	0	1	0	0	0	1	0	1	0

KLRK1	0	0	0	0	0	0	1	0	0	0
LAG3	0	0	0	0	0	0	1	0	0	0
LAIR1	0	0	0	0	0	0	1	0	0	0
LCK	0	0	0	0	0	0	1	0	0	0
LIF	0	0	0	0	1	0	0	0	0	0
LILRA1	0	0	0	0	0	0	0	0	0	1
LILRA3	0	0	0	0	1	0	0	0	0	0
LILRB2	0	0	0	0	0	0	1	0	0	0
LILRB4	0	0	0	0	0	0	1	0	0	0
LRRC32	0	1	0	0	0	0	0	0	0	0
LY9	0	0	0	0	0	0	1	0	0	0
LY96	0	0	0	0	0	0	1	0	0	0
LYZ	0	0	0	0	0	0	1	0	0	0
MAGEA1	0	0	1	0	0	0	0	0	0	0
MAGEA12	0	0	1	0	0	0	0	0	0	0
MAGEA4	0	0	1	0	0	0	0	0	0	0
MAGEA6	0	0	0	0	0	1	0	0	0	0
MAP3K7	0	0	0	0	0	0	0	1	0	0
MAP3K8	0	0	0	0	0	0	0	0	1	0
MAPK10	0	0	0	0	0	0	0	1	0	0
MAPT	0	0	0	0	0	0	0	1	0	0
MGMT	0	0	0	0	0	0	0	1	0	0
MICA	0	0	1	0	0	0	0	0	0	0
MLH1	0	0	0	0	0	0	0	1	0	0
MMP11	0	0	0	0	0	1	0	0	0	0
MMRN2	0	1	0	0	0	0	0	1	0	0
MRE11	1	0	0	0	0	0	0	0	0	0
MSH6	0	0	1	0	0	0	0	0	0	0
MYBL2	0	0	0	0	0	1	0	0	0	0
MYCT1	0	1	0	0	0	0	0	0	1	0
NCAM1	0	0	0	1	0	0	0	0	0	0
NCR1	0	0	0	0	0	0	1	0	0	0
NDUFA4L2	0	0	0	0	0	0	0	1	0	0
NEIL1	0	0	0	0	0	0	0	1	0	0
NFAM1	0	0	0	0	0	0	1	0	0	0
NFIL3	0	0	0	0	0	0	0	0	1	0
NFKB2	0	0	1	0	0	0	0	0	0	0
NFKBIA	0	0	0	0	0	0	0	0	1	0
NKG7	0	0	0	0	0	0	1	0	0	0
NLRC5	0	0	0	0	0	0	1	0	0	0
NOD2	0	0	0	0	0	0	1	0	0	0
NOTCH1	0	0	0	0	0	0	0	1	0	0
NT5E	0	0	0	0	0	0	0	0	1	0
OLR1	0	0	0	0	0	0	1	0	0	0
PC	0	0	0	0	0	0	0	1	0	0
PCK2	0	0	1	0	0	0	0	0	0	0

PDCD1	0	0	0	0	0	0	1	0	1	0
PDCD1LG2	0	0	0	0	0	0	1	0	0	0
PDK1	0	0	0	0	0	0	0	1	0	0
PF4	0	0	0	0	0	0	0	1	0	0
PFKM	0	0	0	0	0	0	0	1	0	0
PIK3CA	0	0	0	0	0	0	0	0	1	0
PIK3CG	0	0	0	0	0	0	1	0	0	0
PIK3R1	0	0	0	0	0	0	0	0	1	0
PIK3R5	0	0	0	0	0	0	1	0	0	0
PLA1A	0	0	0	0	0	0	1	0	0	0
PLOD2	0	0	0	0	0	0	0	0	1	0
PPARGC1B	0	0	0	0	0	0	0	1	0	0
PRF1	0	0	0	0	0	0	1	0	0	0
PRKAA2	0	0	0	0	1	0	0	0	0	0
PRKACB	0	0	0	0	0	0	1	0	0	0
PRKCA	0	0	0	0	0	0	0	1	0	0
PROM1	0	0	0	0	0	0	0	1	0	0
PTEN	0	0	0	0	0	0	0	0	1	0
PTGER4	0	0	0	0	0	0	0	1	0	0
PTPRC	0	0	0	0	0	0	1	0	0	0
PVRIG	0	0	0	0	0	0	1	0	0	0
RAD51	0	0	1	0	0	0	0	0	0	0
RELA	0	0	1	0	0	0	0	0	0	0
REN	0	0	0	0	0	0	0	1	0	0
RIPK2	0	0	0	0	0	0	0	0	1	0
RIPK3	0	0	0	0	0	0	0	1	0	0
ROCK1	0	0	0	0	0	0	1	0	1	0
RPL7A	0	0	0	0	0	0	0	1	0	0
RUNX3	0	0	1	0	0	0	1	0	0	0
S100A8	1	0	0	0	1	0	0	0	0	0
S100A9	1	0	0	0	0	0	0	0	0	0
SAMSN1	0	0	1	0	0	0	1	0	1	0
SELE	0	0	0	0	1	0	0	0	0	0
SERPINA1	0	0	0	0	0	0	1	0	0	0
SFRP4	0	0	0	0	0	0	0	0	1	0
SH2D1A	0	0	0	0	0	0	1	0	1	0
SIGLEC1	0	0	0	0	0	0	1	0	0	0
SIGLEC5	0	0	0	0	0	0	0	1	0	0
SIRPB2	0	0	0	0	0	0	1	0	0	0
SLAMF7	0	0	0	0	0	0	1	0	0	0
SLC16A1	0	0	0	0	0	0	1	0	0	0
SMAD5	0	0	0	0	0	0	0	1	0	0
SMAP1	0	0	0	0	0	0	0	1	0	0
SOCS1	0	0	0	0	0	0	1	0	0	0
SRP54	0	0	1	0	0	0	0	0	0	0
STAT4	0	0	0	0	0	0	1	0	0	0

STC1	0	0	0	0	1	0	0	0	0	0
STING1	0	0	0	0	0	0	1	0	0	0
SYK	0	0	0	0	0	0	0	1	0	0
TAP2	0	0	0	0	1	0	0	0	0	0
TAPBP	0	0	0	0	1	0	0	0	0	0
TBX21	0	0	0	0	0	0	1	0	0	0
TBXAS1	0	0	0	0	0	0	1	0	0	0
TDO2	0	0	0	0	0	0	1	0	0	0
TGFB3	0	0	0	0	0	0	0	0	1	0
TGFBR1	0	0	0	0	0	0	0	0	1	0
TICAM1	0	0	0	0	0	0	0	0	1	0
TIGIT	0	0	0	0	0	0	1	0	0	0
TLR2	0	0	0	0	0	0	1	0	0	0
TLR8	0	0	0	0	0	0	1	0	0	0
TLR9	0	0	0	0	0	0	0	1	0	0
TMEM140	0	0	1	0	0	0	1	0	0	0
TMEM45B	0	0	0	0	1	0	0	0	0	0
TNF	0	0	0	0	0	0	0	0	0	1
TNFAIP3	0	0	0	0	0	0	0	0	1	0
TNFRSF10	0	0	0	0	0	0	1	0	0	0
TNFRSF11	0	0	0	0	0	0	0	1	0	0
TNFRSF18	0	0	0	0	0	0	1	0	0	0
TNFRSF1B	0	0	0	0	0	0	1	0	0	0
TNFRSF4	0	0	0	0	0	0	1	0	0	0
TNFRSF8	0	0	0	0	0	0	1	0	0	0
TNFRSF9	0	0	0	0	0	0	1	0	0	0
TNFSF13B	0	0	0	0	0	0	1	0	0	0
TNFSF18	0	0	1	0	1	0	0	0	0	0
TNFSF4	0	0	0	0	0	0	1	0	0	0
TNFSF8	0	0	0	0	0	0	0	0	1	0
TNFSF9	0	0	0	0	0	0	1	0	0	0
TNKS	0	0	0	0	0	0	0	1	0	0
TP53	0	0	0	0	0	0	0	1	0	0
TRAF1	0	0	0	0	0	0	1	0	0	0
TRAT1	0	0	0	0	0	0	1	0	1	0
TWIST1	0	0	0	0	0	0	0	0	1	0
TWIST2	0	0	0	0	0	0	0	0	1	0
UBE2C	0	0	0	0	0	1	0	0	0	0
UBE2T	0	0	0	0	0	1	0	0	0	0
VCAN	0	0	0	0	0	0	0	0	1	0
VEGFA	0	0	0	0	0	0	0	1	0	0
VSIR	0	0	0	0	0	0	1	0	0	0
WDR76	0	0	1	0	0	0	0	0	0	0
WNT11	0	0	0	0	0	0	0	1	0	0
WNT2	0	0	0	0	0	1	1	0	0	0
WNT5A	0	0	0	0	0	0	0	1	0	0

XCL1	0	0	1	0	0	0	0	0	0	0
XCL2	0	0	0	0	0	0	1	0	1	0
ZAP70	0	0	0	0	0	0	1	0	0	0
ZC3H12A	0	0	0	0	0	0	1	0	0	0
ZEB1	0	0	0	0	0	0	0	0	1	0

Supplementary Table 8: Breast CPI-Dynamics cohort genes categories and clinical outcomes

Gene	group	OR	OR_P_val	HR	HR_P_val	TCGA_HR	TCGA_HR_P_val
APOL6	Response_pos	1.8727688	0.60608696	0.466507724	0.0048434	0.930398	0.7046969
AQP9	Response_pos	3.8368869	0.02695652	0.797015007	0.0694907	1.078635	0.3574409
B2M	Response_pos	2.016424	0.4973913	0.553289306	0.0052078	0.87645	0.5644276
BNIP3L	Resistance_pos	0.3916964	0.55043478	1.092384498	0.7962692	0.73248	0.3159059
C1QA	Response_pos	3.2621595	0.15130435	0.469137102	0.0003951	1.146844	0.3972109
C1QB	Response_pos	3.1471283	0.15130435	0.53394734	0.000962	1.233022	0.2064369
C2	Response_pos	2.9769284	0.20608696	0.527749295	0.0067578	1.161534	0.3482862
CASP1	Response_pos	0.9427519	0.84434783	0.670867549	0.0410696	1.111915	0.5665043
CCL3	Response_pos	16.106601	0.00173913	0.658268684	0.0266653	1.04404	0.7666475
CCL5	Response_pos	1.6984632	0.39826087	0.656356515	0.0032072	0.994727	0.9629122
CCL8	Response_pos	1.8355021	0.20608696	0.692242094	0.0300202	1.083292	0.4659459
CCR5	Response_pos	2.0097843	0.20608696	0.564590915	0.0009785	1.02168	0.8733989
CD2	Response_pos	1.5788148	0.44608696	0.692021854	0.0062276	0.990083	0.9262206
CD244	Response_pos	1.5399066	0.7226087	0.593645726	0.0080028	1.001172	0.9926234
CD27	Response_pos	1.9748343	0.35304348	0.59656293	0.0026742	0.971863	0.7994015
CD274	Response_pos	2.0598546	0.31130435	0.632127869	0.0115716	0.861943	0.3850193
CD300A	Response_pos	1.7830192	0.55043478	0.485764764	0.0068075	1.341231	0.1871815
CD38	Response_pos	2.3677243	0.15130435	0.687609499	0.012684	1.039678	0.6901508
CD3D	Response_pos	1.5105031	0.39826087	0.667992286	0.0020263	0.992414	0.9406984
CD3E	Response_pos	1.5973933	0.35304348	0.632218101	0.0022872	1.007853	0.9392108
CD3G	Response_pos	1.4469164	0.44608696	0.710888892	0.0074528	0.992228	0.9257048
CD4	Response_pos	1.9862914	0.31130435	0.615815227	0.0087922	1.086013	0.6551488
CD40	Response_pos	2.5222572	0.20608696	0.426130594	0.0007434	1.049805	0.7972772
CD48	Response_pos	1.5811139	0.55043478	0.638879333	0.0053871	0.994563	0.9677738
CD69	Response_pos	1.3375743	0.60608696	0.672416139	0.0196796	0.956307	0.7265311
CD7	Response_pos	2.0560772	0.31130435	0.616072227	0.0131005	1.097075	0.3992328
CD80	Response_pos	7.3173158	0.08869565	0.36481559	0.0044464	1.131748	0.4125652
CD8A	Response_pos	2.4038542	0.1773913	0.577413948	0.0014054	0.972925	0.8083929
CD96	Response_pos	1.5427036	0.55043478	0.659244821	0.0040888	0.954424	0.6818473
CLEC7A	Response_pos	1.7877954	0.4973913	0.543615625	0.0309616	1.092617	0.5502292
COL4A5	Response_neg	0.1319368	0.01391304	1.397472218	0.131112	0.836181	0.0720149
CTSS	Response_pos	2.3848869	0.15130435	0.425477785	0.0021864	1.078472	0.6713194
CTSW	Response_pos	1.5935135	0.31130435	0.697480825	0.0029142	0.985039	0.8898861
CXCL10	Response_pos	1.7867266	0.27304348	0.532060343	0.0015043	1.009508	0.9231619
CXCL11	Response_pos	1.2570643	0.7226087	0.706740894	0.0065507	0.994675	0.9537942
CXCL9	Response_pos	1.6297351	0.20608696	0.622371227	7.06E-05	0.920947	0.2970732
CXCR6	Response_pos	1.5883122	0.35304348	0.71883688	0.0062317	0.998445	0.9900835
CYBB	Response_pos	2.6376467	0.35304348	0.415545075	0.0004278	1.096389	0.5476625
EOMES	Response_pos	1.6507559	0.39826087	0.643926769	0.0012749	0.992799	0.9323568
FASLG	Response_pos	2.2721221	0.1773913	0.52806843	0.0001853	1.026172	0.7720422
FCGR1A	Response_pos	3.7710668	0.05826087	0.582379752	0.0072804	1.01598	0.9357926
FCGR3A	Response_pos	15.478905	0.02	0.65039902	0.0413582	1.121014	0.5312954
GBP1	Response_pos	1.2187028	0.60608696	0.664196192	0.0289438	0.958132	0.7592807
GBP4	Response_pos	1.7252202	0.35304348	0.573311031	0.0016244	0.890426	0.3954902
GPC4	Resistance_neg	1.9391881	0.55043478	0.761321405	0.1931634	0.743567	0.025895
GZMA	Response_pos	1.4413757	0.60608696	0.683407105	0.0016215	1.035465	0.7475453
GZMB	Response_pos	1.4524105	0.23826087	0.660639736	0.0076209	1.061966	0.4834415
GZMH	Response_pos	1.9751422	0.20608696	0.591270676	0.0016592	0.98276	0.838995
GZMK	Response_pos	1.4644465	0.4973913	0.712099875	0.0021508	1.010798	0.8833837
H2AX	Response_pos	399.77826	0.01391304	0.529973149	0.1942965	1.479863	0.0652074
HCK	Response_pos	2.0101034	0.60608696	0.495041353	0.0037299	1.066144	0.7243606

HLA-A	Response_pos	2.1418575	0.60608696	0.522651844	0.0046923	1.024855	0.8913822
HLA-B	Response_pos	1.4150549	0.60608696	0.636166021	0.0320963	0.949225	0.779425
HLA-C	Response_pos	2.5488483	0.4973913	0.524363016	0.0241763	0.950805	0.8233445
HLA-DMA	Response_pos	2.7255712	0.20608696	0.461524573	0.0044813	0.965037	0.8532132
HSD11B1	Response_pos	1.8417798	0.1773913	0.608525842	0.0032466	0.917073	0.5072741
ICAM1	Response_pos	1.9300497	0.55043478	0.491683631	0.0092482	1.179045	0.3339128
ICAM5	Response_neg	0.3188997	0.05826087	1.3436427	0.2441818	0.918708	0.3692608
ICOS	Response_pos	1.6210377	0.31130435	0.594317605	0.0020682	1.024759	0.7657114
IL12RB2	Response_pos	1.7140107	0.55043478	0.721521347	0.1830081	1.038279	0.6396861
IL18	Response_pos	1.3821521	0.7826087	0.732471504	0.0505896	0.982481	0.9157297
IL1B	Response_pos	2.3424282	0.35304348	0.73214715	0.238327	1.048561	0.7480361
IL21R	Response_pos	1.6245405	0.4973913	0.741509979	0.04081	0.8979	0.4021277
IL2RA	Response_pos	2.0853543	0.1773913	0.552242063	0.0008321	1.131879	0.2968318
IL2RB	Response_pos	1.8051226	0.35304348	0.598332446	0.0010297	0.99344	0.9592589
IL2RG	Response_pos	1.7621512	0.27304348	0.578692911	0.0009076	0.987675	0.9157327
IL32	Response_pos	1.715288	0.4973913	0.585204327	0.00214	1.240051	0.1251099
IRF1	Response_pos	1.67437	0.4973913	0.526715286	0.0046664	0.918593	0.6661763
IRF2	Response_pos	3.6444514	0.31130435	0.34174643	0.0077753	0.662163	0.3649318
ITGAL	Response_pos	2.0094758	0.27304348	0.596540146	0.004346	0.863865	0.3263692
ITGB2	Response_pos	2.5084302	0.20608696	0.505363279	0.0016231	1.220132	0.2222516
JAK2	Response_pos	1.1620986	0.60608696	0.566378195	0.0145919	0.640733	0.0862139
KLRD1	Response_pos	0.9139911	1	0.765628198	0.0804123	0.92471	0.5419633
LAIR1	Response_pos	3.0321774	0.27304348	0.436434267	0.0006413	1.215952	0.3224262
LCK	Response_pos	1.4987382	0.35304348	0.683295565	0.0030617	1.07803	0.5002889
LILRB2	Response_pos	4.3648143	0.12782609	0.431700139	0.0014693	1.15104	0.3964733
LILRB4	Response_pos	3.257336	0.10695652	0.498061101	0.0013892	1.084379	0.6129286
MAGEB2	Response_pos	2.1027086	0.1773913	0.540426028	0.0229617	0.996688	0.9437196
MRE11	Resistance_pos	0.05854	0.27304348	2.948050226	0.0668811	1.193176	0.6353976
NFAM1	Response_pos	2.0426104	0.4973913	0.491920225	0.0099563	1.051607	0.770427
NFKBIE	Response_pos	4.2898839	0.31130435	0.48074352	0.0712047	1.357126	0.1824776
NLRC5	Response_pos	0.8646258	0.90608696	0.717398086	0.0553694	0.968708	0.8549624
NOD2	Response_pos	0.8275153	0.96869565	0.750646302	0.3494646	1.003736	0.9812758
NRAS	Response_neg	1.73E-05	0.00347826	10.88469319	0.0007866	1.205364	0.3994173
P2RY13	Response_pos	1.5047645	0.55043478	0.651385864	0.0052866	0.916808	0.5364938
PARP4	Response_pos	2.372713	0.44608696	0.263181078	0.0144021	1.132266	0.6497639
PDCD1LG2	Response_pos	1.669749	0.35304348	0.667170485	0.0063942	0.948497	0.7404324
PIK3CD	Response_pos	0.694687	0.7826087	0.660489879	0.082078	1.081108	0.6594495
PIK3R2	Response_neg	0.0068779	0.00347826	2.706627815	0.0128095	1.003149	0.9666504
PRF1	Response_pos	1.9653056	0.15130435	0.573325872	0.0003575	1.018359	0.8755632
PSMB10	Response_pos	3.0145675	0.44608696	0.350796797	0.0008475	1.188004	0.4433316
PSMB8	Response_pos	2.0007949	0.39826087	0.505706056	0.0065241	1.050075	0.8127474
PSMB9	Response_pos	1.7489316	0.39826087	0.578086373	0.0029984	1.003774	0.9805083
REN	Response_pos	1.8393047	0.04608696	0.762884835	0.2717526	0.92895	0.0970617
S100A9	Resistance_pos	0.5527255	0.27304348	1.253637516	0.0807752	1.111464	0.0865664
SERPINA1	Response_pos	1.9285453	0.20608696	0.760771355	0.0059628	0.784721	0.0325136
SH2D1A	Response_pos	1.4786712	0.4973913	0.67672812	0.0031885	0.981288	0.8405735
SIRPB2	Response_pos	3.1666116	0.27304348	0.467065165	0.002602	1.022898	0.9047704
SLAMF7	Response_pos	1.894553	0.23826087	0.624488615	0.0053671	0.974354	0.8217151
STAT1	Response_pos	1.4862267	0.4973913	0.597102299	0.0041554	0.859178	0.416492
TAPBPL	Response_pos	4.2068566	0.31130435	0.210854597	0.0021226	0.522729	0.0189107
THBS1	Response_neg	0.6154778	0.08869565	1.223349835	0.3994572	1.040266	0.84027
TIGIT	Response_pos	1.8086689	0.1773913	0.557898427	0.0007049	1.025084	0.7996627
TLR1	Response_pos	1.4867459	0.7826087	0.263737687	0.0028767	1.401717	0.0630324
TLR4	Response_pos	2.3527181	0.31130435	0.488348995	0.0005001	1.055089	0.7976589
TLR7	Response_pos	1.1479385	0.84434783	0.54696705	0.0188242	1.037815	0.8230126
TLR8	Response_pos	2.3925039	0.12782609	0.43591917	0.0001103	1.068416	0.5824449
TMEM140	Response_pos	1.6687205	0.60608696	0.501617256	0.0044197	0.79696	0.4579628
TNF	Response_pos	1.5391945	0.44608696	0.583915221	0.0088525	1.100408	0.4121489

TNFAIP3	Response_pos	2.02881	0.44608696	0.528292944	0.0105354	1.02986	0.8763139
TNFRSF1B	Response_pos	1.40374	0.55043478	0.550348851	0.0069184	1.064865	0.7264621
TNFRSF9	Response_pos	2.5006557	0.1773913	0.590686275	0.0067948	1.022754	0.8495044
TRAT1	Response_pos	1.328379	0.4973913	0.741793225	0.0101494	0.989101	0.8879631
XCL1	Response_pos	1.4575638	0.96869565	0.685585065	0.0310655	1.008005	0.9337037